Study of protein membranes formed by interfacial crosslinking using microfluidic flow

Chang, Hong

Study of protein membranes formed by interfacial crosslinking using microfluidic flow

By

Hong Chang

Supervisors: Professor Pankaj Vadgama

Dr. Steve Dunn

Submitted for the Degree of Doctor of Philosophy

School of Engineering and Materials Science

Queen Mary, University of London

2012

I hereby declare that the work carried out and presented in this thesis for the degree of Doctor of Philosophy is original and my own.

Hong Chang

Abstract

Microfluidic membranes are used in myriad applications, including use in microbioreactors. They serve as bio-catalyst surfaces or allow cell adhesion. However, creating such membranes requires complex manufacturing processes including multi-step self assemble. Recently, a nylon membrane was produced in situ in a flow channel [17]. This process is completed rapidly (within a few minutes), but such membranes are essentially only gas permeable. Control of the thickness and inclusion of porosity is important for effective membrane permeably for general solute transfer and could be sensitive for a given size range of molecules. In the present work, a simplified in situ fabrication technique has been used to produce a robust and novel protein micro-membrane. The proteins studied were BSA and fibrinogen with an acyl chloride to achieve protein crosslinking. Three acyl chloride crosslinkers were tested each crosslinker also generated unique surface morphologies and cross section morphological structures. Permeability of these membranes was tested by diffusion studies using dye molecules as well as the electrochemically active.

A simplified approach of using ethanol to further modify the porosity of the membrane was established. Antibacterial membranes were achieved by exposing the protein membranes to copper sulphate solution. Tensile tests on the membranes showed that there was variation in membrane strength that was related to the crosslink or molecule type, and was also related to porosity.

Acknowledgements

I'm thankful to say I have reached the end of my PhD study. There have been many ups and downs during this period, the experiences has been exhilarating, painful and damn right depressing, but I have gained a wealth of knowledge about new techniques and met a great set of colleagues and friends in the process.

At first I would like to thank my supervisors Professor Pankaj Vadgama and Dr Steve Dunn. I am grateful for their guidance and support throughout the course of this research project and for their advice during the drafting of this thesis. A special mention will go to Professor Wen Wang who has provided so much support and understanding during my study.

I would also like to extend my thanks to the people who provided me with exciting opportunities to test my experiments on their systems. Dr Andrei Sapelkin in the physics department provided his laboratory for fabricating the microfluidics system. Dr Zofia Luklinska provided so much help with SEM. Bill Gillin in the physics department facilitated the use of their DekTak profilometer. Dr Andy J Bushby provided his Nanoindentation system for membrane test. Dr Nima provided his intellectual stimulation and continued interest in the development of the project, without which all enthusiasm might have been lost, for which I am indented to you. I am grateful for the admin support provide by Jonathon and Catherine (Jones).

I am thankful for all the advice given to me (work or otherwise!) by my colleagues in my group. It has been great knowing Zimei. Rong, Rachel Khan, Anna Spehar-Délèze and Salzitsa Anastasova. They were the ones that made this PhD entertaining. Also the most important friends in office 146 and 147, without them life would not have been as interesting or amusing.

Last but not least, my family. My Mum and Dad have been so supportive from Day one. My husband Biplab for always being around and providing me with lots of love and support! I really could not ask for any better.

Table of Content

List of Figures

List of Tables

Chapter2

Chapter 3

Chapter 4

Chapter 5

Chapter 6

List of Symbols and Abbreviations

MEMS: Microelectromechanical system

PDMS: Poly(dimethylsiloxane)

PMMA: Poly(methylmethacrylate)

PMGI: Poly(methyl glutarimide)

E: Modulus of elasticity

$G_{0:}$ Shear modulus at zero time

$G\infty$: Shear modulus at infinity

C_r: Creep ratio

BSA: Bovine serum albumin

TCL: Terephthaloyl chloride

IDCL: Isophthaloyl chloride

SCL: Sebacoyl chloride

EGCG: (-)-Epigallocatechin-3-gallate

PVA: Polyvinyl alcohol

PSF: Polysulfone

GC: Gas chromatography

BioMEMs: Biomedical microelectromechanical systems

ρ: Fluid density

V: Fluid viscosity

v: Characteristic velocity of the fluid

D: Hydraulic diameter

d: The distance a particle moves

t: Time

x: The spatial coordinate

ϕ: Concentration.

CVD: Chemical vapour deposition

KOH: Potassium hydroxide

EDP: Diamine pyrochatechol

TMAH: Tetramethyl ammonium hydroxide

C.V.: Coefficient of variation

NAPQI: N-acetyl-p-quinoneimine

GOD: Glucose oxidase

PBS: Phosphate buffer saline

CSS: Copper sulphate solution

PTFE: Polytetrafluoroethylene

DMEM: Dulbecco's Modified Eagle's Medium

FBS: Fetal Bovine Serum

DPBS: Dulbecco’s Phosphate Buffered Saline

SEM: Scanning Electron Microscopy

FTIR: Fourier Transform Infrared Spectroscopy

EDS: Energy-dispersive X-ray spectroscopy

PVC: Polyvinyl chloride plastic

Chapter1: Introduction

Microfluidics systems have been the subject of considerable attention in recent years [1]. Their inherent small size not only reduces the sample volume that may be required for a give reaction or measurement process, but there are particular advantages with respect to associated short diffusion distances. Diffusion time varies with the square of diffusion distance, so when diffusion distance is reduced one order of magnitude, diffusion time is reduced two orders of magnitude. Also, in contrast to a macro- system, microfluidics allows for new flow functionality with a fundamental shift in fluid handling, based on the level of dominance of viscous vs. inertial flow effects, i.e., the attribute of a low Reynolds number regimen [2]. A large surface area to volume ratio and surface tension based interactions also facilitate tuning of solid/liquid interactions.

Laminar flow is a particular feature, and while a drawback when rapid, turbulent mixing is intended, it permits more uniform solute exchange driven by Fickian diffusion alone. Laminar flow has been exploited at parallel fluid flows, where convective fluid mixing has been avoided, and diffusive exchanges between separate fluid streams variously used for chemical assay and particle sorting. Since the 1970s [1,3], microfluidics have experienced additional development, with new specialist applications emerging, such as microfabricated glucose responsive valves for closed loop insulin delivery [4] and microfluidics

incorporated materials for application in tissue engineering, drug delivery and prosthetic implants, respectively [5].

Microelectromechanical system (MEMS) was developed in the 1970s and utilised silicon to fabricate microfluidics devices [6]. Due to the lack of optical transparency, observational and analytical studies were limited, and glass based micro-devices were then developed. However, any MEMS technique is costly, labour intensive and requires specialized skills and facilities. As an alternative to such hard micro- devices, therefore, soft polymer based structures were advanced, offering less expensive, more rapid to manufacture capabilities. Poly(dimethylsiloxane) (PDMS) [7] and also poly(methylmethacrylate) (PMMA) have been used. Fabrication approaches have included lithography with photoresists, micro-moulding and laser ablation. However, many microfluidic applications do not require precision techniques. We have achieved low Reynolds number operation for laminar flow with optical transparency using simple geometric assemblies of glass microscope slides with UV glue bonding [8, 9].

The development of microfluidics for analysis is indicated by many recent publications, and as a part of this, the integration of mass transport control membranes in microfluidic flows has been considered [10]. This has made it possible, for example, to extract analyte to extend instrumental detection limit and to remove unwanted solvent [11]. Biopolymers as scaffolds and membranes are already used for tissue engineering and as culture surfaces, and could offer advantages for micro-reactors [12]. Membranes formulated from biopolymers,

as used for tissue engineering, could also offer advantages within micro-bioreactors [13].

The fabrication method used for incorporation of a membrane into a microfludic device depends on both the membrane material and the nature of the micro-device. Two fabrication methods [11] are conventionally used: incorporation of a pre-formed membrane by clamping and adhesive bonding; *in situ* membrane deposition. Pre-formed membrane use, of course, allows for the widest choice of membrane material and morphology, as well as being technically simple. Its major disadvantage, however, is the potential for fluid tracking outside of the clamped membrane area and adhesive tracking into the membrane material due to capillary forces. With *in situ* membrane deposition, an unmodified micro-device can be used, but there is a limit to the materials usable, and control over final properties may be limited. For in situ membrane deposition, different types of microchannel structure have been tested. T-channel geometry exhibits non-uniform velocity profile development at high flow rates, which may lead to non-uniform membrane formation. For the membranes obtained using Y-channels, performance improved giving better quality membranes at high flow rates (about 2000 μl/min), and as flow rate increased, the structure of membranes become more continuous and thinner. The improvement with the quality of the membranes compared well with T-channels due to the orthogonal line of approach of the fluids in these structures. Higher flow rates lead to the reduction of the reaction zone; however the velocity

profile development then becomes non-uniform. The Y-shape structure, with an input angle of 45°, offers a smoother development of the velocity profile at the fluid interface, which results in a thinner membrane near the inlet. Again, as the flow rate increases, the reaction zone becomes even thinner, which facilitates the development of a smooth membrane [8].

In situ membrane formation by interfacial polymerisation constitutes a particular subset for fabrication that is operationally straightforward. Freger [14] used interfacial polymerization and Moorthy and Beebe [15] used emulsion photopolymerization. Song et al [16] incorporated acrylate in fused silica chips by laser induced phase separation polymerization. Hisamoto et al [17] incorporated nylon membranes by interfacial polymerization; hereby, two immiscible solvent flows containing the monomers came together, and the fast nylon polymerisation led to an intact barrier membrane. We have incorporated a similar nylon membrane into linear micro channels, and optimised both membrane formation and wall adherence through control of variables such as flow rate and the flow entry angle [8]. Because a homogeneous nylon layer is impermeable to all but gas molecules, we subsequently tried crosslinked bovine serum albumin (BSA) protein membranes through interfacial polymerization using a highly reactive acyl chloride bifunctional reagent; terephthaloyl chloride [9]. However, while the formed membrane was permeable to ammonia, it again proved relatively impermeable, assessed by optical tracking of the dye

molecules: phenolphthalein, permanganate, rhodamine B, Meldola Blue and Ponceau S. So for the purposes of achieving microsolute transport e.g., for nutrient delivery to cells, there was no advantage over nylon. Complementary to experimental work, mathematical models were reported of interfacial polymerization processes that led to thin films [18, 19], but did not allow for prediction of permeability.

In this study, another two different crosslinkers have also been used for forming the membranes, they are sebacoyl chloride and isophthaloyl dichloride. The effectiveness of the three acyl chloride crosslinkers have been compared, surface morphologies and cross section morphological structures of different crosslinked membranes has been studied, and a systematic, measurement of electroactive microsolute has been determined. Also, the thickness of membranes and growth rate vs. time has been determined.

Furthermore, a robust and novel variable porosity copper protein membrane has been achieved. Copper is one of the natural antimicrobial materials, known at least from the nineteenth century [20]. French and co-workers began synthesizing metal binding ligands as potential antitumor agents since the 1960s, during this research the metal complexes such as copper and iron showed strong cytotoxic [21]. In 1999 Nelson found that toxic metals can interact with DNA and proteins causing oxidative deterioration of biological macromolecules. Thus, the process of breakdown of metal-ion homeostasis has been involved in a

plethora of diseases [22, 23, 24]. In this study the copper binding crosslinked protein membranes was developed for antimicrobial utilization. Through microbial studies we can conclude the release of copper to produce some antibiotic activity. The porosity of the membrane can be controlled by exposed time in copper sulphate solution.

Moreover, crosslinked membranes have many uses but before a suitable application can be made the unknown mechanical properties need to be known so the material can be defined as to have it is different to other materials available for these applications. The mechanical properties of a material define its limitations and capabilities, without this information the reliability of the material is inaccurate or remains unknown.

In this study the membranes as an entire entity was studied and tested it as a material. Its mechanical properties gave it a measure of what the strength of the material made was which could give an indication as to how it compares with other materials. To test the mechanical properties of a membrane which is micrometers thick specialised methods have to be implemented. Nanoindentation has been a chosen method for membranes of similar dimensions. Through testing different protein membranes in different conditions sensible assumptions and conclusions can be made as to what mechanical properties the films possess. The mechanical properties of interest are modulus of elasticity (E), instantaneous shear modulus at zero time (G_0), the shear

modulus at infinity (G_∞) and the creep ratio (C_r). The data was critically analysed and conclusions made from this analysis.

Aim and Objectives

- Created practically useful crosslinked protein membranes.
- Controlled the permeability of protein membrane for different application.
- Characterization of crosslinked protein membranes with SEM, FTIR et.
- Tested the mechanical properties of protein membrane using nanoindentation method.
- Study the cells attachment to protein membranes.
- Prepare crosslinked protein membranes in micro-fluidic channels using interfacial crosslinking reaction.
- Permeability of these membranes was tested by diffusion studies using dye molecules as well as the electrochemically active compounds.

Chapter2: Literature Review

2.1 Protein membranes

Crosslinking of polymers have become a new, innovative way of producing membrane films; it has great interest for many reasons in various industries. Proteins are well known natural polymers so become an ideal material to crosslink. Albumin and fibrinogen are natural occurring proteins which have great interest in their role for different medical benefits. For example, albumin can be used for expanding blood plasma volume, significantly reduced the circulatory dysfunction that often occurs after large-volume paracentesis and also significantly reduced the occurrence of hyponatremia (low blood sodium levels) [25]. Fibrinogen concentrate was prescribed for acute bleeding episodes in patients with congenital fibrinogen deficiency [26].

2.1.1 Bovine serum albumin

Bovine serum albumin (BSA) is a large globular protein (66,000 Da) which constitutes 585 amino acids in one polypeptide chain [25], which primarily EXISTS in the α-helix form. Earlier publications on BSA structure by Hughes [26], Bloomfield [27] and Wright and Thompson [28] suggested the structure of BSA to be an oblate ellipsoid with dimensions of 140 × 40 Å. More recent experiments have continued to support these dimensions [29, 30]. However, a

study by Bos [31] indicated that BSA was heart-shaped showing as in Figure 2.1 [32]. This result was also suggested by Cater [33] using X-ray crystallographic data. Albumin is a highly abundant plasma protein with a concentration of 35 of 45 mg/mL. By binding to different solutes albumin can transport them around in the plasma; these materials include fatty acids, drugs bilirubin and metals [34]. This makes materials which would usually be insoluble in water able to be soluble while being bound to the albumin. As there are many functional groups along the polypeptide chain which are reactive, albumins can be manipulated into membranes or nano spheres. There has been an interest in albumin and it has been a common topic of research due to its ability to inhibit fibrinogen, platelet aggregation and adsorption, this makes albumin an ideal biomaterial coating candidate to enforce its blood compatibility [35].

The BSA molecule is made up of three homologous domains (I, II, III) which are divided into nine loops (L1-L9) by 17 disulphide bonds (see Figure 2.2). The structure of these nine loops comprises a series of residues as shown in table 2.1. BSA has an isoelectric point of 4.7 and so will carry a negative charge at pH 7.4 [36].

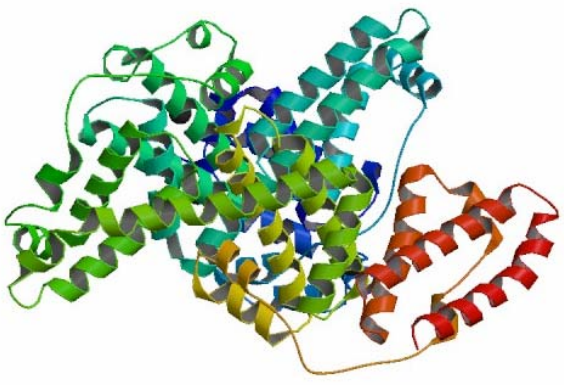

Figure 2.1 BSA molecule shape

Table 2.1 Amino acid composition of BSA [37, 38, 39, 40, 41]

Amino acid	Chemical formula	Number of units	Amino acid	Chemical formula	Number of unit
Ala	$C_3H_7NO_2$	48	Cys	$C_3H_7NO_2S$	35
Glu	$C_5H_9NO_4$	58	Phe	$C_9H_{11}NO_2$	30
His	$C_6H_9N_3O_2$	16	Gly	$C_2H_5NO_2$	17
Lys	$C_6H_{14}N_2O_2$	60	Leu	$C_6H_{13}NO_2$	65
Met	$C_5H_{11}NO_2S$	5	Asp	$C_4H_7NO_4$	14
Pro	$C_5H_9NO_2$	28	Arg	$C_6H_{14}N_4O_2$	26
Ser	$C_3H_7NO_3$	32	Thr	$C_4H_9NO_3$	34
Val	$C_5H_{11}NO_2$	38	Try	$C_9H_{11}NO_3$	21

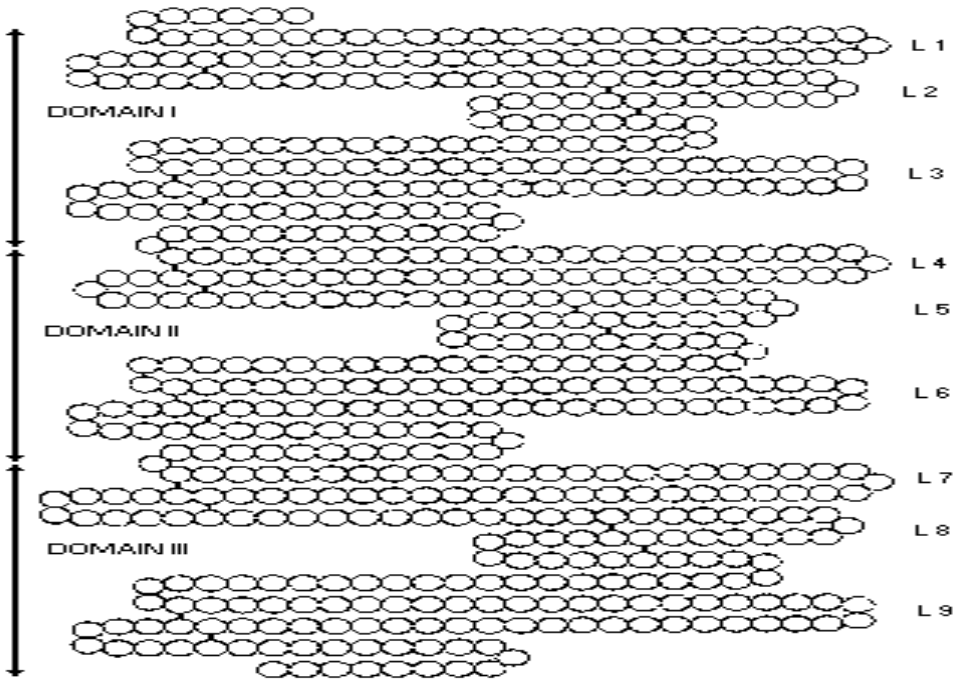

Figure 2.2 The molecule structure of bovine serum Albumin

2.1.2 Fibrinogen

Fibrinogen is a larger linear protein as shown in figure 2.3. It plays a central role in the mechanism of coagulation and thrombosis. The earliest publication a fibrinogen structure was written by Hall and Slayter [42]. Fibrinogen is a plasma protein which is water soluble, although it has been described as a member of the least soluble of the plasma proteins [43]. It has a high level presence in plasma, constituting to 200-450 mg/dl as around concentration [44, 45]. Much literature spanning many year has explored fibrinogen's structure and function [42, 46, 47]. It is a large protein (340,000 Da). Each subunit is an elongated molecule; the long axis is 47.5 nm±2.5. Fibrinogen also has a trinodular structure [49] (Figure 2.4, Domains D, E, D). The central module is 5 nm in diameter and another two nodules are 6.5nm in diameter, referred to as terminal domains. The primary sequence consist of three pairs of polypeptide chains Aα, Bß and γ, these are linked by 29 disulfide bonds. The structure of the Aα, Bß and γ chains of fibrinogen comprises various different amide acid residues, such as Lys, Arg, His, Asp and Glu. They carry different charges under different pH environments. pH 5.5 has been determined as the isoelectric point of bovine fibrinogen, so at pH 7.4 fibrinogen is negatively charged [48].

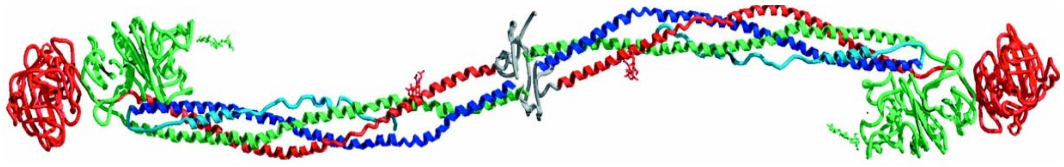

Figure2.3 Fibrinogen molecule shape [50，51]

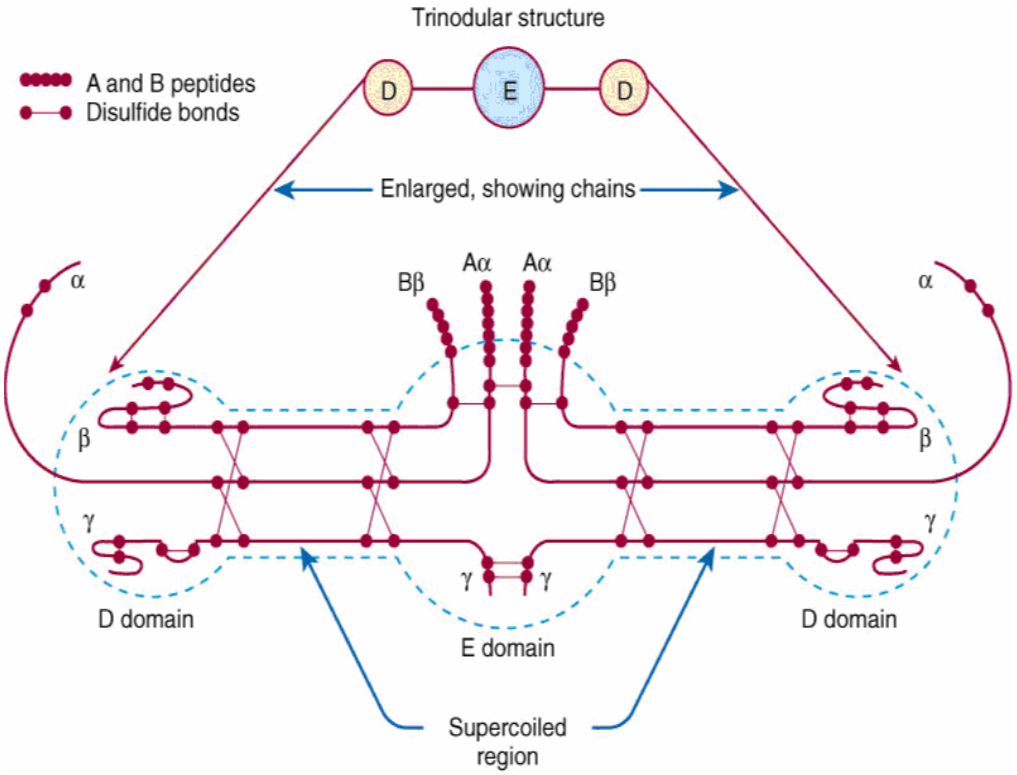

Figure 2.4 The structure of bovine serum fibrinogen

2.1.3 Protein – protein comparison

Fibrinogen is much larger than the globular protein albumin. Its mass is 273.5 kDa higher. Fibrinogen's shape had been described as rod-like [52]. This particular study investigated controlled protein adsorption and it concluded that both Albumin and fibrinogen's structure change more when being adsorbed at hydrophilic surfaces as compared with hydrophobic surfaces. This suggests that both these proteins form more stable when adsorption occurs with a surface which is hydrophobic. Also, in this study the denaturation of these proteins

where investigated, in relation to the curvature of a surface. Albumin was found to have greater stability than fibrinogen as small surfaces with high curvature values. The reasons for this were judged due to the structural differences between the proteins. Roach [52] suggested that the rod like shape of fibrinogen wraps around a smaller surface and therefore causing greater denaturation of the proteins structure.

2.1.4 Crosslinking agent

A crosslinked polymer is defined as a linear polymer system where formation of chemical bonds between the linear polymer chains has to infinite networks [53]. This is typically achieved by crosslinking groups, atoms or single bonds. This classification is commonly used when the crosslinks are significantly shorter than the chain parts in between the crosslinks. A popular way of crosslinking these linear polymers have been to incorporate into the polymer, a group which is eager to crosslink. This method could, eg, create free radicals attached to the linear polymer chain, and they could have the ability to crosslink [54].

The crosslinking are polymerisation of monomers alter chemical properties and develop new functionality. Some proteins or polymers would not be able to perform a function alone so in many cases the two materials complement one another creating a better material for a specific function. It is through

investigation into the possibilities of crosslinking, which allow new materials to be created. R.Arshady, explained that “mechanical strength, chemical strength and biodegradability can be controlled by crosslinking” [55]

Different crosslinking agents have been chosen to create solid protein membranes. An acid chloride is very reactive towards amino groups at room temperature. In this study terephthaloyl chloride and isophthaloyl chloride were used as crosslinking agents. Terephthaloyl chloride (TCL, 1, 4-benzenedicarbonyl chloride) and isophthaloyl chloride (IDCL) are acid chlorides with the chemical formula $C_8H_4Cl_2O_2$, the structure as shown in Figure 2.5. They are white crystalline solids at room temperature, soluble in organic solvents. TCL and IDCL are used as key agents for crosslinking polymers. The polymers that are crosslinked by TCL and IDCL can provide good chemical resistance, temperature stability, are light weight, and usually very high strength [56]. Sebacoyl chloride with the formula $C_{10}H_{16}Cl_2O_2$ is a light-yellow liquid with a pungent odor, soluble in hydrocarbons and ethers. It can be reacted with hexamethylenediamine, to give the crosslinked polymer, nylon-6,10. The structure is shown in Figure 2.5c. They all can be used to crosslinked with protein molecule. Further more after formation they are expected to provide different membrane morphology structure.

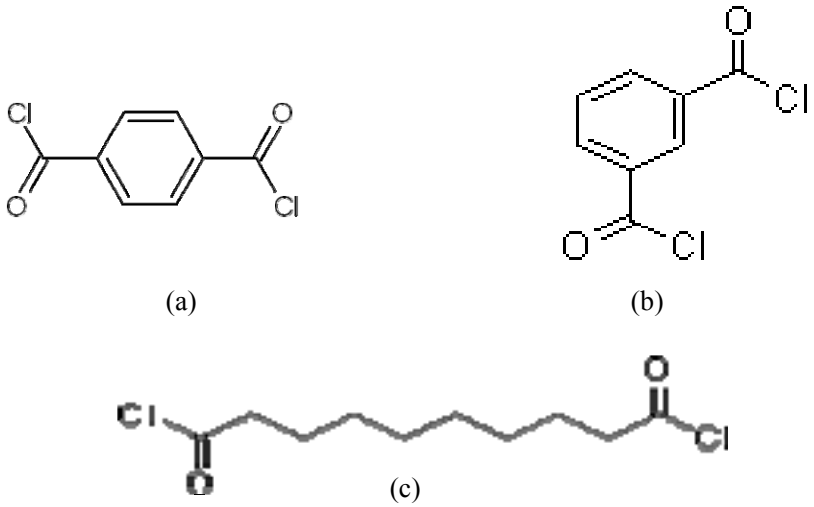

(a) (b)

(c)

Figure 2.5 Chemical structure of (a) terephthaloyl chloride, (b) isophthaloyl dichloride, (c) sebacoyl chloride

The reaction scheme for amino-based protein crosslinking with terephthaloyl chloride is shown in as scheme 1. The crosslinking reaction involves a nucleophilic substitution between protein and acid chloride, which includes a nucleophilic attack by the lone-pair electrons of the amino groups on the protein on the polarised carbon atom of acid chloride. The outcome is C=O double bond re-formation, chloride ion removal as well as the subtraction of hydrogen from the nitrogen, with hydrochloric acid as product.

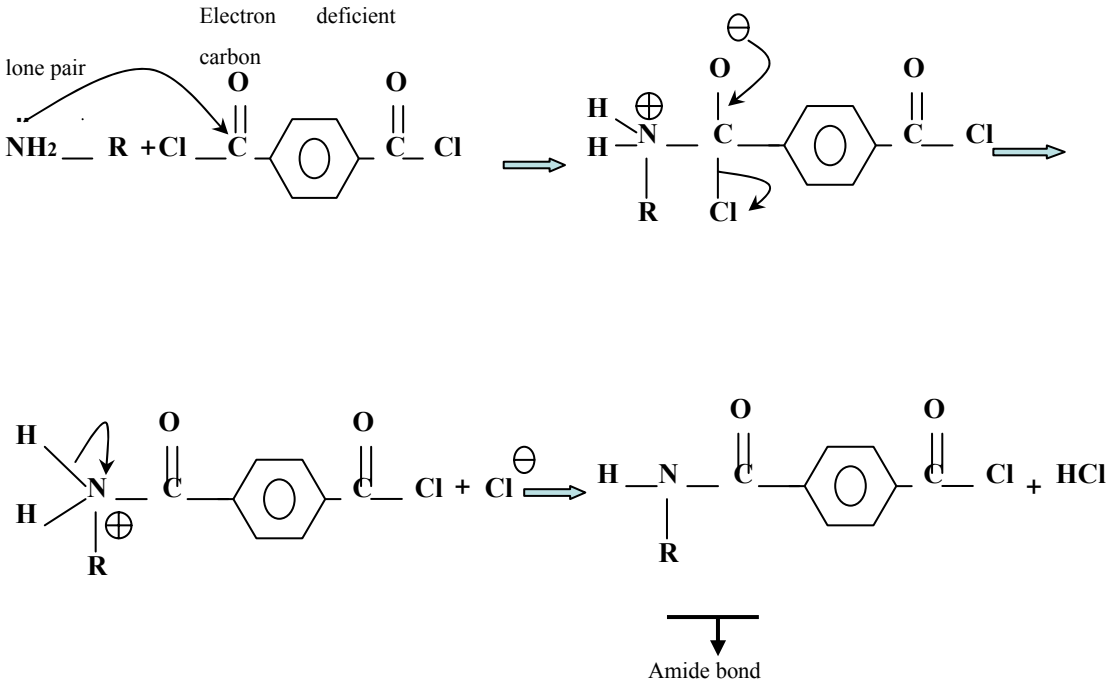

Scheme 1

2.2 Copper for protein membranes

2.2.1 History

Copper ions, either alone or in copper complexes, have been used to disinfect liquids, solids and human tissue for centuries. Today copper is used as a water purifier, fungicide, nematocide, molluscicide as well as an antibacterial and anti-fouling agent. Copper also displays potent anti-viral activity.

In the Smith Papyrus which is an Ancient Egyptian medical text and the oldest known surgical treatise on trauma. It describes the application of copper to

sterilize chest wounds and drinking water [57]. Greeks, Romans, Aztecs, and others also used copper or copper compounds for the treatment of such ailments as headaches, burns, intestinal worms, and ear infections and for hygiene in general [58]. In *1832* a *cholera epidemic* reached *France*, however, the copper workers appeared to be immune to cholera. In the 19th and early 20th centuries, the use of copper in medicine became widespread and a variety of inorganic copper preparations were used to treat chronic adenitis, eczema, impetigo, scrofulosis, tubercular infections, lupus, syphilis, anemia, chorea, and facial neuralgia [59]. The use of copper as an antimicrobial agent was not developed further after 1932, because the advent of commercially available antibiotics, copper is still a well known selfsanitizing agent. A 1983 report documenting the beneficial effects of using brass and bronze on doorknobs to prevent the spread of microbes in hospitals remained largely unnoticed [59]. Recently, copper vessels have been used to render water drinkable as a low-cost alternative for developing countries [60].

2.2.2 Antimicrobial property with copper

Copper is an essential element in most living organisms, and more than 30 types of copper-containing proteins are known today. Here are a few well-known examples lysyl oxidase, which is involved in the cross-linking of collagen, tyrosinase, required for melanin synthesis, dopamine-hydroxylase, which

functions in the catecholamine pathway, cytochrome *c* oxidase, the terminal electron acceptor of the respiratory chain, and superoxide dismutase, required for defense against oxidative damage.

In these enzymes, copper serves as an electron donor/ acceptor by alternating between the redox states Cu(I) and Cu(II) [61]. Other copper proteins, such as plastocyanins or azurins, act as electron carriers. Depending on the type of coordination of the copper to the protein, the redox potential of copper can vary over the range +200 mV to +800 mV. On the other hand, the redox properties of copper can also cause cellular damage. A number or mechanisms have been suggested. Reactive hydroxyl radicals can be generated in a Fenton- type reaction (scheme 2a). The extremely reactive hydroxyl radical can participate in a number of reactions detrimental to cellular molecules, such as the oxidation of proteins and lipids [62]. Copper ions can also lead to depletion of sulfhydryls, such as in cysteines or glutathione, in a cycle between reactions b and c in scheme 2:

$$Cu^{+} + H_2O_2 \longrightarrow Cu^{2+} + OH^{-} + OH^{-} \quad \text{(a)}$$

$$2\ Cu^{2+} + 2\ RSH \longrightarrow 2\ Cu^{+} + RSSR + 2H^{+} \quad \text{(b)}$$

$$2\ Cu^{+} + 2\ H^{+} + O_2 \longrightarrow 2\ Cu^{2+} + H_2O_2 \quad \text{(c)}$$

Scheme 2

The hydrogen peroxide thus generated can in turn participate in reaction (a) and lead to further generation of toxic hydroxyl radicals. It is still not clear to what

extent reactions (a) to (c) cause copper toxicity. Cells try to keep H_2O_2 at very low levels, and reaction (a) may not be the chief toxic mechanism, although this has been frequently claimed. An alternative route for copper ion toxicity is the displacement of iron from iron-sulfur clusters [63]. Similarly, copper ions may compete with zinc or other metal ions for important binding sites on proteins. The toxic effect of copper on microbes is utilized in agriculture for the control of bacterial and fungal diseases [64], which in fact led to the first thorough investigation of bacterial resistance to copper ions [65].

Bacteria evolved a range of mechanisms to protect themselves from the toxic effects of copper ions: extracellular sequestration of copper ions, relative impermeability of the outer and inner bacterial membranes to copper ions, metallothionein- like copper-scavenging proteins in the cytoplasm and periplasm, and active extrusion of copper from the cell. The latter appears to be the chief mechanism of copper tolerance in bacteria and has been extensively studied in Gram-positive and Gram-negative bacteria. In *Escherichia coli*, the CopA coppertransporting ATPase resides in the cytoplasmic membrane and pumps excess Cu(I) from the cytoplasm to the periplasm [66]. In the periplasmic space, the multicomponent copper efflux system CusCFBA and the multicopper oxidase CueO control the copper level and redox state, respectively. In addition to these chromosomally encoded systems, *E. coli* strains can harbor related, plasmid-encoded systems which further increase copper tolerance [67]. All the

components of this copper detoxification machinery are transcriptionally upregulated by copper via two regulatory circuits. In Gram-positive bacteria, which are devoid of a periplasmic space and an outer membrane, only CopA-type copper exporters are present and a single regulatory circuit usually controls their expression [68, 69]. A number of other components, like copper-binding proteins, copper reductases, etc., support these basic defense systems against copper and have been described elsewhere [71, 72, 73, 74].

In contrast to copper defense, copper utilization by bacteria is much less well understood. In synechocystis, it appears that a special copper uptake ATPase serves in supplying copper to the photosynthetic components in its thylakoid membranes [70]. On the other hand, methanotrophic bacteria that require copper for particulate methane monooxygenase secrete siderophore-like substances, the methanobactins, to scavenge extracellular copper [71]. In Gram-negative bacteria, such as *E. coli*, it is believed that the metalation of cuproenzymes takes place in the periplasmic space and does not require special copper uptake systems across the cytoplasmic membrane. Finally, many novel proteins of unknown function which are regulated by copper have been identified in the Gram-positive organism *Lactococcus lactis* [75], and further efforts will be required for an in-depth understanding of copper handling by bacteria.

2.2.3 Copper and membrane applications

Recently the potential for wide application of copper with membranes has been exampled are shown in table 2.2

Table 2.2 Applications of copper membrane

Ref.	Author (s)	Year	Materials and Method	Application
[76]	Matthew et al.	2011	Use copper-mediated synthesis to prepare 4-thiazolyl imidazole analogs	As an antibacterial template for Gram positive bacteria growth inhibition
[77]	Sun	2011	(-)-Epigallocatechin-3-gallate(EGCG)-Cu(II) complex electronspun into polyvinyl alcohol (PVA) nanofibers	The fibrous membrane has good antimicrobial activity. Cu(II) can increase the antimicrobial activity and stability of EGCG.
[78]	Sivakumar et al.	2011	Marine paint with $CuSO_4$	for decreasing the formation of marine biofilm.
[79]	Qiu	2011	immobilized copper (II) ions on the microporous polysulfone (PSF)+Poly(4-vinylpyridine) brushes membranes	Could serve as a good starting point for the fabrication of antibacterial membranes for waste-water treatment applications.

2.3 Nanoindentation

2.3.1 Basic principles

Nanoindentation is a form of mechanical testing done in the micro scale. It uses the elastic modulus of a known material (the indenter) to discover the properties of the material being tested which are unknown. The nanoindentation test pushes the indententor tip into the film; a measurement of load against displacement is recorded and plotted in a graph. The displacements of the indenter tip against the load being applied are the two factors which are incessantly being measured [80]. The nanoindentation test can be customised for the purpose of your unknown property such as the elastic modulus, stain-hardening effects or viscosity. In the case of brittle materials the fracture toughness can also be calculated [81].

2.3.2 Berkovich Indenter

This indenter shape is that of a 3-sided pyramid. The plastic depth of penetration is measured to determine the contact pressure [81]. This indenter appear has been used by Li and Chung [82] to test ultrahigh strength carbon nitrite thin films. The yield strength of these films was greater than 5 GPa which is more than for common metals or ceramics. The tip was focused to work well for a material with such high yield strength but was unsuitable for softer protein thin

membrane films.

2.3.3 Vickers Indenter

This indenter shape is a 4-sided pyramid. This tip is used to determine the Vickers diamond hardness; it relies on the impression's surface area as well as the load of the indenter [81]. Doerner and Nix [83] used a Vickers indenter for their depth sensing tests as a means to test the elastic and plastic properties of thin films. They used data from the loading curves to determine the hardness of the films by the load-displacement data minus the elastic load. The Young's modulus was calculated with the use of the linear portion of the unloading curve.

2.3.4 The Cube Corner indenter

Here the indenter shape is of a 3-sided pyramid with perpendicular sides. This is a good indenter for low load crack initiation. It has also been used in studies to create radial cracks in materials [82]. Zheng et al conducted nanoindentation fracture tests on $Pb(Zr_{0.52}Ti_{0.48})O_3$ ferroelectric films. The loads in this experiment went up to 300mN. Although they found that the theories made for the relationship between load and the radius of the indentation imprint only applied at smaller loads, they suggested this was the case because if the

indentation depth exceeded the thickness of thin films then the substrate would affected the results of the indentation [83].

2.3.5 Conical Indenter

The shape of the indenter is conical here with, axial symmetry. The depth of penetration here is measured from the outside surface of the circle in the cross-section [81]. Vella et al. investigated the mechanical properties and fracture toughness of organo-silicate glass. In this study the conical indenter was used to create “delamination blisters” which is the plastic region around the indent, this required forces of up to 600 mN [84]. The Young’s moduli of these low-k thin films were in the range of 6.90-11.7 GPa. The variation in porosity was suggested as the cause for the linear relationship between hardness and Young’s modulus of the films.

2.3.6 The Spherical Indenter

This indenter shape is spherical. It is known for its ability to transfer from elastic to elastic plastic contact with the materials surface. The depth of penetration here increases as strain increases [87].

Studies [88, 89] have shown that the spherical indenter can be used to measure the residual stress and yield strength. So it makes the tip able to accurately

determine the quantities for soft material [81].

The spherical indenter was known to be the ideal solution for linear viscoelastic materials. Despite alignment between the tip and the materials surface being an important factor when proceeding with a nanoindentation test, this tip is less delicate to the alignment [90], making it compatible to film surfaces which can be tempe ramental at the nanoscale.

The spherical indenter is most suitable to measure. For incompressible materials the shear modulus G is given by Bembey and Bushby [91]. Where P is the load, h is the displacement and R is the radius of the spherical tip.

$$G = \frac{3P}{16h^{\frac{3}{2}}\sqrt{R}}$$

Figure 2.6 shows a typical load-displacement curve for polymer film [91].

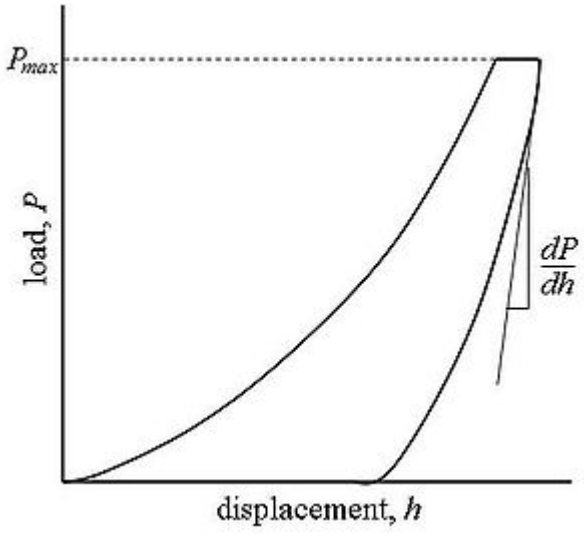

Figure 2.6: A typical load/displacement curve for polymer film

The coefficients G0 and Gi were obtained by the least-square curve fit from

experimental data. The shear modulus varies with time. The shear modulus at time zero G0 is given by [91], where C0 is creep constant and Ci is creep compliance coefficient

$$G_0 = \frac{1}{2(C_0 - \sum C_i)} (2)$$

Where the time approaches infinity (eg. 10 hours was considered to be infinity in the present work). The shear modulus $G\infty$ is calculate by

$$G\infty = \frac{1}{2C_0} \quad (3)$$

Thus, the creep ratio Cr is given by:

$$C_r = 1 - \frac{G\infty}{G_0} (4)$$

The creep ratio is an parameter/quantity that measures the elasticity /viscosity of materials. The value of Cr close to zero indicates strong elasticity of material while whereas the value of Cr close to 1 indicates strong viscosity of materials.

2.3.7 Uncertainty anlysis

Thermal drift

This can either be thermal drift from the material as plastic flow is a result of a load being held on a material or creep of the machine due to thermal changes.

Discrepancy in the initial penetration depth

If the indenter is not sufficiently contact to the sample material, this results in either failure of measurement or a larger discrepantly.

Instrument Compliance

If the machine has a discrepancy which does not allow correct measurements for the displacement of the indenter it can lead to false results

Surface roughness

If the film is not enough flat to be tested it can throw the indenter out of range and result in the test failing.

Results gained under these pretences will be disregarded on this basis.

2.4 Background of microfuidic

2.4.1 What is microfluidics

Microfluidic systems are miniaturized flow systems for chemical, biological, and medical applications. They normally have a cross-sectional dimension that is the order of 10-100 μm. These applications can be divided into four broad areas: miniaturized analytical systems, biomedical devices, tools for chemistry and biochemistry, and systems for fundamental research [1]. Therefore, microflidics are a central technology for a number of miniaturized systems. They offer the ability to work with smaller reagent volumes, because diffusion times can be short, microchannel, can provide shorter reaction times.

2.4.2 The *history* and *development* of microfluidics

The first microfluidic device was reported in the 1970s [3]. It was a miniaturized gas chromatography (GC) system, and was not developed further. With the growth of molecular biology, especially genomics, microfluidic system, have been found to be useful for the analysis of complex mixtures, especially DNA and proteins. From the 1990s the biomedical microelectromechanical systems (BioMEMs) were not only just concentrated in the academic area but also moved towards commercialization. For example, a MEMs-based DNA sequencer which can measure different complementary DNA sequences in order to detect the presence or significance of biomolecules and pathogens (Smart CyclerR) is currently being installed in post offices for Bio-agent detection [92] to detecte anthrax and other deadly pathogens. By the US. Postal Service intends to have Biohazard Detection System units installed at 283 mail-processing centers throughout the US. Bio-MEMS drug delivery systems are also used by many investigators and companies [93], and introduce systems that integrate silicon and electroactive polymer technologies for controlled delivery [94].

Most of the early systems were fabricated with silicon and glass. In the beginning these systems were developed for analyzing aqueous solutions [2]. Compared with glass, silicon is quite expensive, also it has a further disadvantage; it is opaque in the visible UV region of the spectrum, and so unsuitable for analysis of that need optical detection. Glass has the advantage of being optically transparent.

Normally both these materials can be manufactured with an etch method, following by sealing which generally requires a clean-room environment. However, many biomedical devices require to be made of soft materials that can conform to smooth, non-linear surfaces. Patients may prefer them to other materials due to their comfort and resistance to fracture. There are many polymeric materials that are suitable such as silicone rubber, isobornyl acrylate, and polyimide [7]. Polymers can provide an advantage as soften interface with biological tissue. Also, polymers can be made in relatively tough, glassy states or in a soft, rubbery, state. Finally, most polymers are low cost. However, the disadvantages of polymers are that some are incompatible with organic solvents and high temperatures. Recently polymer microfluidics systems made of Poly (dimethylsiloxane) (PDMS) [95] have been reported. PDMS is an excellent material for fabricating microchannel systems. The polymer can be cured at low temperatures, it is optically transparent down to 280 nm; it can handle most of organic solvents and non-toxic.

2.4.3 Fluid physics at the microliter scale

Reynolds number

In contrast to a macro- system, microfluidics allows for new flow functionality with a fundamental shift in fluid handling, based on the dominance of viscous *vs* inertial flow effects, i.e., the low Reynolds number regimen [2]. The Reynolds

number can be calculated by

$$R = \frac{\rho V D}{\mu} \quad (1)$$

Where ρ is the fluid density, v is the characteristic velocity of the fluid, V is the fluid viscosity and *D* is the hydraulic diameter. The hydraulic diameter is a computed value that depends on the channel's cross-sectional geometry.

Re number < 2300, as calculated by the above formula, generally indicates laminar flow. As Re approaches 2300, the fluid begins to show signs of turbulence, and as Re becomes greater than 2300, flow is considered to be turbulent. The literature reports that the Re for transition from laminar to turbulent in microfluidic channels might be different than that predicted by theory.

Laminar flow

Laminar flow is a particular flow feature, and is a condition in which the velocity of a particle in a fluid stream is not treated in 3D space as a random function of time. It also permits more predictable and uniform solute exchange along the laminar flow axis driven by Fickian diffusion alone. So two or more distinct fluid streams moving in the same capillary at low Re do not develop turbulence at the interface between them or at the interface with the capillary wall, the only mechanism of mixing of their components is diffusion across the former

liquid-liquid interface [1]. Because of the small size of microchannels, flow is almost always laminar (a compliance with Re number data).

Diffusion

Diffusion is the process by which a concentrated group of particles in a volume spread out over time by Brownian motion, so that the average concentration of particles throughout the volume is become constant. Diffusion can be modelled in one dimension by the equation

$$d^2 = 2Dt \quad (2)$$

where d is the distance a particle moves in a time t, and D is the diffusion coefficient of the particle. During the analytical process, with small sample volumes the mass transfer is very fast in microfluidics systems. Diffusion time varies with the square of diffusion distance, so when diffusion distance is reduced one order of magnitude, diffusion time is reduced two orders of magnitude Diffusion for a solute of concentration C through a membrane follows Fick's Second Law

$$\frac{\partial \phi}{\partial t} = D\frac{\partial^2 \phi}{\partial x^2} \quad (3)$$

where D is the diffusion coefficient for the solute in the film, t is time, x is the spatial coordinate and ϕ is concentration.

2.4.4 Applications of microfluidic devices

Microfluidic devices can provide technological advantages such as small sample volume, associated short diffusion distances. The decrease in the amount of the sample volum leads to cost reduction.

Controlled laminar flow in microfluidic devices has been utilised to great benefit in a number of industrial applications including diffusion-based separation. Diffusivity increases as particle size decreases, according to equation 3 a larger particle will take more time in this way to diffuse same distance than a smaller particle. Thus particles have been separated by diffusion according to their size.

Since the 1970s, microfluidics have experienced additional developments, with new specialist applications emerging, such as microfluidics incorporated materials for application in tissue engineering and drug delivery [94]. The potential for the wide application of microfluidic systems is high lighted in Table 2.3.

Table 2.3 Applications of Microfluidic Devices

Area	Application
Systems to analysis small amounts of sample	Detection of living single molecules
Small-scale organic synthesis	Combinatorial synthesis[96]
Study the flow of fluids	Studies laminar flow in small channels [97] Studies of diffusion
Biomimetic systems	Development of mimic biological functions [94]
Sample preparation	Purification of biological samples for further analysis[98]
Biomedical devices	Drug delivery, use for cellomics [94]
Miniaturized analytical systems	Analysis sample of blood or interstitial fluids
Genomics and proteomics	Rapid, high density sequencing [99, 100], combinatiorial analysis, forensics
Clinical analysis	Rapid analysis of blood or interstitial fluids, Point of care diagnostics based on immunological [101, 102] or enzymatic assays [103], electrochemical detection.
Environmental testing	*In situ* analysis of environmental contamination[104]

2.4.5 Fabrication techniques

Most fabrication techniques use well understood methods for processing. A clear understanding of the different types of basic microfabrication is important for anyone working in the microfluidic area. Over the last few years, various different types of techniques have been used to fabricate microfluidic structures. Outlined below are the major methods used in the manufacturing of microstructures. Their structures are based on:

(1) Thin-film deposition, which can be used for masking, isolation, and structural purposes. The deposition of a thin-film can be achieved by various chemical or physical techniques.

(2) Lithography, which can be used for transferring a designed pattern on to a certain substrate.

(3) Etching which is the method for forming the channel. A patterned substrate can be etched by using different chemicals and agents in the gas phase.

Additionally, substrate bonding, during the microchip manufacturer is an important part of creative research systems, and can be used for surface change and packaging purposes, for example an etched substrate can be bonded with another substrate piece as the final step in making a microfluidics device. Also, bonding can be used for introducing different multiple functionalities for example, by bonding several pieces of substrates for multiple, different channels.

These steps can be repeated several times depending on the design of the microfluidic system and the manufacture process [102]. The details of the different techniques are as follows.

Thin-film deposition

Oxidation of the substrate is one of the main thin-film deposition techniques. This technique is a simple process which is normally used to deposit thin films for semiconductor substrates. This process is naturally limited to materials that can be oxidized, and it can only form films that are oxides of that material. The process consists of heating the substrate to the temperatures ranging from 800 to 1200 ^{o}C in an atmosphere containing O_2 or H_2O vapour. Film growth is actually downwards into the substrate. The thin film which is produced by this method normally has high quality. For example, if the substrate is silicon, a smooth SiO_2 thin film will be deposed on the surface.

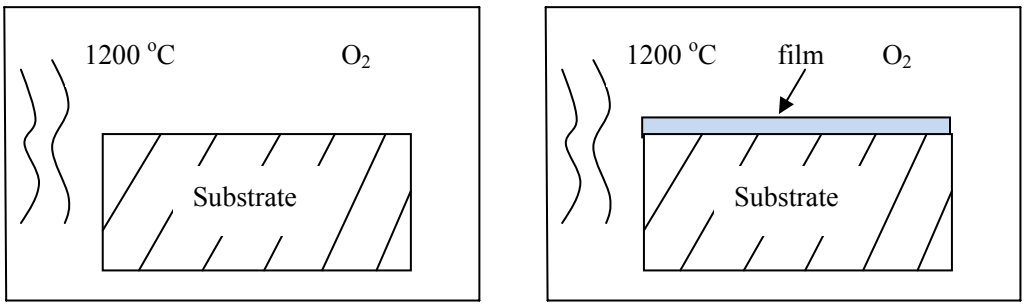

Figure 2.7 Schematic drawing of the oxidation of the substrate step

Chemical vapour deposition (CVD) involves using a chemical reaction from the

gas phase to form a thin film. There are two common techniques used in CVD, Low Pressure CVD and Plasma enhanced CVD. These methods are typically used to deposit inorganic materials such as silicon dioxide, silicon nitride, and polycrystalline silicon (polysilicon).

Low pressure CVD is performed at pressures ranging from 0.1 to 1 Torr and temperatures with the range of 550-900 ^{o}C and the films are usually very conformal to the substrate surface. The main problems with the process are the high deposition temperature (higher than 600°C) and the relatively slow deposition rate. Plasma enhanced CVD however, uses plasma, and has the advantage that it requires much lower temperatures, but the disadvantage is that the films obtained do not always fit the substrate's surface and can be poor quality.

Bonding techniques

During microfluidic device fabrication, bonding techniques can be used to form a channel and as a part of the final microsystem packaging. The earliest technique for making microfluidics is anodic bonding which bonds glass or silicon wafers together at 400 ^{o}C using a high electrical field (1 kV in voltage) [105].

Bonding starts immediately after the voltage and heating has been applied. During this period, ions in the substrate migrate to the cathode and form a depletion layer at the interface. The substrates are contacted together by a

resulting electrostatic force. This electrostatic force results in intimate contact at the interface creating conditions suitable for covalent silicon-oxygen bonds at substrates interface. However, the precise chemistry underlying anodic bonding has not yet been discovered. Figure 2.8 shows a schematic diagram of the bonding setup.

Another important bonding technique is silicon–silicon fusion (or silicon direct bonding) [106]. This technique is used to bond two silicon wafers with or without oxide layer. First the silicon wafers are cleaned thoroughly, to remove all the dust and organic particle. The surfaces are rendered hydrophilic by hydroxylation in HF or boiling in nitric acid. This results in the formation of surface silanosl (-SiOH).

The wafers are then brought together, with high compression force starting from the centre to avoid air remaining between the two wafers. Initially, van der Waals forces keep the surfaces together. On close apposition, hydrogen bonds are formed at the two surfaces as resulting the hydroxylation, causing the substrates to join at an atomic scale. This reaction can happen at room temperature. However, a high temperature annealing (800–1200 ˚C) can be used for increasing the bond strength. It is presumed that an Si–O–Si bridging bond is formed between the surfaces and that a water molecule is liberated as a result.

In addition to the above mentioned techniques, several alternative methods can

be used such as eutectic and a glass frit [107] which uses an intermediate layer. Also, a UV-curable adhesive can be used instead of high temperature bonding of glass –glass substrates.

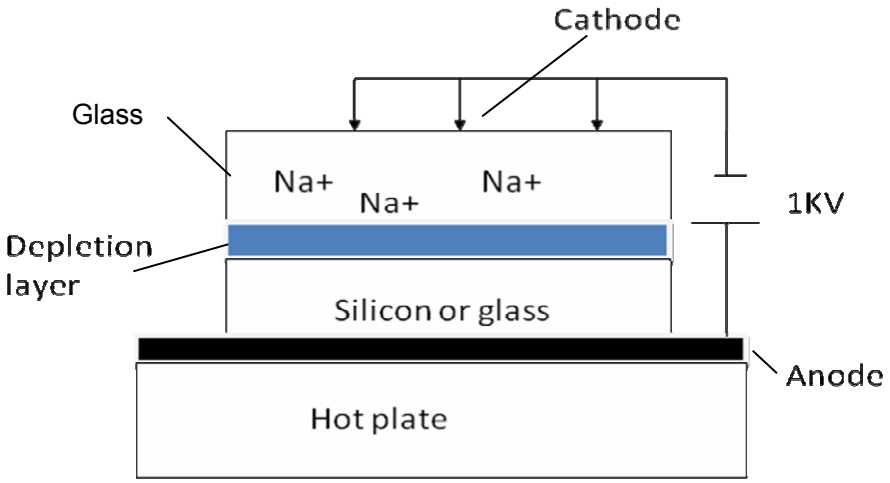

Figure 2.8 Glass to silicon anodic bonding setup

Photolithography

Photolithography uses a photosensitive emulsion layer knows as a resist. Different chemicals may be used for giving the materials the desired property, such as Poly(methyl methacrylate) (PMMA) [109], poly(methyl glutarimide) (PMGI) [110], Phenol Formaldehyde resin (DNQ/Novolac) and SU-8 [109], they are all applied as a liquid . There is another kind of material knows as photo resist dry film. The coating exists as a uniform, semi-solid film coated onto a polyester substrate and the user applies that substrate to the work piece by

lamination.

Computer graphics are used to create a photo mask for a specific design. This is then used to transfer a pattern to a substrate (glass, silicon, etc). This process starts with deposition of material on the substrate followed by spin-coating the photosensitive resist material on top of the substrate (if a dry film is used, the film needs to be deposited on the substrate by lamination). The thickness of the film is typically in the range of 0.5–2.5 um, and depends on the spin speed and the viscosity of the resist. A soft bake (2–10 min at 95–115 ˚C) process is carried on in order to improve adhesion and removes solvents from the resist. Then the resist layer is exposed to UV source; this transfers the pattern from the mask on to the photo resist layer by changing the initial properties due to curing of polymer in the area exposed. For example, SU-8 (Fig. 2.9) is a commonly used epoxy-based negative photoresist. When exposed with UV light, SU-8's long molecular chains cross-link causing the solidification of the material.

Then, development process involves washing off of either UV exposed area or unexposed area. This step is strongly influenced by nature of the photo resist material which can be positive or negative showing as Figure 2.10. Finally, the resist is hard-baked (20–30 min at 120–180 ˚C) in order to further improve the adhesion. The pattern is created on the substrates [111].

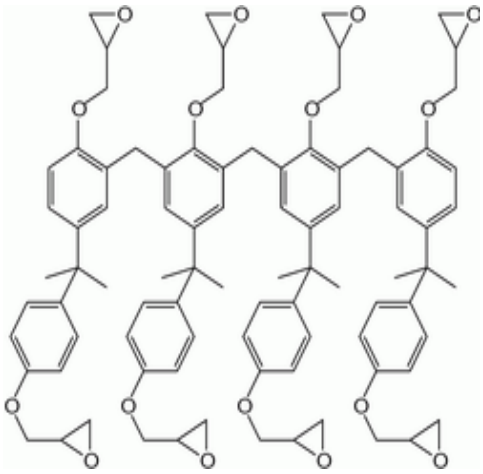

Figure 2.9 SU-8 molecule structures (Sigma Aldrich Co.)

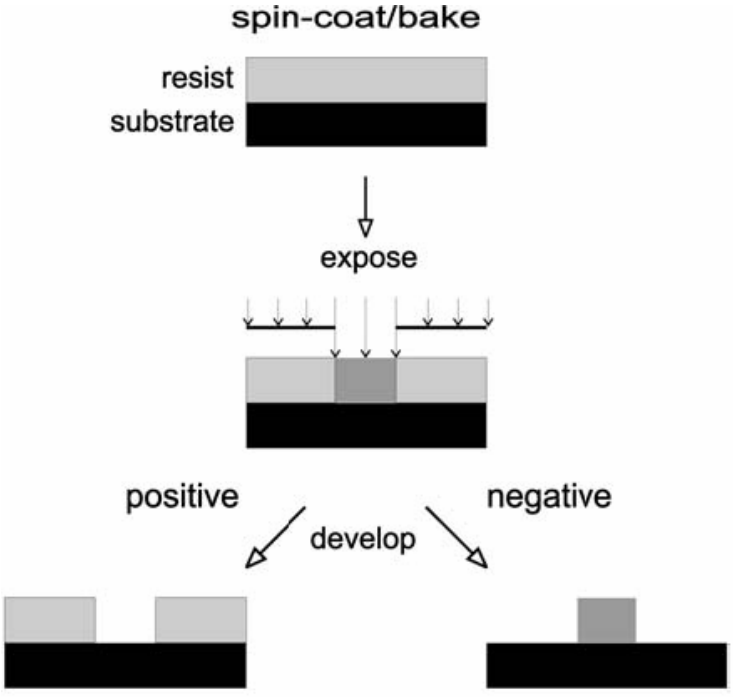

Figure 2.10 Schematic representation of the fabrication process to obtain masters employed in soft-lithography

PDMS

Polydimethylsiloxane (PDMS) is a well used and understood material for

fabricating microfluidic systems, which has known sealing and biocompatibility properties [95]. It is also known as silicone rubber. The structure of PDMS shown in figure 4 is stable due to the methyl groups attached the silicon. In addition, it can be easily chemically bonded to itself, and multilayer structures can be fabricated in this way. Finally, elastic PDMS films can be achieved.

The fabrication process for the PDMS microfluidic can be divided into two main steps:

- Mould fabrication and preparation: a photomask is used to produce a positive relief on a silicon wafer using a positive photoresist. This is known as the ‘master mould’.
- PDMS casting: The prepolymer (may need to perform under vacuum to remove air bubbles) is poured over the mould to generate negative replicas in PDMS. The mould can be used repeater, which reduces costs.

PDMS can adhere to different kind of materials such as itself, glass, and silicon nitride. Using PDMS microfluidics can save fabrication time in long term research compare with glass microfluidic systems. Once the mould is ready, a few PDMS microfluidic structures can be added together by simply pouring the prepolymer in the mould and generating the final structure.

.

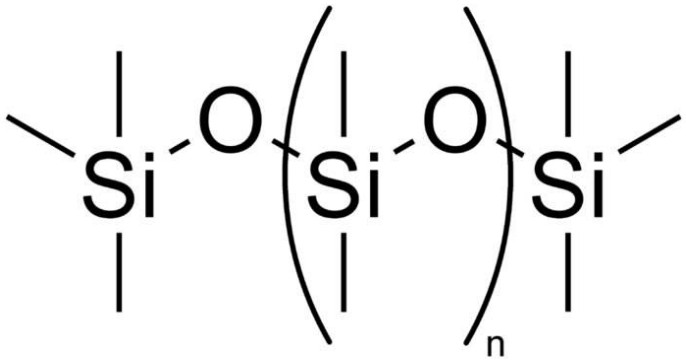

Figure 2.11 Chemical structure of PDMS [95]

Etching techniques

Etching techniques can also be divided into “wet” and “dry” forms [112]. Wet etching can achieve more material selectivity than dry techniques. However, the lateral undercutting involved in wet isotropic etching limits the features to greater than 3μm. The three most important anisotropic silicon etchants are potassium hydroxide (KOH), ethylene diamine pyrochatechol (EDP) and tetramethyl ammonium hydroxide (TMAH). These etchants attack silicon along preferred crystallographic directions. In addition, they all show a marked reduction in the etch rate.

Etching techniques can be employed to make patterned films or removal of selective materials from the substrate. The two important parameters of an etching process are selectivity and directionality [113].

Selectivity is related to the degree to which the etchant can differentiate between the masking material and the material to be etched. Directionality is a function of etch profile under the mask. In an isotropic etch, the cross-section of the channel is shows a semi-circular profile. This is due to attack by the etchant material from top to bottom at the same rate. In an anisotropic etch, the cross-section of the channel normally shows non-circular or totally straight sidewalls profile, this is as a result of the etchant in removing material specific orthogonal direction.

2.5 Membrane technology

Membrane science and technology is a broad and highly interdisciplinary field, where process engineering, material science and chemistry meet. The interfaces of these fields offer many opportunities [98]. Furthermore, biocompatible or biodegradable membranes can be used as cell culture supports for tissue engineering. Membranes also provide a large internal surface area that can be used effectively for the adsorption of solutes. Also, the use of membranes in microfluidics has been a topic of growing interest. Some applications are showing as below (table 2.4)

Table 2.4 application of membrane in microfluidics

Ref.	Author (s)	Year	Membrane in Microfluidics	Major focus/area of author(s) study	Application
[112]	Inamdar Niraj K. et al.	2011	Microfluidic device been separated by the porous membrane (PDMS). the upper channel used for high flow rate, cells culture in the lower channel	Cell culture	Controlling gradients of oxygen and other soluble factors and hemodynamic shear forces in the culture of mesenchymal stem cells
[113]	Liu Changchun	2011	A hydrophobic, porous membrane as debubbler with microfluidic systems made with plastic	Micro filter	Removing bubbles from the flow stream.
[114]	Srigunapalan Suthan et al.	2011	A porous polyethylene terephthalate(PET) membrane sandwiched between two PDMS microchannels.	Clinical analysis	This microfluidic platform can be used to study complex cell-matrix and cell-cell interactions in environments that mimic those in native and tissue engineered blood vessels, and offers the

					potential for parallelization and increased throughput over conventional macroscale systems
[115]	Luo Xiaolong	2010	The microchannels were fabricated with PDMS, Chitosan molecules were deprotonated at the flow interface to form a solid freestanding chitosan membrane.	Biofabrication	Biochemical, bioanalytical, biosensing applications and cellular studies
[116]	Lu Yao	2010	paper-based microfluidic devices in nitrocellulose membrane by wax printing	Biofabrication	protein immobilization related applications

2.5.1 Fabrication membranes in microfluidics

A rough division into four different approaches can be made for membrane microfluidics.

Direct incorporation of membranes

This is the most straightforward way to fabricate a membrane into microchannel. The whole system can be achieved just simply by clamping or gluing of

membrane [119]. The advantages of this method are the simplicity of the process and the wide choice of different type of membranes. The membrane can be purchased from a commercial supplier. Different membranes have been chosen, depending on the application of the microfluidics device. For example, for sample filtration, porous membranes are applied as barriers and transport occurs by a pressure difference [120]. Many gas sensors are based on the dissolution of gas in an analysis liquid, so here the membranes serve as efficient gas-liquid contactors. A high gas permeability polymer such as PDMS can be exploited as a membrane in a microfludics device [39]. But the major problem with direct incorporation of membranes is the sealing step. During adhesive step, due to capillary forces, and hence fluids can easily get sucked in, the whole system can then be complete in blocked.

Membrane preparation as part of the chip fabrication process

This method can be achieved in several ways, such as production of sieves with well-defined pores by etching [121], Preparation of polymeric membranes by casting [122], creation of pores by ion track technology and photo polymerization of ion-permeable hydrogels[123].

The membrane in microfluidics fabricate with this method normally with good control over feature sizes, and good sealing of the membrane. The disadvantages of these technologies in general are the complexity of the production process

with different equipments, and related to this, the high price.

Use of membrane properties of the chip material

This method is quite simple, since no additional fabrication steps are required, just to choose a chip material that has the required membrane properties itself. Normally, the materials required are polymer. When a polymer solution is phase separated on a microstructured mould, a membrane is formed with an inverse replication of the mould features [120]. The membranes with channel networks can be produced in the lateral direction by using rigs on a mould. The disadvantage of this technology is the limited choice of materials, only several polymers can be used, such as polyimides and PDMS. Also with these polymers it is difficult to change the porosity of the membrane limited the application of the microfluidics system.

In situ preparation of membranes

There is a more convenient method can be used for forming polymer membrane within microfluidics. It is interface reaction. Recently Hisamoto et al., [6] successfully demonstrated that highly efficient molecular transport between two phases for analytical and synthetic applications was achievable using aqueous/organic multilayer flows. They utilised the principle of laminar flow to generate polymer membranes within the channel via an interfacial reaction. Based on these ideas, the microfluidics platform in this current work was

fabricated first, then two immiscible liquid flows were designed to be injected in the microchannel at the same time. A liquid–liquid interface can be formed within a short time, based on the controlled laminar flows of two immiscible solutions. This liquid wall was usable for interfacial polymerization. The polymerization reaction (Scheme 1) involved nucloephilic attack at the acyl chloride by a lone pair of electrons at the nitrogen atoms in proteins eventually leading to crosslinking.

By this method a thin membrane was formed along the length of the microchannel. This process was completed rapidly and many different applications can be targeted, simply by changing to different solutions to form different *in situ* protein membranes.

2.6 Diffusion study

2.6.1 Diffusion coefficient correlates of membrane protein

Diffusion at a porous membrane is governed by membrane morphology, and includes parameters such as surface and volume porosity, pore size distribution and pore tortuosity [124]. These micro-structural parameters are not easy to measure accurately, and in any case cannot quantitatively define, or predict final mass transport behaviour through a membrane. A simple defining characteristic

of a membrane is its solute molecular weight cut off, set as the molecular weight at which 90% [125] of a solute is rejected; again this would be difficult to predict on the basis of morphology. However, measurement of diffusion coefficient would be the best functional characteristic to use for membrane porosity.

The diffusion coefficients of model solutes through protein membranes were determined by fitting simulated amperometric sensor current responses at membrane covered electrodes to experimental data following a step change in diffusant concentration. A typical fit of hydrogen peroxide diffusion through a crosslinked fibrinogen membrane is shown in Figure 18. The coefficient of variation (C.V.) for the curve in Figure 18 is in fact 1%. This was typical for the estimations of membrane permeability. Moreover, the closeness of fit to the Fick's model for diffusion across the time series can be ascertained by the closeness of fit to the experimental curve. The method thus gives an exceptionally precise, and readily validated, measure of diffusion coefficient. Any differences in measured diffusion coefficients are, therefore, likely to be related to either the reproducibility of the sensor based method or to differences between membranes as shown Table (4). The variation in measurements for single membrane locations is within 30% C.V., and allows a valid comparison across the solute range.

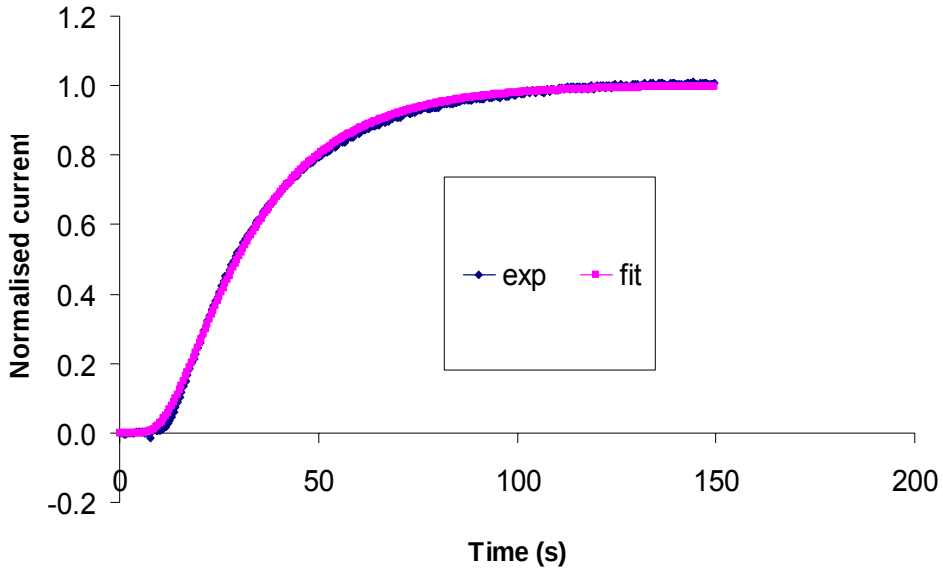

Figure 2.12 Normalised experimental (solid diamond blue) and simulated (solid square pink) transient amperometric currents for hydrogen peroxide diffusion through a crosslinked fibrinogen membrane.

2.6.2 Chemical compounds for diffusion studies

Ponceau S

The molecular weight of Ponceau S is 673 (as show in Fig. 2.13). The molecule structure shows ponceau S would be negative charged. The pKa of Ponceau S in H_2O_2 is about -2 (H_2SO_4 is about -3). **(** from Bordwell pKa Table)

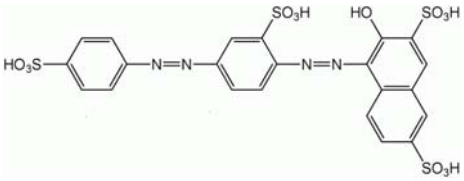

Figure 2.13 The structure of Ponceau S

Meldola blue

The molecular weight of Meldola blue is 277, the structure is shown in Figure 2.14. It is neutered at pH7.4 and a positively charged ion in solutions which of less than pH7.4 [126].

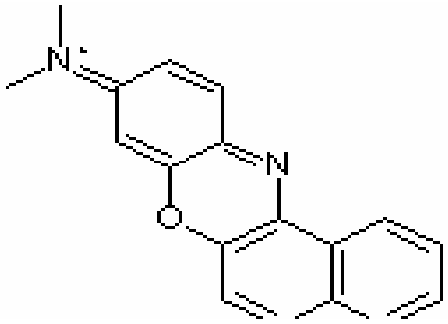

Figure 2.14 Structure of meldola blue

Catechol

Catechol, also known as pyrocatechol or 1,2-dihydroxybenzene, is an organic compound with the molecular formula $C_6H_4(OH)_2$. It is the *ortho* isomer of the three isomeric benzenediols. This colorless compound occurs naturally in trace amounts.

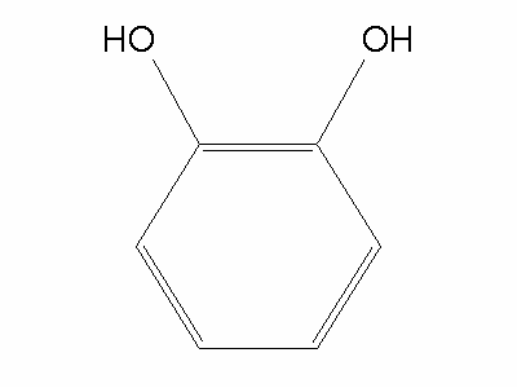

Figure 2.15 Structure of Catechol

In the presence of oxygen, the catalytic reaction of catechol is as scheme 2 [127]. The generated *o*-quinone is then reduced at the electrode. The generated *o*-quinone is then reduced at the electrode. In our study, the response current of the sensor is detected by the amperometric method during the reduction of *o*-quinone.

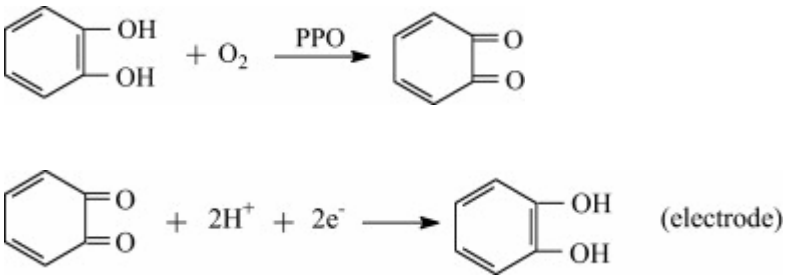

Scheme 3

Acetaminophen

Acetaminophen (ACAP), also known asN-acetyl-p-aminophenolor paracetamol, is an effective analgesic and antipyretic drug with rather limited anti-inflammatory properties. This substance is commonly used for relieving

mild to moderate pain associated with headache, backache, arthritis and postoperative pain, and is used universally for reducing fevers of bacterial or viral origin [128], have used electrochemical detection to overcome these difficulties, which have proven to be promising detection for ACAP because of its electroactivity at solid electrodes.

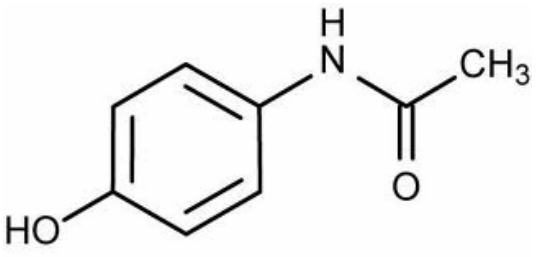

Figure 2.16 Structure of acetaminophen

According to previous reports, oxidation of ACAP at bare GCE is an irreversible reaction, involving a two-electron and two-proton transfer process to produce the unstable, oxidized product N-acetyl-p-quinoneimine (NAPQI) as shown in scheme 3. The hydrolysis of NAPQI is then reduced at the electrode [129, 130].

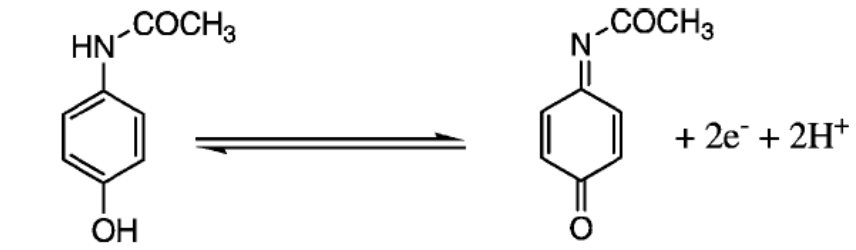

Scheme 4

acetaminophen (ACAP)

N-acetyl-*p*-quinoneimine (NAPQI)

Hydrogen peroxide

Hydrogen peroxide (H_2O_2) is the simplest peroxide (a compound with an oxygen-oxygen single bond) showing as figure. It is also a strong oxidizer. Hydrogen peroxide is a clear liquid, slightly more viscous than water. In dilute solution, it appears colorless.

Hydrogen peroxide is an electroactivity chemichal compounds, it is known as the final product of glucose electron reaction based on the following principle:

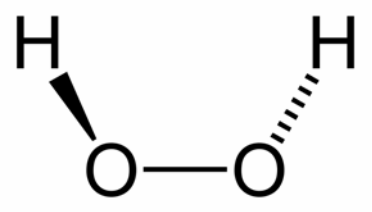

Figure 2.17 Structure of Hydrogen peroxide

$$\text{Glucose} + O_2 \xrightarrow{GOD} \text{Gluconic acid} + H_2O_2$$ **Scheme 5**

Diffusion of H2O2 from bulk to the electrode surface (step a) followed by electron transfer steps (reactions b and d) is expected to result in the amperometric method [131].

(a) H_2O_2 (bulk) → H_2O_2 (surface)

(b) H_2O_2 (surface) + e^- → O_{Had} + OH^-

(c) OH^- + H^+ → H_2O **Scheme 6**

(d) O_{Had} + e^- → OH^-

(e) O_{Had} + H^+ + e^- → H_2O.

Chapter3: Experimental Procedure

3.1 Solution preparation

3.1.1 Phosphate buffer saline (PBS)

The composition of the phosphate buffer saline (PBS) was 52.8 mM Na_2HPO_4 (BDH, Dorset, UK), 15.6 mM NaH_2PO_4 (BDH, Dorset, UK) and 5.1 mM NaCl (Sigma, Dorset, UK). In a 50.00ml volumetric flask, all the materials were added with distilled water and the solution stirred until dissolved. For changing the pH value of the buffer solution for the pH studies, an addition of 5 M phosphoric acid was used to adjust pH to 6 and an addition of 5 M NaOH was used to adjust pH to 9, respectively.

3.1.2 Protein solution

3.1.2.1 Bovine serum albumin (BSA)

To make 20 wt% of BSA solution, 1.25g of BSA (Fraction V-initial fraction by heat shock treatment) was purchased from Sigma Aldrich UK mixed with 5ml of PBS. The solution was left in a clean room at room temperature (23 ºC) without stirring for 4 hours giving the solution time to mix thoroughly.

3.1.2.2 Fibrinogen solution (different pH)

To make 3.8 wt% of fibrinogen solution, 0.2g of fibrinogen was purchased from Sigma Aldrich UK mixes with 5ml of PBS. The solution was left in a clean room without stirring for 4 hours giving it time to mix thoroughly.

Table 3.1 Fibrinogen dissolved in PBS at different pH

Membrane	Solvent	dissolved temperature
pH6	pH6 PBS	23˚C
pH7.4	pH7.4 PBS	23˚C
pH9	pH9 PBS	23˚C

3.1.2.3 BSA ethanol solution preparation

20 wt. % BSA solutions were prepared using PBS followed by careful addition of 5, 10 and 15 v/v % ethanol (97.7% w/v) to BSA solutions to determine the optimal processing concentration. Solutions were mechanically stirred for 2 hours at ambient temperature (23 °C).

3.1.3 Crosslinker solution

Terephthaloyl chloride (TCL), isophthaloyl dichloride (IDCL), sebacoyl chloride (SCL) and distilled xylene were purchased from Sigma Aldrich UK. TCL, IDCL and SCL (1 wt. %) cross-linking agent was dissolved in xylene, and stirred for 2 hours at room temperature in a sealed container.

3.1.4 Other solutions

3.1.4.1 Copper Sulphate solution

1 g of copper sulphate (Sigma, Dorset, UK) powder was dissolved in distilled water, and stirred until the solution mixed thoroughly.

3.1.4.2 analyte stock solutions

Dye diffusion

Ponceau S and Meldola Blue were prepared using pH 7.4 PBS with concentrations of 0.04 wt%.

Electrochemical diffusion study

Different chemical compounds showed different microsolute transport and diffusivity through membranes such as crosslinked BSA and crosslinked fibrinogen. In the present case, a range of chemical compounds: 4-acetaminophenol (MW 151), catechol (MW 110) and hydrogen peroxide (MW 34) were selected to give a rage of molecular weight diffusants.

4-Acetaminophenol, Catechol and Hydrogen Peroxide were purchased from Sigma Aldrich. Solutions were prepared using pH 7.4 PBS to give concentrations of 0.1 M as stock solutions.

3.2 Membrane preparation

3.2.1 Experimental procedure for forming large surface protein membranes

Figure 3.1 shows the vessel used for membrane formation. The protein solution was first introduced into the beaker, and subsequently, xylene with crosslinking agent (TCL, IDCL, SCL) was carefully layering over the aqueous phase; xylene has a low specific gravity (SG ~ 0.87). An immediate, opaque, uniform membrane disc was formed across the liquid interface. To vary crosslinking reaction conditions, crosslinking temperature was changed from 23 ºC to 4 ºC. The membrane formed totally across the vessel diameter and was now sufficiently large to be readily detached from the wall of the beaker and was also relatively easy to handle. Membrane thickness was determined by mounting the wet membrane between two glass cover slips, and using light microscopy to determine the spacing between the refractive glass surfaces. Membranes of thickness around 160 μm were used for diffusion measurements, as they were easier to handle than the thinner membranes that formed immediately after the reagent interaction in the beaker. The membranes were washed thoroughly in distilled water, and dried in an ambient atmosphere.

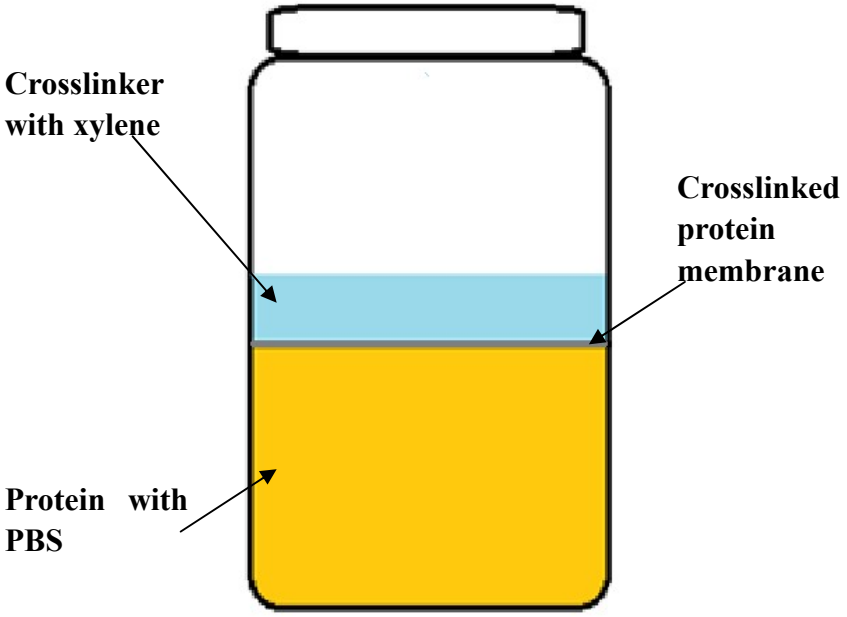

Figure 3.1 Vessel for large surface area membrane formation

3.2.2 Crosslinked Copper Protein Membranes

The large surface protein membranes (as Chapter 3.2.1) were washed thoroughly in distilled water three times, then exposed to 250mM copper sulphate solution (as Chapter 3.1.4.1) for 0sec, 30sec, 1min, 5mins, 10mins, 30mins, 1hour, 2hours and 24hours. The membranes were then washed thoroughly in distilled water for further use.

3.2.3 Experimental procedure for *in situ* protein membranes

Membrane formation utilized an interfacial reaction at the liquid-liquid interface involving the following steps:

(1) Microfluidic chips fabricated in glass were coupled to the KdScientific 200 syringe pumps (Royem Scientific Ltd, UK) by the Tygon tubing (1.6 mm i.d, 3.2 o.d).

(2) BSA solution (as chapter 3.1.2.1) at a flow rate of 300μl/min and the crosslinker solution (as chapter 3.1.3) at a flow of 700 μl /min were pumped into the flow cell to give parallel laminar flow streams and therefore to give interfacial crosslinked membranes. This was achieved along the full length of the channel under the continuous positive pressure driven laminar flow.

(3) Fibrinogen solution (as chapter 3.1.2.2) at a flow rate of 300μl/min and the crosslinker solution (as chapter 3.1.3) at a flow rate of 600μl/min to form crosslinked membranes

Such microfabricated membranes could extend the separation potential of any microfluidic structure providing a stable barrier layer.

3.3 Measurement of membranes thickness

Membrane thickness was determined by Dektak shown in Fig 3.2. To vary crosslinking reaction conditions, crosslinking time was changed from 5 mins to 72 hours. The Dektak is a profilometer for measuring step heights or trench depths on a surface. This is a surface contact measurement technique where a very low force stylus is dragged across a surface. The display range of the data is 200Å to 655,000 Å (65.5 um) with a vertical resolution of ~ 5 Å. The lateral resolution is limited by the tip shape. A video camera with variable magnification allows for manual placement of the stylus and the system is programmed for scan length and speed. Data leveling is done in the software and printouts with cursor locations and step heights are provided. The data can also be saved to a PC for further analysis.

3.3.1 Membrane formation

There were two methods used to develop membrane for measuring their subsequent thickness. One method was to develop the membrane inside of open vessel for set growing times from 6 to 72 hours as (Chapter 3.2.1). The membrane was now sufficiently large to be readily detached from the wall of the beaker and was relatively easy to handle.

With the above method if the growing time was less than 6 hours, the membrane

were thin and difficult to handle. So another method was used to grow the membrane on a solid cover glass surface for growing time from 5mins to 1hour. Here first protein solution was dropped on to the cover glass, then xylene with crosslinking agent was dropped over the protein solution. An immediate, opaque, uniform membrane disc formed across the liquid interface. Every 5mins layering of an aqueous solution over the xylene ensured there was an aqueous phase on top, three acyl chloride crosslinkers were tested in these experiments: TCL, SCL and IDCL, After membranes was crosslinked washing them with PBS.

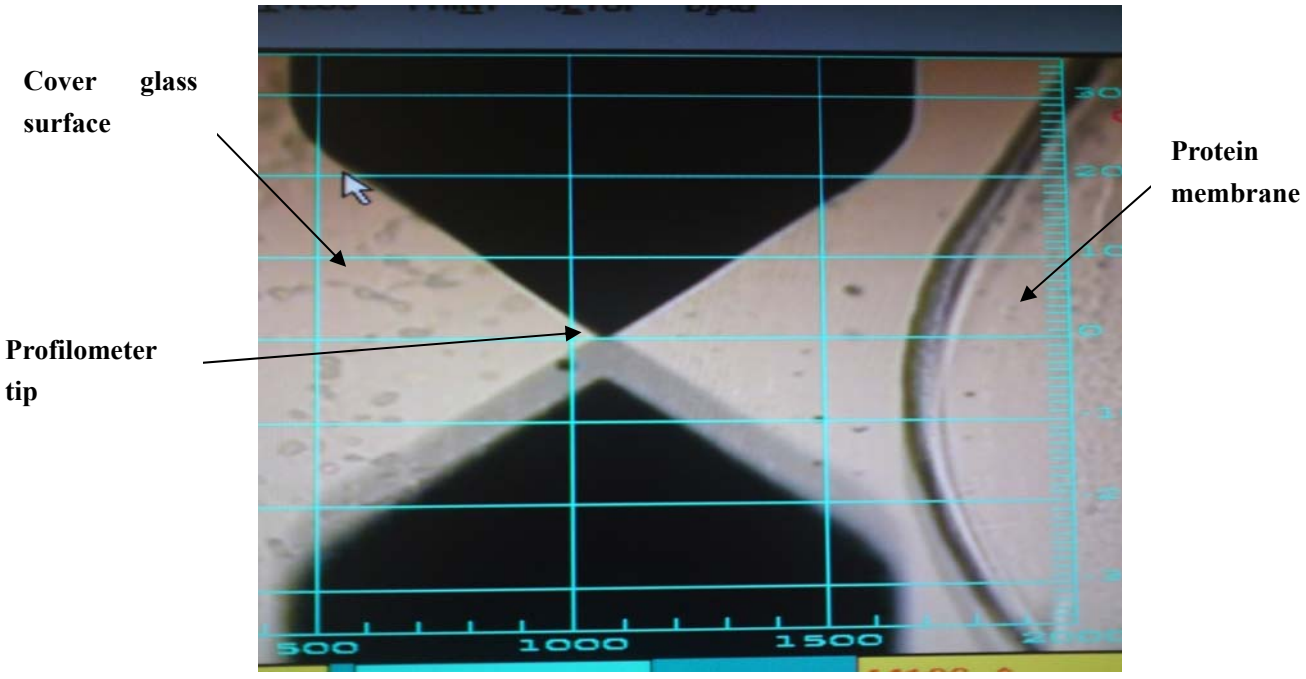

Figure 3.2 Measurement of thickness with DekTak instrument

3.4 Nanoindentation test for membranes

3.4.1 Preparation of corsslinked protein samples

There were four membranes: fibrinogen TCL, fibrinogen IDCL, BSA TCL and BSA IDCL, all were tested in wet conditions.

The crosslinked protein membrane was placed in a Petri dish, usually the membrane adhered to the bottom of the dish. Tissue paper was placed around the inner circumference of the dish and approximately 2.5mL of distilled water was applied to the tissue paper to keep the sample hydrated. The Petri dish was fixed to a metal stage mount using superglue (Loctite 385, Henkel), the glue was applied to the metal stage and the Petri dish was held to it for 15 seconds. The metal stage was then placed in position in the nanoindentation machine (UMIS 2000, CSIRO).

3.4.2 Preparation of crosslinked copper protein samples

There were two membranes: copper fibrinogen-TCL and copper BSA-TCL, they are tested in wet and dry conditions.

The crosslinked protein membrane was first placed it a Petri dish using glass slides, let the membrane adhered to the bottom of the dish. Then add 250mM copper sulphate solution. The membranes were exposed in for 24hours. Finally the membranes were washed

thoroughly in distilled water for further using. For the dry condition membranes, just leave the sample under clean room condition over night. For wet condition, tissue paper placed around the inner circumference of the dish and approximately 2.5mL of distilled water was applied to the tissue paper to keep the sample hydrated. The petri dish was fixed to a metal stage mount using super glue (Loctite 385, Henkel), the glue was applied to the metal stage and the petri dish was held to it for 15 seconds. The metal stage was place in position on in the nanoindentation machine (UMIS 2000, CSIRO).

3.4.3 Machine formation

With the use of tweezers, the diamond indentation tip named "RJ" with a radius of 20μm was fitted into the indenter. Using the software the position of the sample was adjusted so the tip was directly over a flat part of the film which was to be tested. The tip was lowered approximately 3mm above the sample area chosen. The working distance was set using a programme on the software, which allowed the indenter to make contact with the surface then distance itself away from it.

The parameters for the test were set as, contact force of 0.10mN exceeding to a maximum force of 10.00mN. The test consisted of 5 rows of 5 indents 100 μm apart. Each row was 100 μm apart also so the area covered was a 400 square μm. To stabilise the conditions inside the indentation machine it was set to start the test with a delay period of 30 minutes. The film was allowed to dry in the

indentation machine for a few hours until the tissue paper around the circumference of the petri dish was completely dehydrated. The indenter was moved to a new 400 square μm of film and the test repeated using the same parameters.

3.4.4 Procedure to acquire results

Once the test was completed the indentation information files were converted to ASCII files on a floppy disk. The ASCII files were imported into Excel, and with the use of Origin8 software the creep graphs were established. The standard deviations and error bars were performed in Excel, as well as the students T-test to acquire the P-Values.

3.5 Diffusion study

For studies of permeation; two methods were used. Firstly, dye diffusion was carried out with a single membrane inside the channel. Also, the crosslinked protein membrane which formed without using microfluidics was tested using Rank cell (Fig 3.3) electrodes with different electroactive chemical compounds.

3.5.1 Dye diffusion study with *in situ* crosslinked membrane

Dye solution (as Chapter 3.1.4.2) was passed through one side of a channel separated by a membrane and pH7.4 PBS on the other side. Both the solutions were passed at a rate of 100µl/min for 3 minutes, and flow was then stopped to monitor dye diffusion across the membrane. Dye transport was followed over 30 minutes and images were recorded.

3.5.2 Diffusivity of crosslinked protein membranes

3.5.2.1 Equipment

In this study the amperometric measurement was logged using a micro Autolab potentiostat instrument (Eco Chemie, Netherlands). A planar Pt working electrode (Fig 3.3) was used as part of a standard electrochemical cell (Rank Brothers Ltd, Cambridge, United Kingdom). The diameter of the Pt electrode disc was 2 mm. A platinum wire (MW-1032, Bioanalytical System Inc., Warwickshire, United Kingdom) served as a counter electrode, and solutions were stirred using a magnetic stirrer (MR 100, Heidolph, Kelheim, Germany)

3.5.2.2 Method

Experiments were carried out at room temperature (25 ºC) using amperometric

measurement of electrochemically active compounds. 5 ml PBS was placed in the Rank cell and stirred with the magnetic stirrer. For amperometric measurements, a μ-Autolab potentiostat was used. The electrochemically active diffusants, hydrogen peroxide, acetaminophen or catechol (solution prepared as Chapter 3.1.4.2), was added to the stirred solution in the electrochemical cell following the application of a polarising voltage of +0.65V *vs* Ag/AgCl and the establishment of a stable baseline current. For practical measurement of diffusion profile at a membrane, its thickness requires to be less than one tenth of working electrode diameter to avoid edge effects [132]; in the present study membranes of < 200 μm were considered to be suitable.

In order to check repeatability, every diffusion study with the same membrane was carried out 3-5 times.

Figure 3.3 Rank cell electrode

3.6 Bacterial study for copper protein membrane

3.6.1 Membranes preparations

During this test, crosslinked protein membranes (BSA and fibrinogen) were prepared using the large surface area membrane formation method as Chapter3.2.1. The crosslinking time was 48 hours，during this time the thickness of the crosslinked BSA membranes can grow to ~70 μm, and the thickness of the crosslinked fibrinogen membrane was ~300 μm which made them easier to handle. Four pieces each of the protein membranes were kept as control samples. The rest of the membranes were washed thoroughly in distilled water three times, then they were exposed to 250mM copper sulphate solution (CSS) for 12hours, and finally washed thoroughly in distilled water for further use.

3.6.2 Bacterial strain culture (Provided by Mark wilks)

Strains *S. epidermidis* RP62A (ATCC 35984) [133] were selected to study bacterial adhesion on membranes surfaces. Bacterial colonies of the strains were stored at 4 °C and then cultured at 37 °C for 24 h in tryptic soy broth (TSB for *S. epidermidis*) in a 125 ml flask (Pyrex) containing 60 ml media covered with aluminum foil on an orbital shaker at 250 rpm. Bacterial cultures were collected by centrifugation at 1360*g* for 10 min. The pellet was washed with PBS, and then resuspended in PBS, and the concentration of bacteria was measured by a

spectrophotometer at 600 nm. Using a 30-gauge needle to reduce bacterial aggregation, bacteria were suspended in PBS or 25% pooled human plasma in PBS at a final concentration of 1×10^8 cfu ml^{-1}. 50 ml of test suspensions inoculated with bacteria was added to a 100 ml PTFE beaker for measurement of bacterial adhesion.

3.6.3 Bacterial adhesion on protein membrane surface

Two control membranes (BSA and fibrinogen each) and four copper protein membranes (BSA and fibrinogen two each) were incubated in bacterial solution for 24 hours. Another two control membranes (BSA and fibrinogen each) and four copper protein membranes (BSA and fibrinogen two each) were incubated in bacterial solution for 48 hours. All the membrane samples were washed with pH7.4 PBS by sequential addition and aspiration, and then washed with DI water to eliminate salt particles from PBS. Finally the samples were left to dry overnight in a clean room at the room temperature. The membranes were examined by SEM.

3.7 Cell attachment to membranes

B50 rat neuronal cells [134] were cultured in Dulbecco's Modified Eagle's Medium (DMEM), supplemented with 10% Fetal Bovine Serum (FBS),

Penicillin- Sterptomycin solution and L-glutamine solution. Cells were incubated at 37^{o}C in 5% CO_2 for 3-4 days until grown to confluence before trypsination. Subsequently the cells were resuspended in DMEM before 1 ml of 2×10^{6} cell/ml suspension was dispensed into each well of an 8 well cell culture plate consisting of different planar crosslinked protein membranes cast on glass coverslips. During day 1 and day 3, the morphology of the cells was examined by light microscopy, and cell viability studies conducted by staining cells with Trypan Blue. After day 1 of initial culture, media was removed from each well and washed with Dulbecco's Phosphate Buffered Saline (DPBS). Cells were then fixed with 25% (w/v) glutaraldhyde and stored for 1 hour at 4ºC before an additional fixation period of 2 hours with 50% (w/v) glutaraldhyde at 4 ºC. Each coverslip was then washed three times using distilled water and left to dry overnight at room temperature.

3.8 Fabrication of microfluidic system

In this study, different types of materials were used for the fabrication of the microfluidic channels. The design of the channel however was the same. The main channel is 2mm width and 100μm depth. The two smaller channels as input were 1mm in width and 100μm depth shown in Fig 3.4b. Cell culture media/ nutrients and various other chemicals flowed through these channels.

3.8.1 Fabrication of protocol Glass structures

The microfluidic structures were fabricated in-house using three layers of glass microscope slides: 76×26×1 mm as the lower base, and variously, 22×22×0.1 mm as an upper cover and as channel slide walls. The top view of the structure of channel is shown in Fig 3.4. The main channel was of 2mm width and 0.1 mm depth. To create a bifurcated geometry, whilst the covering and base glass slides were used as received, the intermediate layer glass slides were cut to the required size and shape so that a 2×0.1 mm Y channel could be formed. The glass slides were bonded with UV-curable adhesive (Loctite® 3211, Henkel, UK). For the input fluid connectors, conical tips (5mm length) from 1 ml pipette tips (Eppendorf pipette, purchased from VWR UK) were bonded to the short Y-microfluidic channels by UV adhesive. To prevent leakage around the structures, all junctions were further sealed using an extra layer of epoxy resin (Araldite® Huntsman Advanced Materials UK) and left to set overnight for full bonding. By this simple technique a wide range of flow geometries, e.g., input angle, were readily accessed and tested.

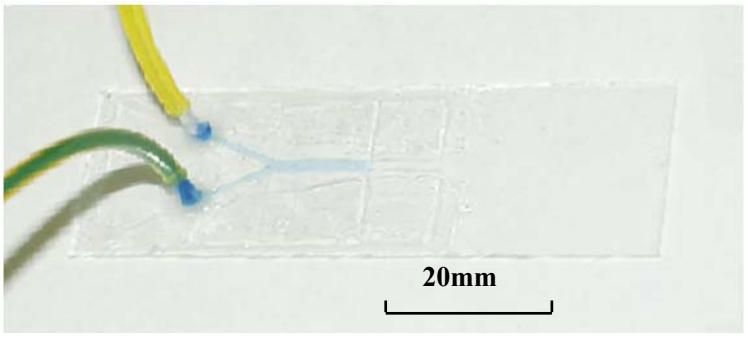

(a)

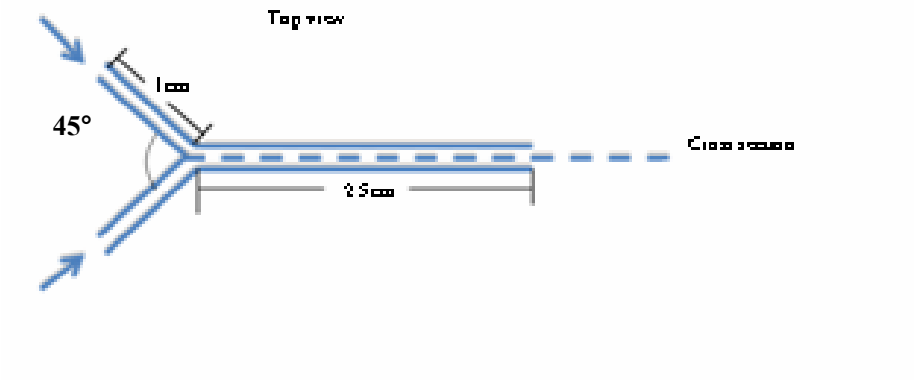

(b)

Figure 3.4 (a) Image of the Y shape microfluidic channel, (b) schematic of the Y shape channel.

3.8.2 The fabrication process for the PDMS Microfluidic channel

This used D.I. water, 2-3% (w/v) sulfuric acid solution, silicone resin, curing agent, isopropyl alcohol, a hot plate and microscope glass slides.

The aim of this study was to develop a microfluidic channel that was cost effective and easy to use. The fabrication process for the PDMS microfluidics can be divided into four main steps:

1. Mould fabrication;
2. PDMS casting;
3. Fluidic port drilling ;
4. Channel sealing.

Step 1 during this study, a mould was made by etching a Y channel on an iron block as figure 3.5 from Queen Marry workshop.

Step 2 PDMS casting

The components for preparing the elastomers were supplied in two parts, Sylgard-184A and Sylgard-184B. As obtained, Sylgard-184A and Sylgard-184B contained 30–60 and 10–30 wt%, respectively, of dimethylvinylated and trimethylated silica fillers, as reported by the manufacturer. A 10:1 Sylgard-184A/Sylgard- 184B mixture [93] by mass was prepared and stirred in a plastic cup using a glass rod. Trapped air bubbles resulting from the agitation of the mixture were removed by applying gentle vacuum for 1 hour to remove air bubbles. Once, all the air had been evacuated curing was carried out in an oven at 65ºC for 2 hours to form the crosslinked PDMS network. Immediately after the cure was complete the castings were peeled off from the mould.

Step 3 Fluidic port drilling

Drilling was performed using a flat-tipped 20-gauge syringe needle. This was used to drill four holes in the PDMS pieces, the sharp needle edge ensured that clean cuts were made into the PDMS.

Step 4 channel sealing

Oxygen plasma is created by exposing oxygen gas at a low pressure (O_2) to high power radio waves, which ionise it. It was used to form a hermetic seal between

the PDMS channel casting and the glass cover slides. Before insertion of the PDMS castings and the glass slides in the oxygen plasma both were washed again in isopropyl alcohol and dried with nitrogen gas. Within 10-15 seconds the glass slide and PDMS were taken out of the chamber. The surfaces were pressed together, sealing the channels. The pressed slabs needed to be kept at room temperature for two days to ensure sealing was complete.

Figure 3.5 Fabricated metal mould made by Queen Marry workshop

3.9 Instrumentation

3.9.1 Scanning Electron Microscopy (SEM)

The surface of the membranes was examined by Scanning Electron Microscopy (SEM). The Scanning Electron Microscopy (Jeol-high field) provides measurement with a micron scale resolution and so can determine microstructures and local values of physical properties. SEM samples are coated with a very thin layer of gold by a machine called a sputter coater, and then the sample is placed inside the microscope's vacuum column through an air-tight door.

3.9.2 Fourier Transform Infrared Spectroscopy (FTIR)

FTIR spectra of modified and unmodified polymer films ($1cm^2$) were obtained in the mid infrared region ($4000\text{-}400cm^{-1}$) at $8cm^{-1}$ resolution, using an interferometer mirror velocity of 0.633cm/s with a modulation frequency of 10 kHz, averaging 256 scans. The sample chamber of the photoacoustic spectrum (PAS) cell was purged with dry helium gas (pre-dried over a column of magnesium perchlorate). A background scan was obtained prior to each set of tests using carbon black specimen. According to Schubert [135] 5-10μm depth of the polymer surface was sampled with these settings.

Chapter 4: Development and Characterisation of Crosslinked Protein Membranes

4.1 Introduction

With the fast growth of biotechnology and the pharmaceutical industry, polymer membranes are widely used in biomedical applications. A common application is separation of components, such as gas-liquid separation due to the permeability of a membrane [7]. It is also possible to use biocompatible or biodegradable membranes as cell culture supports for tissue engineering as tissue scaffolding. Membranes also provide a large internal surface area that can be used effectively for adsorption of solutes. The mechanisms for transport cell morbidly and application depend strongly on membrane morphology and membrane structure. Two typical morphologies have been distinguished: porous and dense.

Crosslinked membranes have many uses but before a suitable application can be made the mechanical properties need to be determined. The material can be defined as suitable for a correct range of applications.

In this study, two types of proteins, fibrinogen (340kDa) and BSA (66kDa), were crosslinked to form the solid membrane and comparisons of different forming conditions made. Also, to obtain different protein membrane

morphologies three types of acyl chloride crosslinkers have been tasted. They were terephthaloyl chloride, sebacoyl chloride and isophthaloyl dichloride. The surface morphologies and cross-section morphological structures of different crosslinked membranes were studied, BSA with different concentrations of ethanol was crosslinked with TCL, and the surface morphologies of those membranes were compared. Additionally the growth rate of membranes was determined as a background to effects of protein vs. crosslink agent.

Additionally, there was little control over the final porosity and the membranes were not mechanically robust. A truly self-supporting membrane was not produced as it still required some other structural substrate. During the process of exploring permeability to copper ion [Cu^{2+}], a series of more robust protein membranes were produced which appeared to be competitive with the strength of values cellulosic membranes (an industry standard). Moreover, the duration of copper exposure appeared to determine porosity, which could be well enhanced over the current copper free membranes. Essentially, after the membrane was formed, there was controlled exposure to copper sulphate solution. Two control features were achieved: thickness control of the protein membrane based on the liquid-liquid interfacial polymerisation process and porosity on the basis of exposure time in copper sulphate solution. Such membranes could allow for a new generation of materials, with niche applications, and the protein surface would have advantages for biological use.

4.2 Large area membrane

4.2.1 Surface structure of large surface membrane (SEM)

The aqueous and organic sides of the membranes exhibited different morphologies, as shown in Figure 4.1. This was consistent with previous findings of asymmetric membranes with interfacial formation and bulk formation. In conventional, bulk interfacial polymerization, a microporous support membrane is typically used to provide an interfacial barrier that allows only transport of monomers by diffusion. Once the support is impregnated with the aqueous amine solution and placed on top of the organic chloride solution, the interfacial polymerization occurs via a polycondensation reaction between two monomers [18]. The smooth surface indicates that the interface of the two flows is smooth. Once the protein and acyl chloride starts crosslinking, the reaction is rapid and leads to a smooth surface. After the formation of a membrane skin, during the initial reaction a rate-limiting barrier for the transport of the acyl chloride from the organic side into the protein solution, formed the random porosity and native membrane structure of this membrane skin was inhomogenous, so possibly the solute diffused unevenly, also the morphology of the membrane becomes asymmetric (Fig. 4.1)

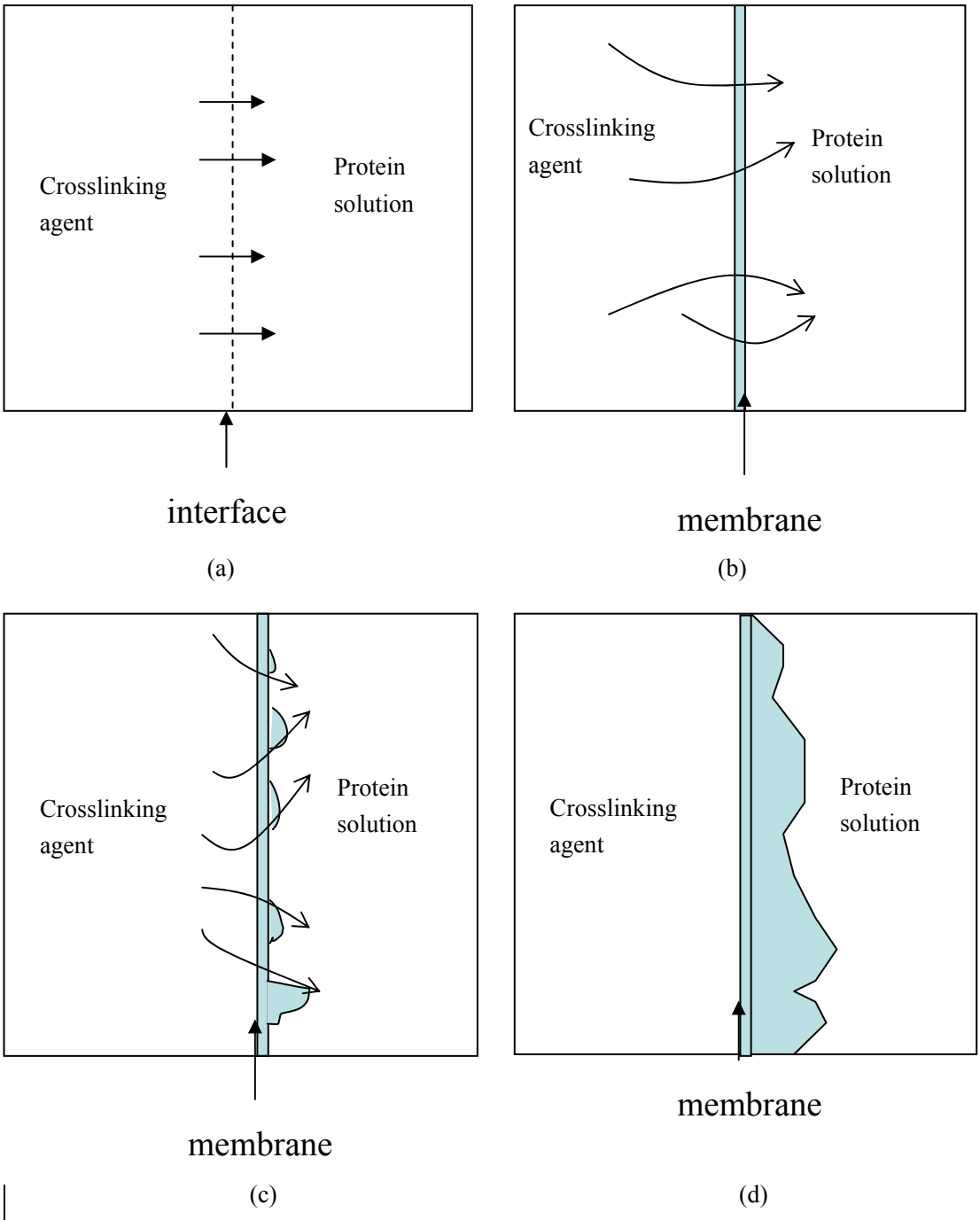

Figure 4.1 membrane formation process (a) interfacial crosslinking formation (b) monomers diffuse through microporous membrane (c) solute diffuse through the inhomogeneity membrane (d) unevenly membrane format in microchannel

4.2.2 Comparison fibrinogen membrane with BSA membrane

The surface roughness of the protein membrane was characterized with membranes made of different proteins first. Figure 4.2 shows SEM images of albumin and fibrinogen membranes. On the organic solvent side during membrane formation, no obvious pore structure is seen for the albumin membrane, but for the fibrinogen, there are defined pores in the range 0.01 – 0.10 μm. If they are continuous through the material, this would account for the observed membrane permeability differences. On the protein solution side both BSA and fibrinogen membranes showed a rough structure. The protein side as used during membrane formation of the fibrinogen membrane show a more ridged structure compared to the BSA membrane. That may be because fibrinogen is a larger linear protein but BSA is a small globular protein, when they start crosslinking with the same crosslinker the distance between two crosslinking points may have been different, also there may have been pre-crosslinking solubility units. The lower solubility fibrinogen may have formed colloidal aggregates that allowed for clumping of material during crosslinking and therefore pores. This could be possible reasons for the more open and porous membrane networks and higher solute diffusivity in the membrane made of protein with nominally higher molecular weight and larger hydrodynamic ratio. Also, when membranes were formed using BSA solution, a crosslink skeleton made of a smaller and globular molecular size would assemble into a smaller

sized structure and aggregate and from fewer granularities. This may be the reason that the surface of a crosslinked BSA membrane was smoother than that of a membrane made of the linear fibrinogen protein.

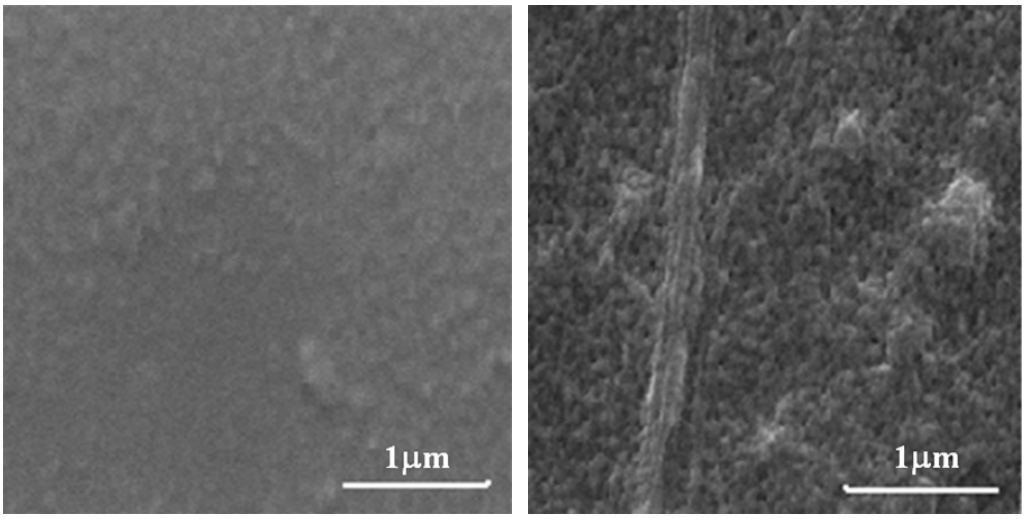

(a) organic side **protein side**

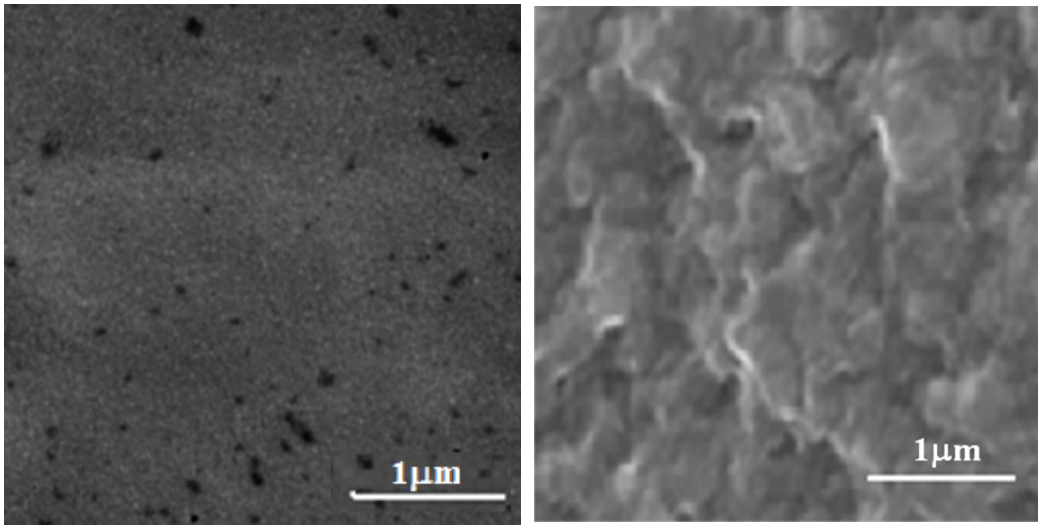

(b) organic side **protein side**

Figure 4.2 (a) BSA terephthaloyl chloride membrane (b) fibrinogen terephthaloyl chloride membrane

4.2.3 FTIR analysis

The FTIR peak near 1650 cm^{-1} in Figure 4.3 was considered to be the amide I band. It results from the C=O stretching vibrations of the peptide bond. This band is sensitive to changes in secondary structure and has therefore been widely used for protein conformational studies [136]. Similarly, the peaks near 1540 cm^{-1} (N-H bending vibration/C-N stretching vibration) and 1240 cm^{-1} (C-N stretching vibration/N-H bending vibration) are called the amide II band, and amide III band, respectively. The peak near 3300 cm^{-1} is thought to be N-H bending vibration and the peak near 1400 cm^{-1} to result from protein side-chain COO-. As the absorption peak position and shape of the amide I band differ according to the secondary structure, peak analysis can yield information on that structure. The C-H stretching signals appear in the wavenumber range between 2700 and 3100 cm-1. The 1110 cm^{-1} band is typical $HPO4^{2-}$ which from PBS. CO2 group functionality was indicated at 2370 cm-1 may come from the structural environment. Benzene signal which come from the crosslinker could not find from FTIR peak.

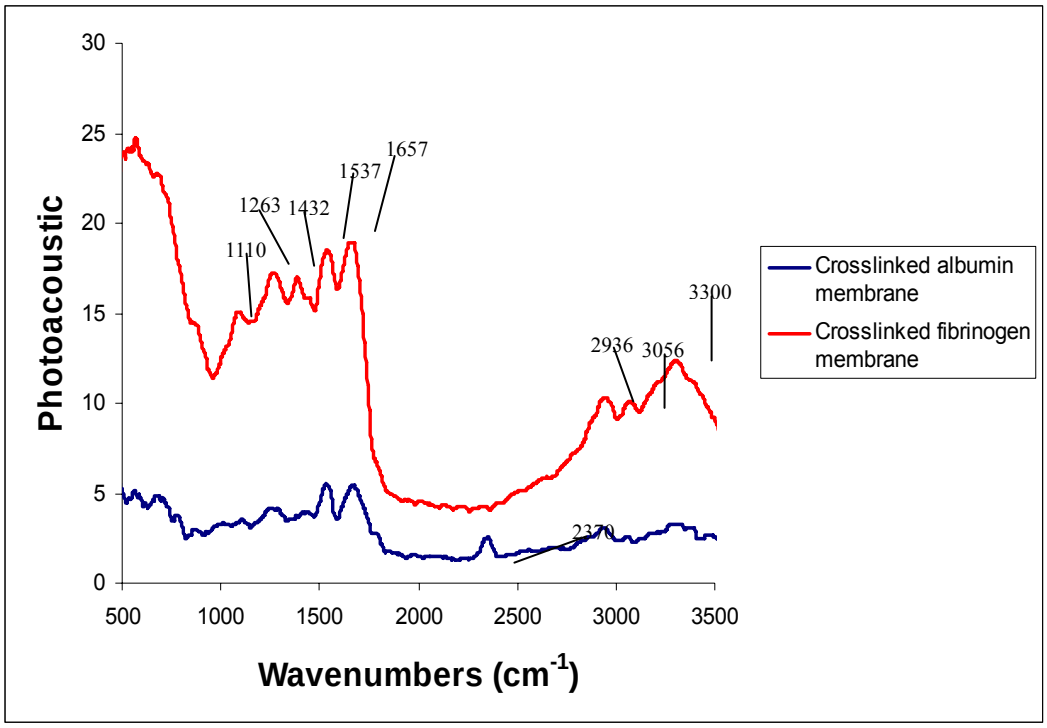

Figure 4.3 FTIR of crosslinked fibrinogen membrane and BSA membrane

4.3 pH dependence of membrane porosity

4.3.1 Surface structure of pH fibrinogen membrane (SEM)

Protein membranes were formed using protein solution at various pH values: 6.0, 7.4 and 9.0. Following equivalent crosslinking time (24 hours), the generated thicknesses of crosslinked fibrinogen membranes were 174, 133 and 118 μm. This suggested that the crosslinker had penetrated the membrane to varying degrees and more effectively so in the case of the lower pH samples. SEM of the membranes (Fig. 4.5) shows that the lowest pH membrane had a coarse uneven

surface with a fibrous structure with large voids. As pH increased, morphology altered to give a smooth surface with discrete nanopores with a range of 10nm to 200nm (Fig. 4.4). The latter decreased in number with increasing pH (data in Table 3.2). It is possible that at the lowest pH (pH 6) the fibrinogen underwent denaturation/desolvation and formed aggregates that produced an uneven membrane surface. Denatuaration of fibrinogen is known to occur at low pH [137]. Also, as pH is raised above the isoelectric point, while the fibrinogen is not denatured, its terminal segments undergo extension due to electrostatic repulsion [138] and such changes might account for membrane structural differences.

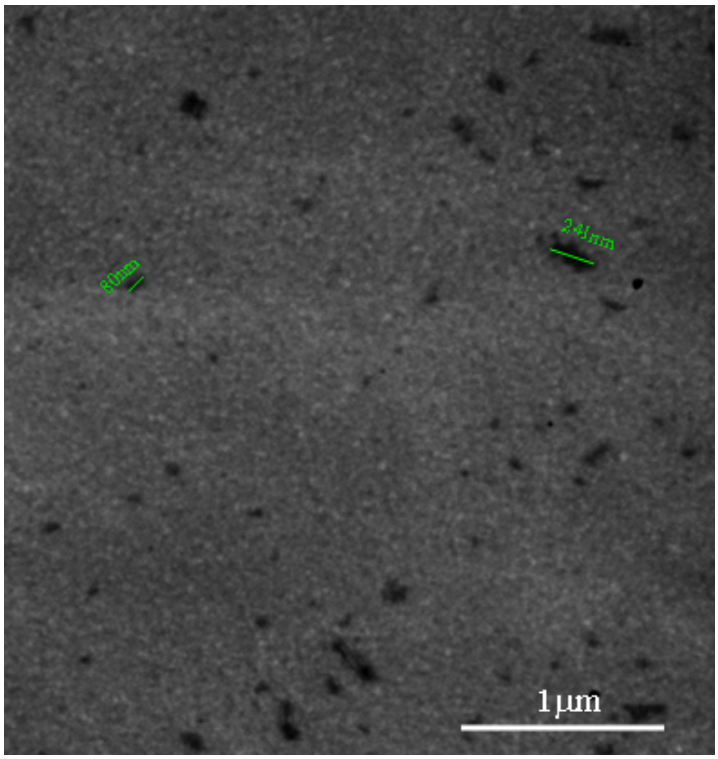

Figure 4.4 SEM images of microstructures of crosslinked fibrinogen membranes formed from PBS at pH 7.4

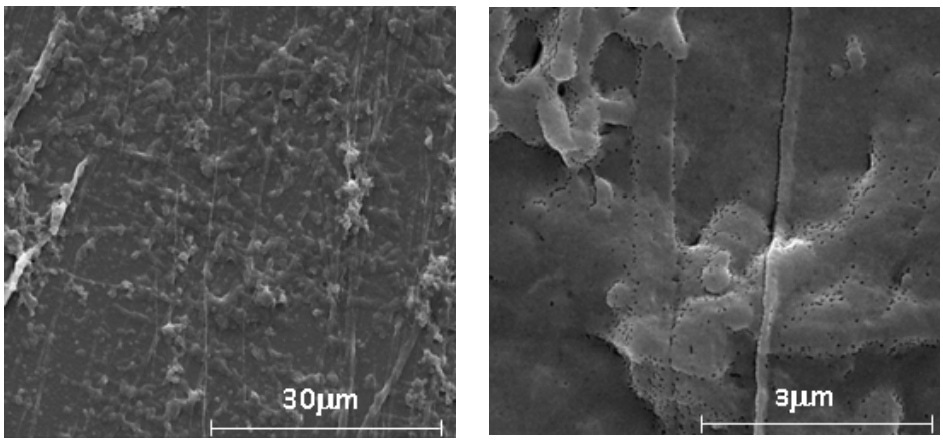

(a) pH 6

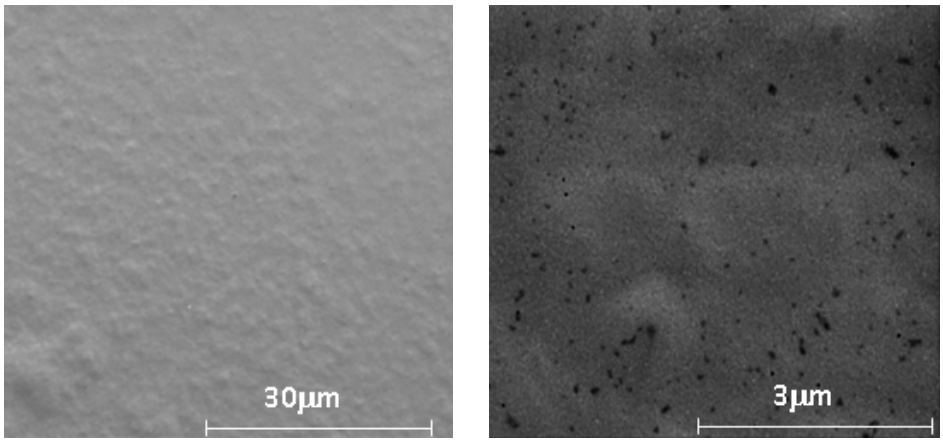

(b) pH 7.4

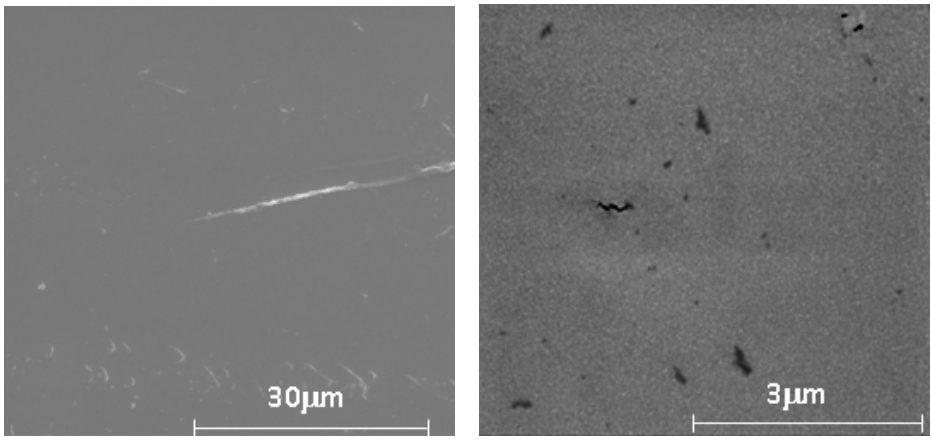

(c) pH 9

Figure 4.5 SEM images of microstructures of crosslinked fibrinogen membranes formed from PBS at pH 6, 7.4 and 9 with 3.8% w/v fibrinogen solution, 1% w/v terephthaloyl chloride.

4.4 Effect of temperature on membrane structure

Figure 4.6 shows the surface structure of a fibrinogen membrane formed at pH 7.4 under different crosslinking temperature 22°C (a), and at 4°C (b). The surface of both was smooth, the images show there is a high density of small pores ranging in size from 15 to 100 nm. There is no significant difference between the surface structures of the membranes with different crosslinking temperature.

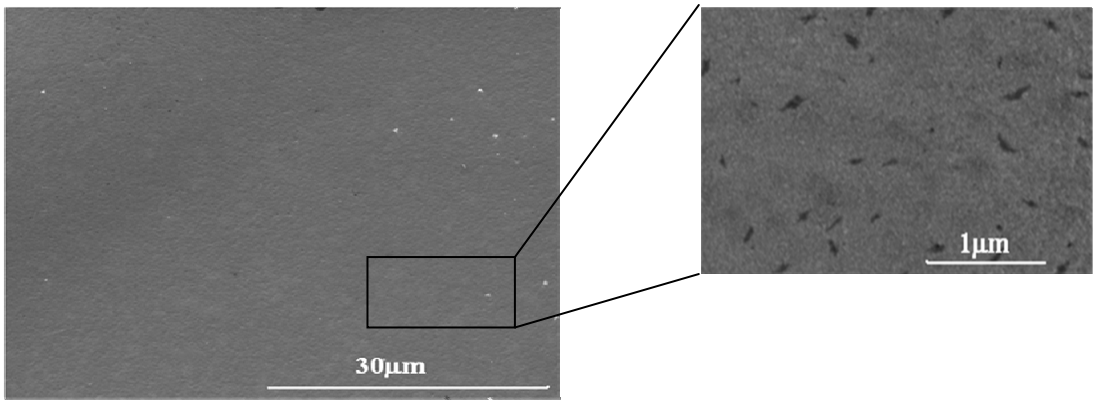

(a)

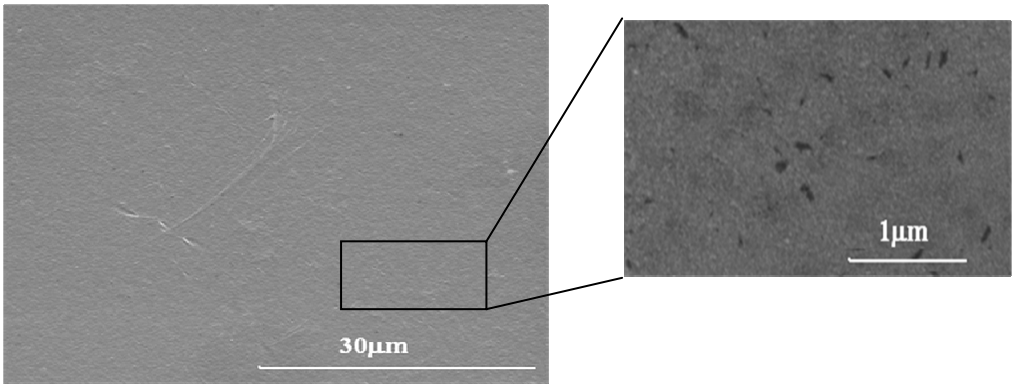

(b)

Figure 4.6 Fibrinogen membrane with pH 7.4 under different crosslinking temperature 22°C (a), and at 4°C (b)

4.5 Ethanol in albumin membranes

4.5.1 Surface structure of large surface membrane (SEM)

Without ethanol the albumin membrane exhibits a smooth and even surface, with few changes of topology as compared with the 2ml ethanol membrane. With the 4ml ethanol membrane, the surface shows wavelike ripples. However with 6ml ethanol, the membrane appears to have stronger wavelike ripples. The localized particles on the membranes may be attributed to crosslinker particles entrapped on the surface during the membrane formation.

SEM results of various membranes indicated no major effect of ethanol apart from the rougher surface. This may suggest that ethanol denatures proteins by disrupting the side chain intermolecular hydrogen bonding. But this hydrogen bonding is very weak compared with the nucleophilic reaction. So this solution should still crosslink with acyl chloride. Stronger wavelike ripples with higher ethanol concentrations due to an increased drying effect from the ethanol which has a lower boiling point than water will have led to quicker evaporation and so to non-uniform aggregation of the polymer, concomitant with reorientation of molecules within the polymer matrix.

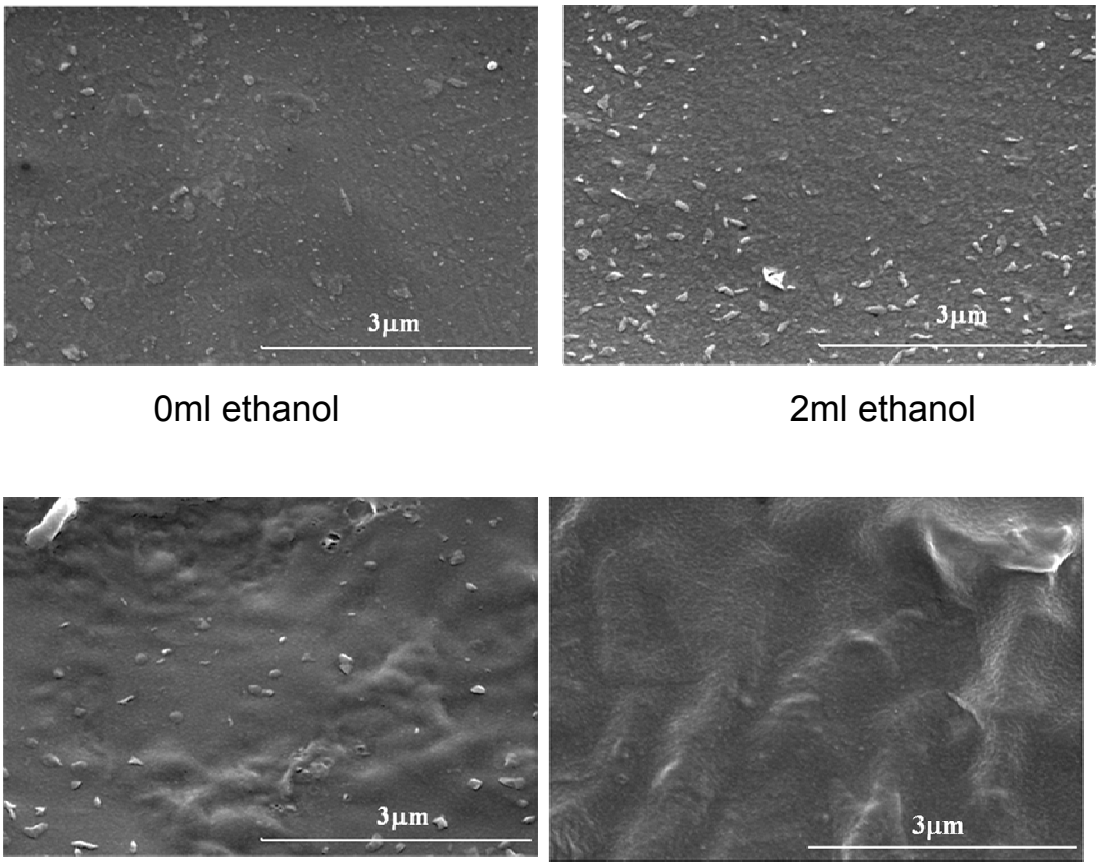

Figure 4.7 electron micrographs of ethanol BSA membrane structures

4.5.2 FTIR analysis

Exposure of a protein to ethanol will cause denaturation, due to that ethanol can affect intermolecular electrostatic forces, hydrogen bonds, and hydrophobic interactions, respectively resulting in the alteration of protein conformation [7]

The surface of the protein, in contact with aqueous solution, will expose hydrophilic amino acid side chains. The hydrophobic residues will normally be

buried inside. This interaction with the surrounding aqueous solution is an important factor in determining stability of a folded protein. When an organic solvent such as ethanol is mixed in, the protein molecules twist and flexes (through free bond rotations within) as the hydrophilic side chains avoid the alcohol. At the same time some interior hydrophobic side chains twist to the surface where they can interact more favorably with the organic solvent. The net effect is as though the protein molecule was trying to turn itself inside out in response to the change in the surrounding solvent. So in the process alcohol disrupts the hydrogen bonding as well as the ionic interactions. The result is a structurally altered, perhaps unraveled, protein molecule. The higher peak of FTIR indicated that the distance between the protein molecule is increase with the amount of the ethanol increase.

FTIR studies performed on membranes (Fig. 4.8) revealed absorption bands as expected from a native BSA at the regions of amide Ⅰ (~1650cm^{-1}) and amide Ⅱ (~1500 cm^{-1}) [139], denaturation does not break any of the primary chemical bonds that link one amino acid to another but it changes the way the protein folds in upon itself.

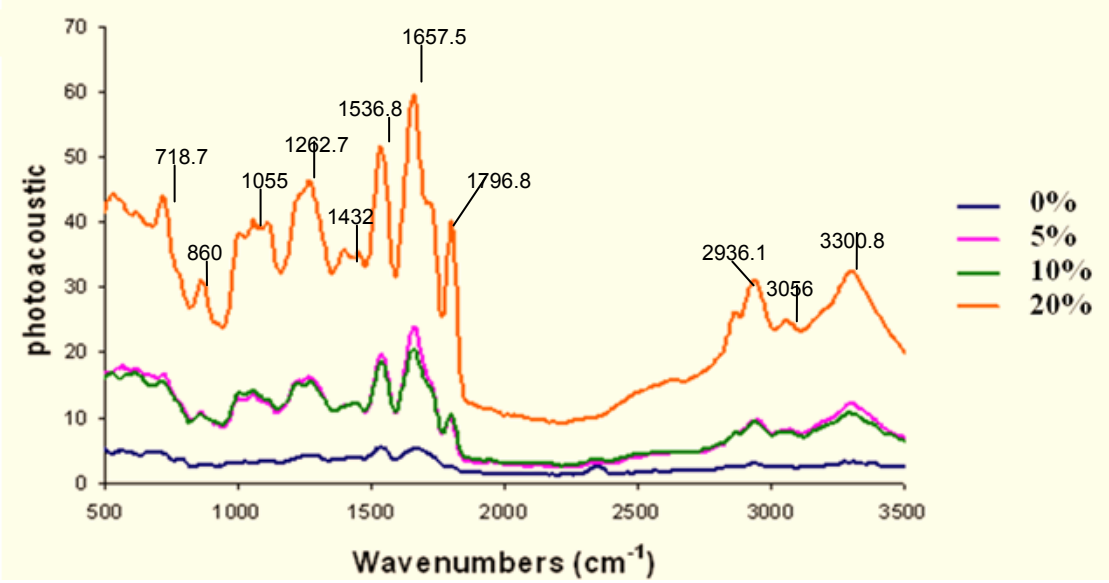

Figure 4.8 FTIR spectra of 20 wt. % BSA membranes prepared using different concentrations of ethanol (0, 5, 10 and 20 %) and corresponding

4.6 Crosslinked protein membranes with different crosslinker

4.6.1 Surface structure of crosslinked protein membranes

The surface topography of fibrinogen and BSA membranes was examined to assess microstructural changes owing to the different crosslinker used. Scanning electron microscopy (SEM) was used to confirm physical appearance.

With a BSA crosslinked membrane (Fig. 4.9), the sample crosslinked with IDCL appeared to be smooth and even on the organic side but for the protein side of the

surface, it showed undulating contours due to IDCL molecule diffused from the organic side to the protein side. This has been perversity shown in chapter 4.2.1. However, the surface of the membrane sample of BSA crosslinked with TCL shows localized particles on the organic side, which may be attributed to dust contamination or to TCL particles entrapped on the surface; apart from that, the surface was smooth. The protein side of this membrane shows a ridge-and-valley structure. The surface structure of a sample with SCL crosslinker shows significant morphological change, with the organic side of the membrane showing evenly distributed pores. On the protein side the surface appeared to be more distorted with clearly visible pores; around these pores there were circular ridges, due to the fast transfer of SCL molecule.

The membrane of fibrinogen crosslinked with IDCL presented a wrinkled appearance, on the protein side of membrane without discrete pores. The organic side shows a smooth surface with some large localized pores possibly due to damage during the sample handling process.

For the TCL crosslinked fibrinogen membrane (Fig. 4.10), the organic side shows a smooth surface with visible pores. On the protein side, the surface appeared to show undulating contours. The organic side of the fibrinogen SCL membrane was an uneven structure; the particles might be due to SCL. The surface of the protein side presentes a strongly wavelike appearance with circular

ridges, furthermore, both sides of the SCL fibrinogen membrane showed pores ranging from 0.1μm to 0.3μm but a lower pore density as compared with IDCL and TCL protein membranes.

Overall, the SCL crosslinker formed membranes that had a coarser, uneven structure with possible large voids for geared solute transport. Fibrinogen SCL membranes were coarser in structure and generally more porous. TCL protein membranes showed a relatively smooth, lower porosity surface compared with the SCL protein membranes. IDCL protein membranes exhibited a smooth and dense surface morphology. According to these findings, the crosslinker structure influences final structure outcome.

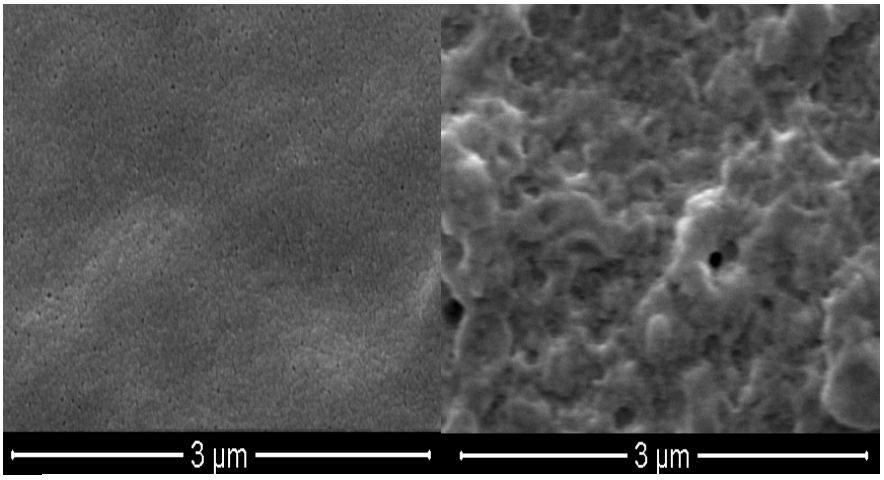

(a) organic side protein side

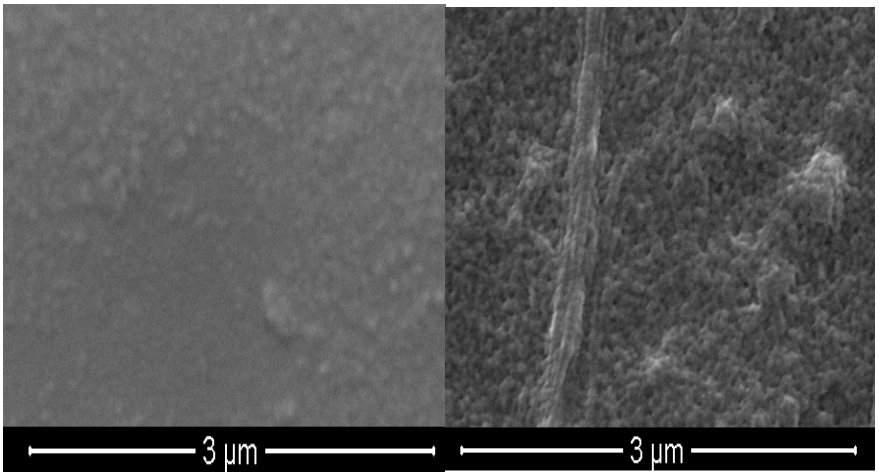

(b) organic side protein side

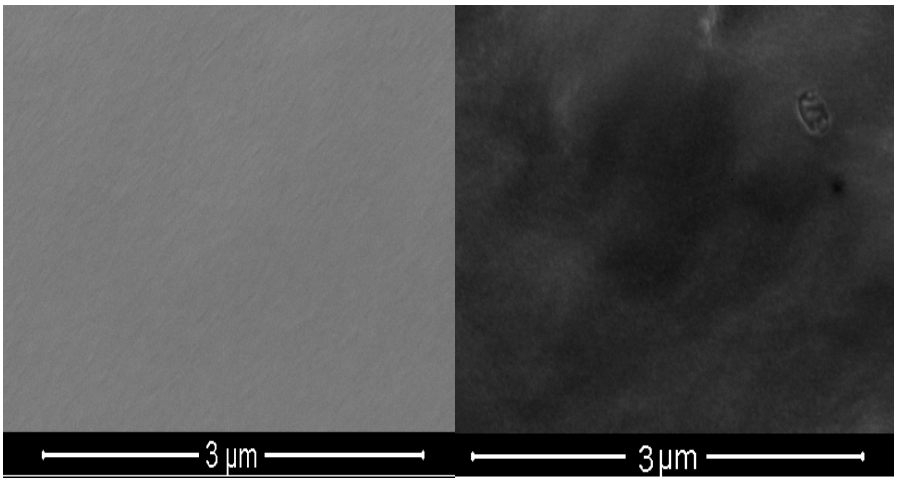

(c) organic side protein side

Figure 4.9 SEM images of surface microstructure for the crosslinked BSA membrane with (a) SCL, (b) TCL and (c) IDCL crosslinker

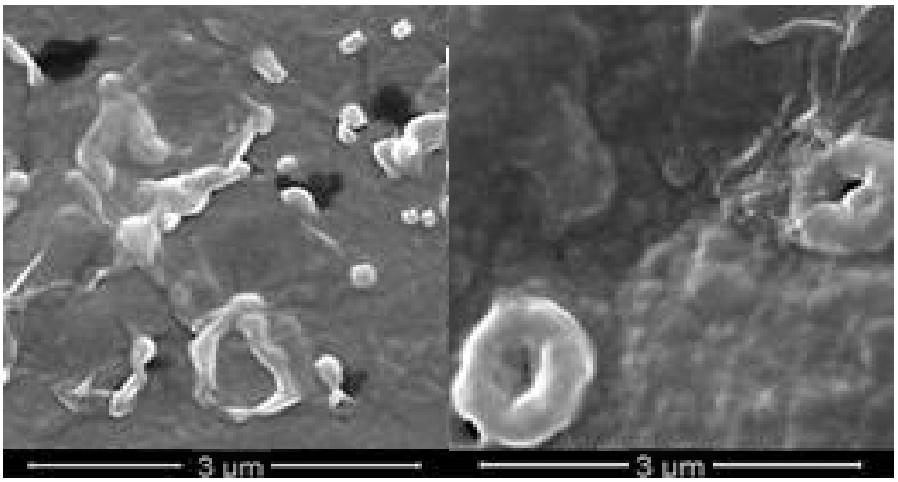

(a) organic side protein side

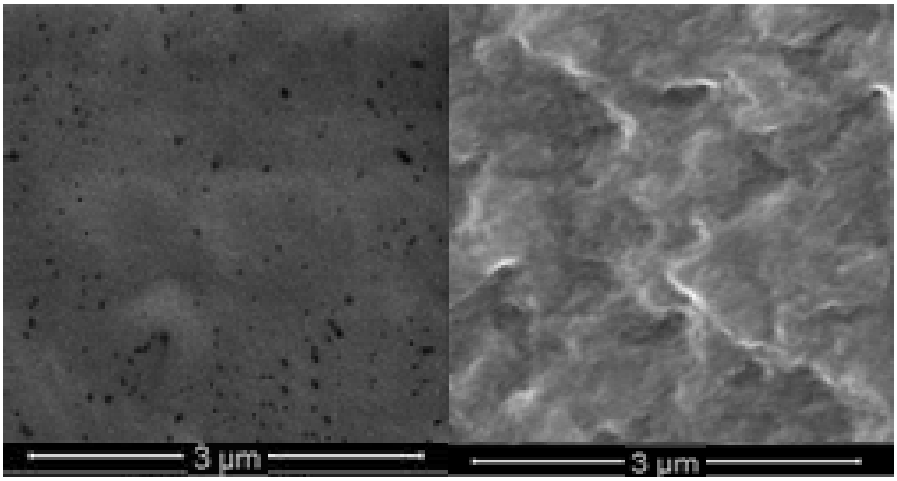

(b) organic side protein

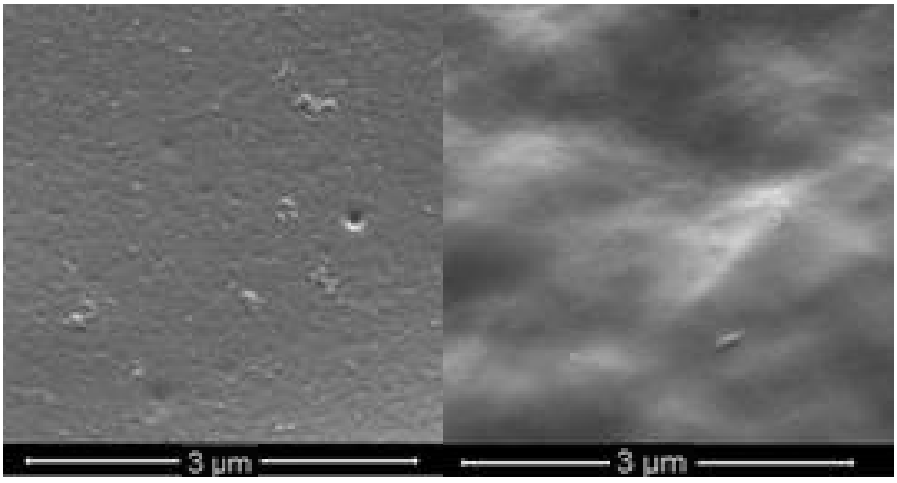

(c) organic side protein side

Figure 4.10 SEM images of surface microstructure for the crosslinked fibrinogen membrane with (a) SCL, (b) TCL and (c) IDCL crosslinker

4.6.2 Cross-section structure of crosslinked protein membranes

SEM was employed to observe the crosssection features of the membranes. Figure 4.12 shows a crosslinked BSA membrane crosssection. For the crosssection of the IDCL-BSA membrane, the structure was dense and very smooth. However, the membranes might still have possessed small pores of the order of a few nanometers that were not observable the SEM. The crosssection of the TCL-BSA membrane reveals that the dense skin layer of the membranes is relatively thin and there is a flaky structure below the relatively thin skin layer. With the SCL-BSA membrane, the crosssection showed stronger porosities with an asymmetric overall structure.

Figure 4.11 shows the SEM micrographs for fibrinogen crosslinked membrane cross sections. The micrographs of the IDCL-fibrinogen membrane showed the expected relatively dense crosssection structure with no pores apparent. The structure of the crosssection of TCL-fibrinogen membrane appeared to show undulating contours. For the crosssection of the SCL-fibrinogen membrane, the thickness of the smooth skin layer of the membranes was relatively thin (0.1μm). There were many pores with a size of approximately 0.1–0.5 μm below the smooth skin layer. The path of these pores is flexural and asymmetric. These differences in structure both on the surface and in the bulk of the membrane can be attributed to a wet phase inversion film-formation process and have also been observed by many researchers [140, 141]

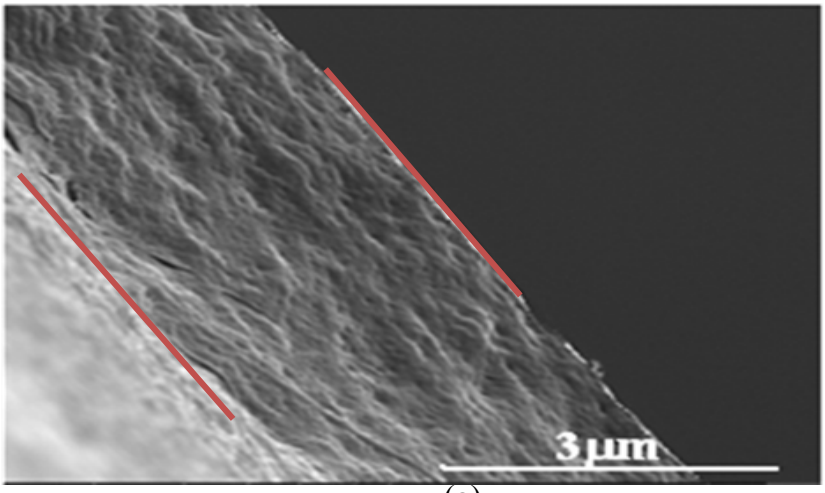

(a)

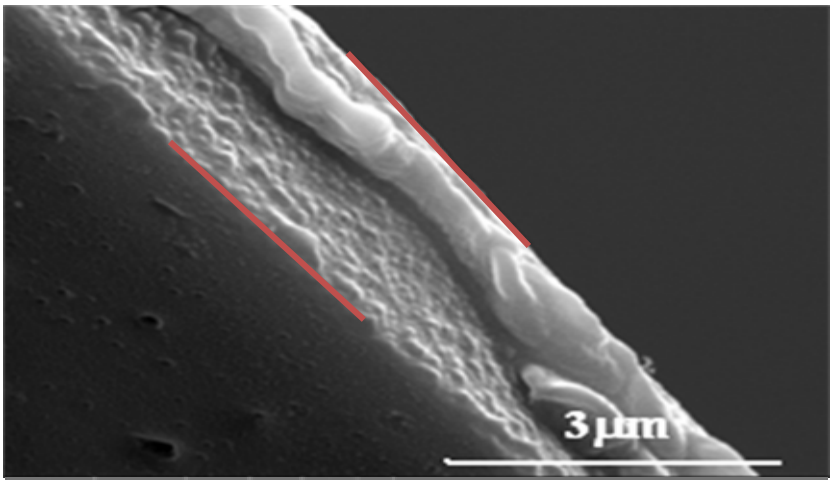

(b)

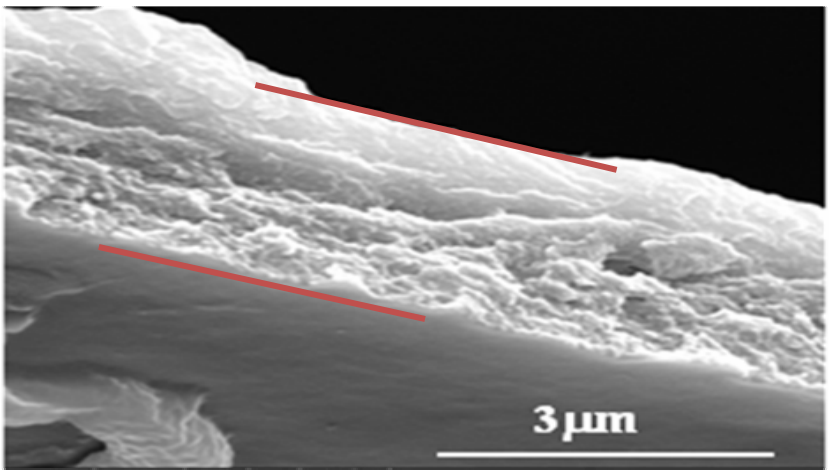

(c)

Figure 4.11 SEM images of cross-section microstructure for the crosslinked fibrinogen membrane with (a) TCL, (b) IDCL and (c) SCL crosslinker

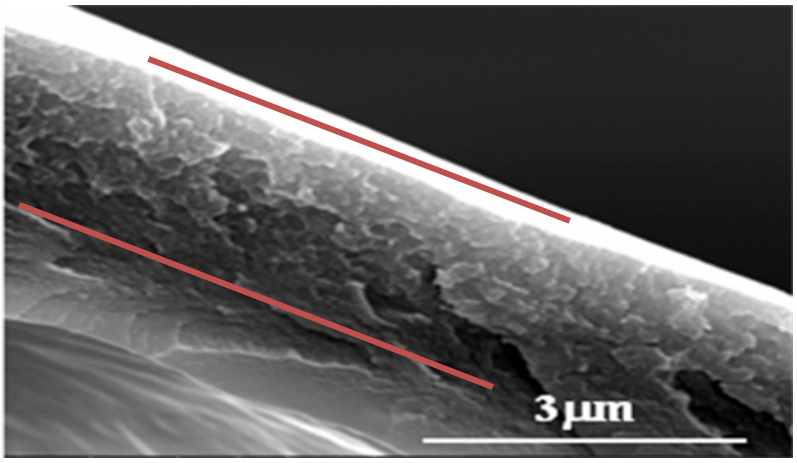

(a)

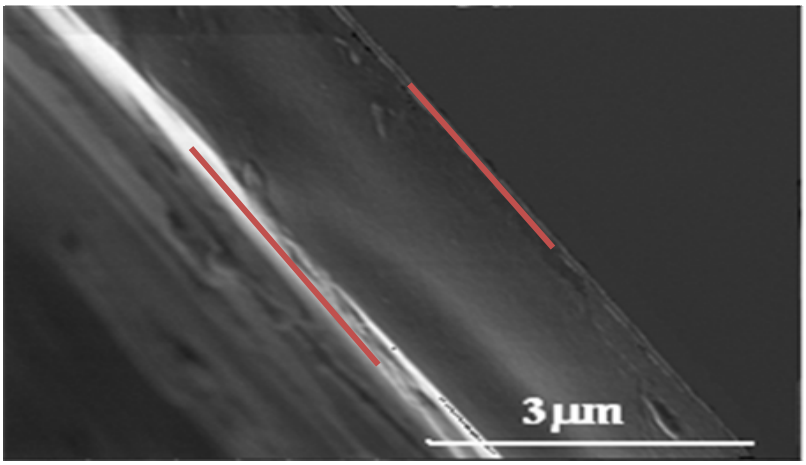

(b)

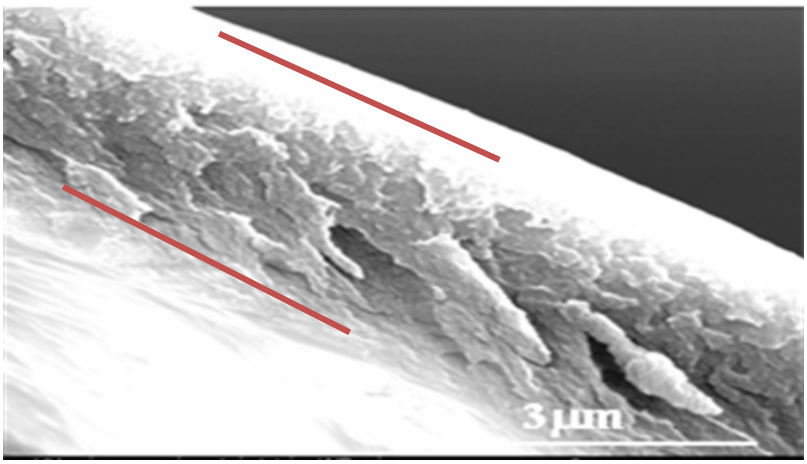

(c)

Figure 4.12 SEM images of cross-section microstructure for the crosslinked BSA membrane with (a) TCL, (b) IDCL and (c) SCL crosslinker

4.6.3 Membranes' thickness with different crosslinking agents

For BSA with TCL, IDCL and SCL membranes, thickness was found to be 11 μm, 26 μm and 12 μm respectively after 5 min crosslinking. The thickness was found to increase to 36μm, 37μm and 33μm respectively at 1 hour. After that the growth rate becomes smaller for all membranes as shown in figure 4.13. The thickness of TCL, IDCL membrane was found to have only had a small degree of extension after considerably extended crosslinking periods, *viz* 62μm and 66μm at 12 hours and 73μm and 80μm at 72 h. This indicated that the BSA membrane forming reaction was crosslinking reagent limited due the diffusion barrier to it imposed by the membrane crosslinking process itself. With the crosslinker SCL, there is a slightly different (Fig.4.13b) growth rate when compared with TCL and IDCL. This suggests that SCL can provide more permeability for crosslinking matured types of protein.

TCL and IDCL have a similar chemical structure. There are two chlorocarbonyls with benzene. SCL is a di-acyl chloride, after crosslinking the membrane with TCL and IDCL always showing more compact surface structure.

The fibrinogen with TCL and IDCL membrane had a thickness of 20 μm after 5 min crosslinking. These thicknesses increased more significantly with extended

crosslinking time, reaching 107 μm, 103 μm at 12 h and 299 μm, 344 μm at 72 hours.

With the crosslinker SCL the growth rate seems slower. The thickness from 18 μm after 5 min crosslinking reaches to 46 μm at 12 hours and 356μm at 72 hours. That may because of the structure of the crosslinked membrane is less strong than other membrane (showing more porous structure), but after increasing the crosslinking time, there was more crosslinking happening within the membrane, so the membrane subsequently had become reinforce with more crosslinked protein and so stronger.

Compared with the two different proteins, the results above suggested a greater permeability for the fibrinogen to the reacting crosslinking species than observed with the BSA. That may have been because of the different structure of the proteins. Bovine serum albumin (BSA) is a globular protein (66,000 Da) with an essential amino acid profile. Earlier publications on the BSA structure suggested the structure of BSA to be an oblate ellipsoid with dimensions of 140 × 40Å. Fibrinogen is a larger protein (340,000 Da) than BSA. It comprises a dimmer, and each subunit is an elongated molecule; the long axis size is 47.5nm±2.5. Fibrinogen has a trinodular structure (Fig. 2.4, Domains D,E,D). Central module is 5 nm in diameter and another two nodules are 6.5nm in diameter, referred to as terminal domains. So after crosslinking, the larger linear protein fibrinogen showing more permeability than the globular BSA.

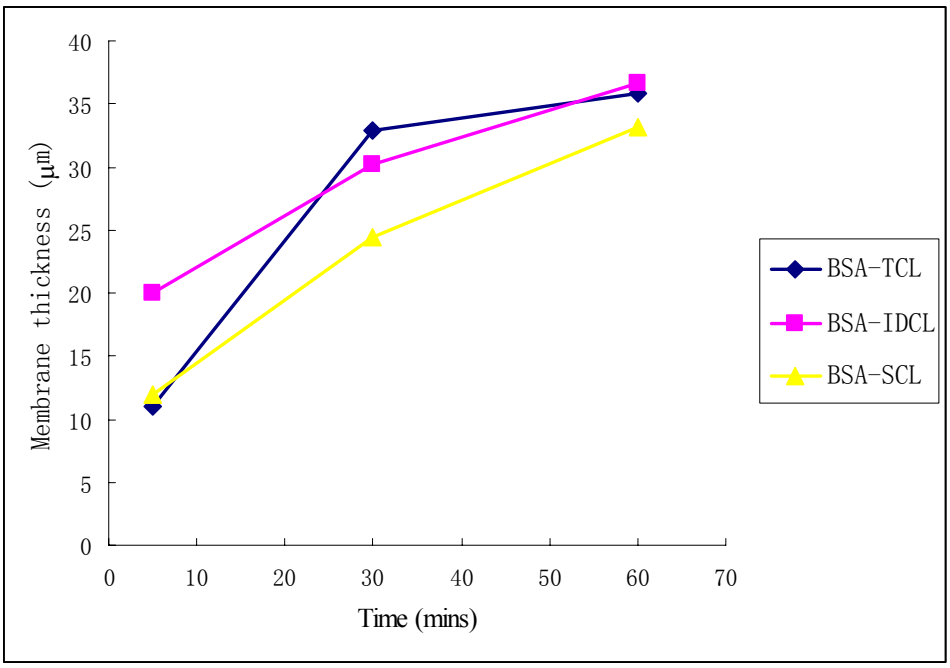

(a)

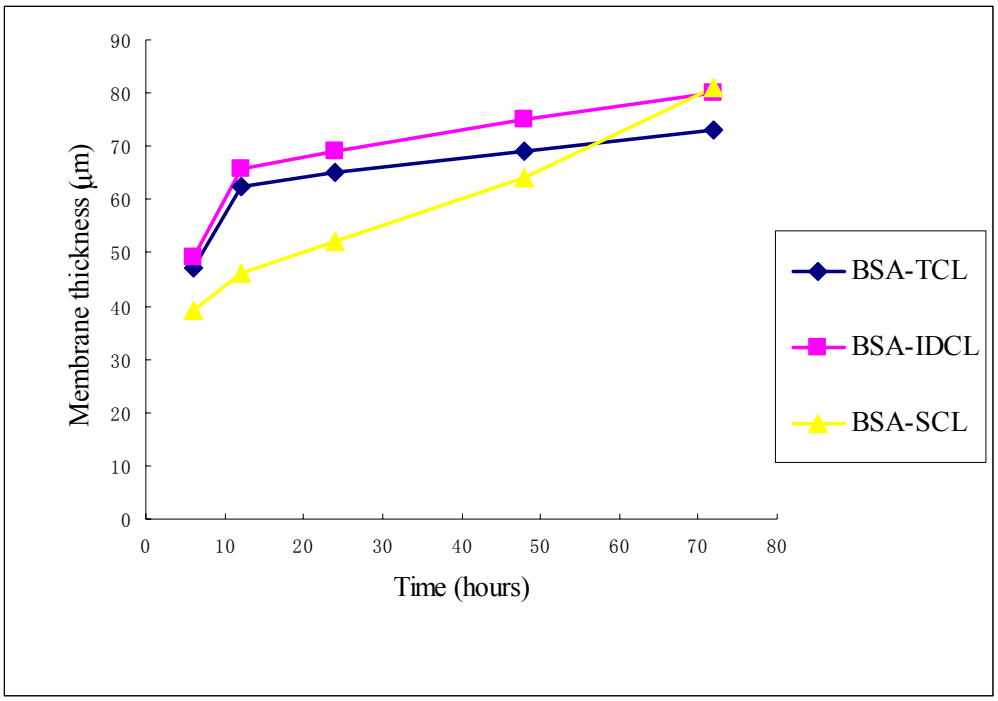

(b)

Figure 4.13 Thickness of crosslinked BSA membrane growing with time (a) membrane grow time from 5 mins to 60 mins, (b) membrane grow time from 6 hours to 72 hours

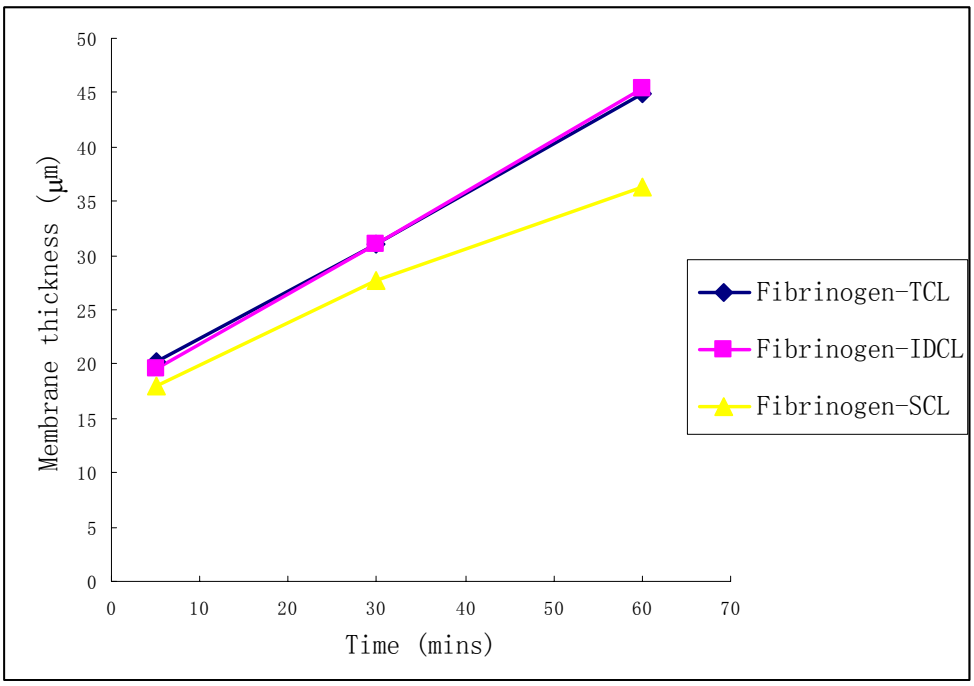

(a)

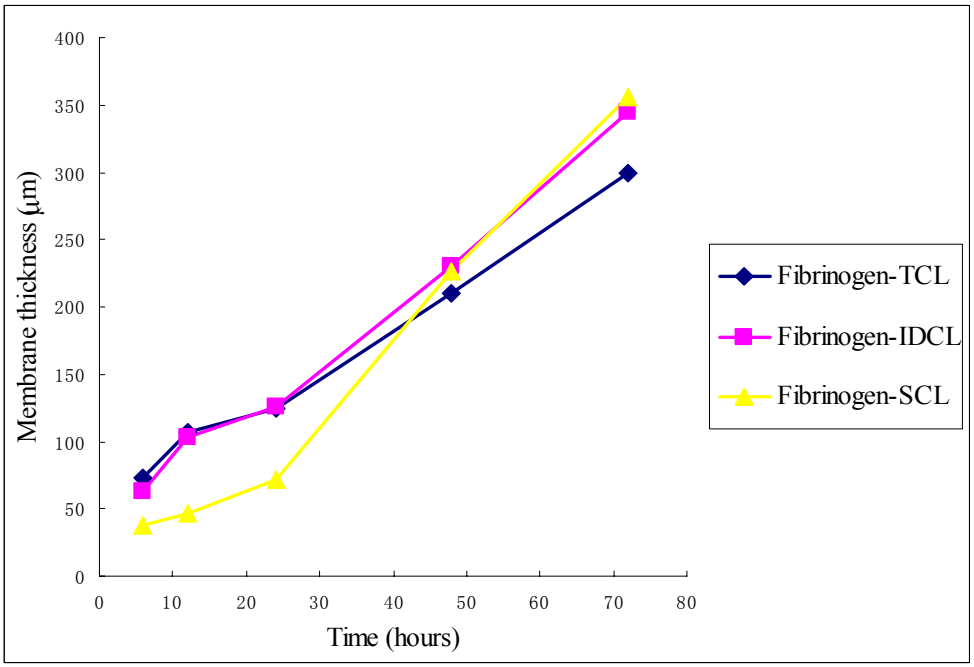

(b)

Figure 4.14 Thickness of crosslinked fibrinogen membrane growing with time (a) membrane grow time from 5 mins to 60 mins, (b) membrane grow time from 6 hours to 72 hours

4.7 Crosslinked copper protein membranes characterization

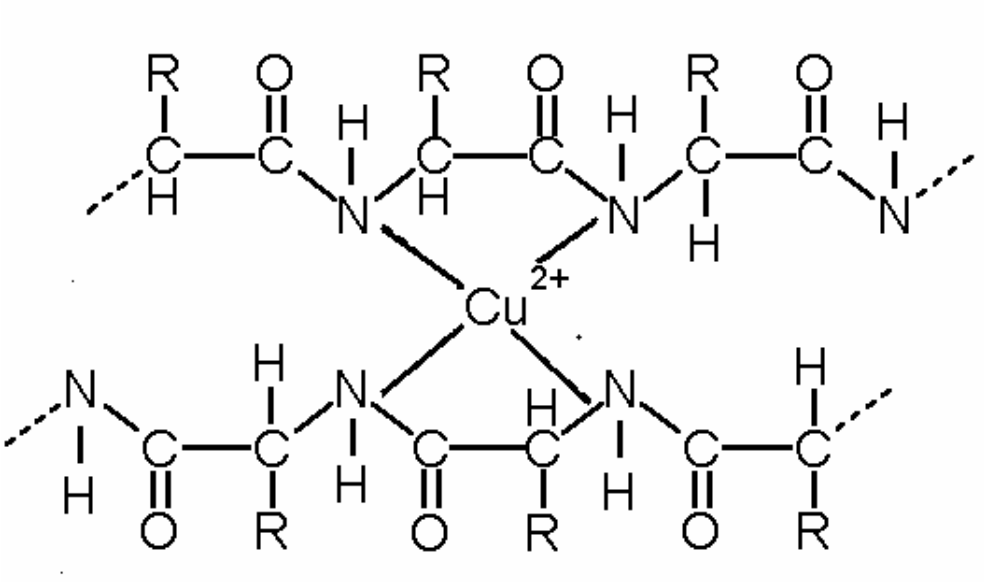

Figure 4.15 Structure of copper protein

4.7.1 Surface structure of crosslinked copper protein membranes (SEM)

4.7.1.1 Surface structure of crosslinked copper fibrinogen membrane

By adjusting the ratio of copper in the protein membrane it proved possible to manipulate membrane morphology. Figure 4.16 shows the surface morphology of the fibrinogen crosslinked membrane and the fibrinogen membrane which was exposed in to 250mM $CuSO_4$ solution for 30sec, 1min, 5mins, 10mins,

30mins, 1hour, 2hours and 24hours respectively. Figure 4.16a shows the morphology of the crosslinked fibrinogen membrane, demonstrating a relatively dense structure with quite small pores (marked by a red ellipse). As seen in Figure 4.16b, after exposing to $CuSO_4$ solution for 30 second, the morphology of the membrane shows noticeable changes. A gradual morphological transition can be found with increasing exposure time. The nanoporous surface was formed with an arrangement of irregularly shaped aggregaties. As seen in Figure 4.16d, a hierarchical porous structure was observed on the membrane surface when the exposure time increased to 5mins. The nanopores (marked by a red ellipse) were about 100 nm to 300nm in diameter and regularly distributed on the membrane. However, by increasing the exposure time to 2 hours, the pores size increase to between 700nm and 1μm. After 24 hours the arrangement of these nanopores were formed more regularly with the diameter of around 1μm (Figure 4.16i). The result indicates that the porous structure evolved gradually when the copper content increased in the membrane. As Cu^{2+} is known to induce combination aggregation of proteins [142], the structure change may have been because the copper (II) ions formed a coordination complex with four nitrogen atoms involved in peptide bonds as Fig 4.15 showing. With copper content increasing, more peptide bonds from the protein start crosslinking with the copper ion and aggregating. So the fibrinogen membrane becomes more rigid, and also possibly the copper ion induced fiber packing that is localised together (Fig 4.17), so as to generable porous structure.

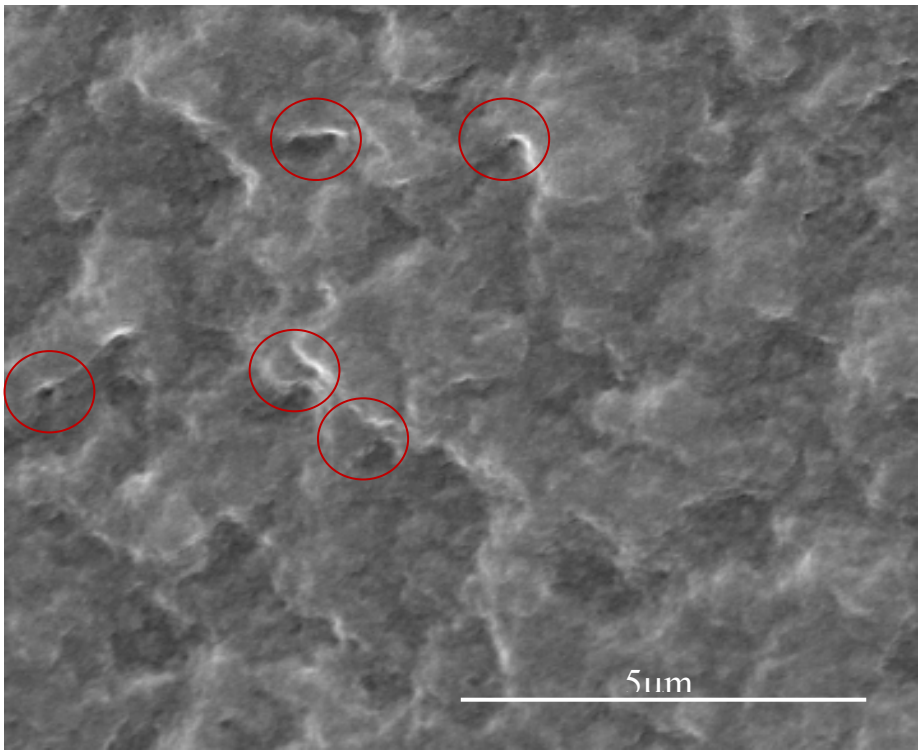

(a)

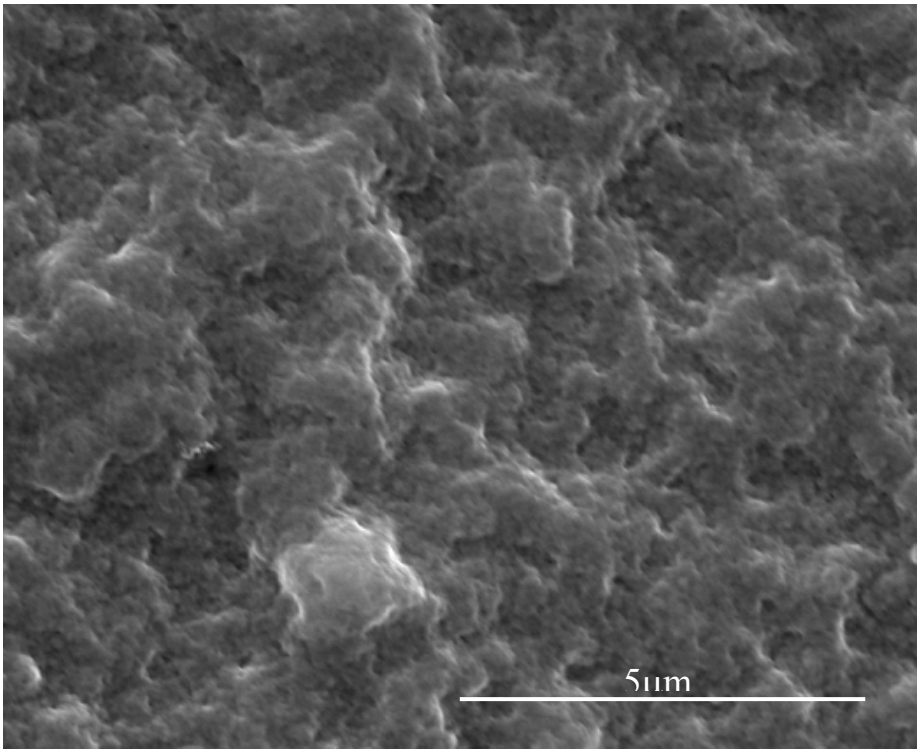

(b)

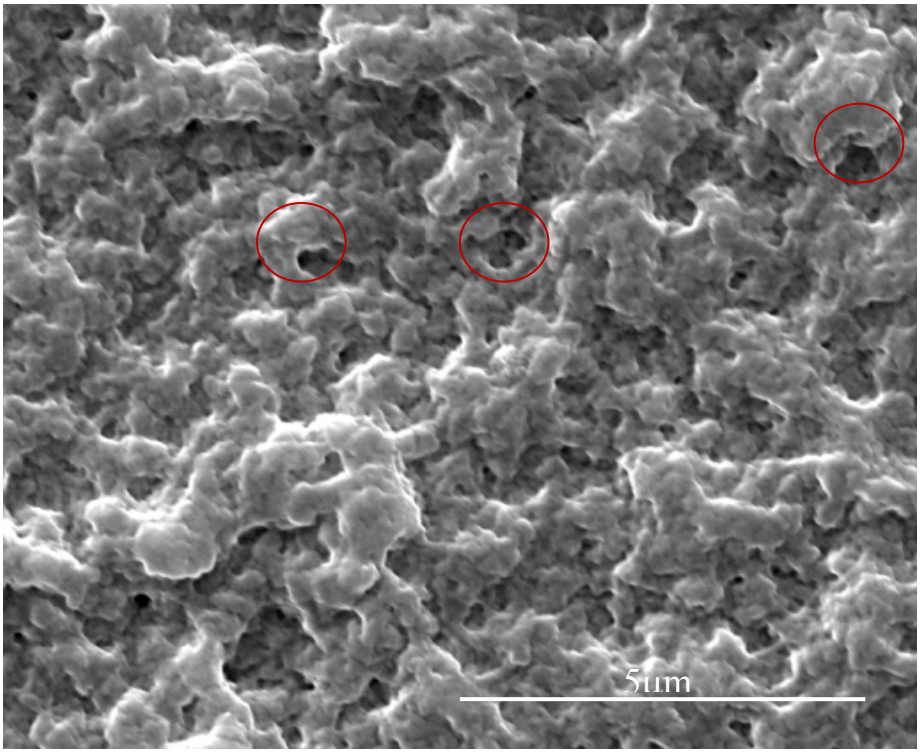

(c)

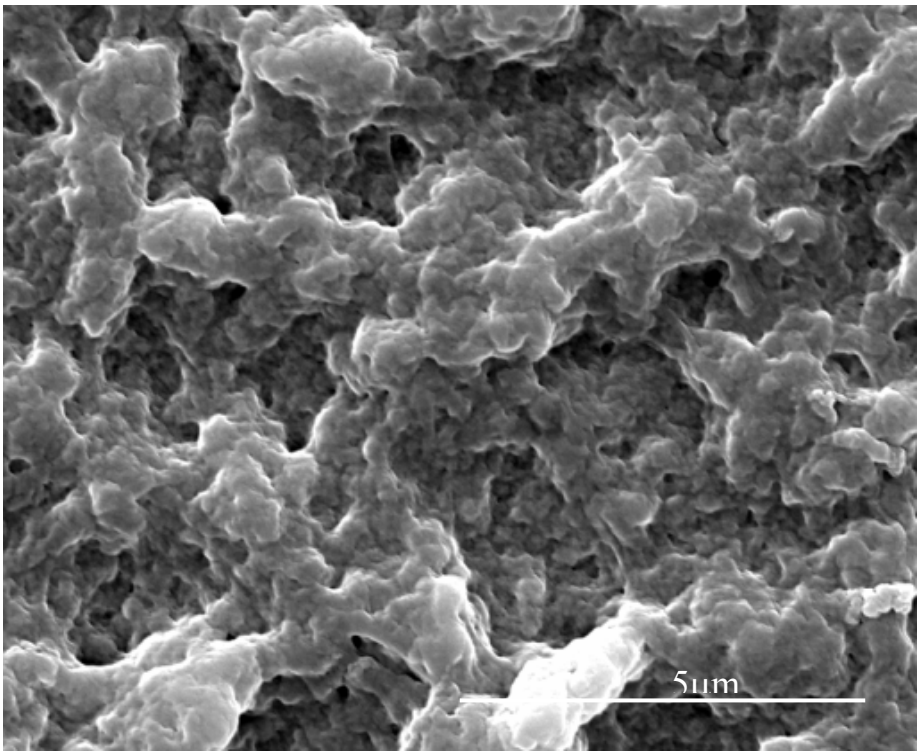

(d)

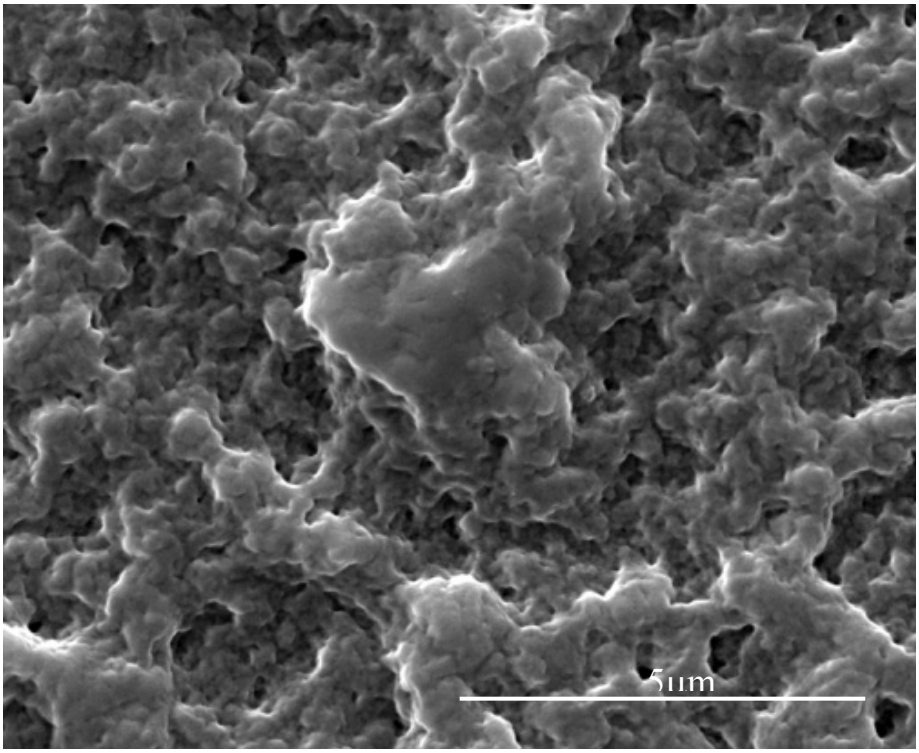

(e)

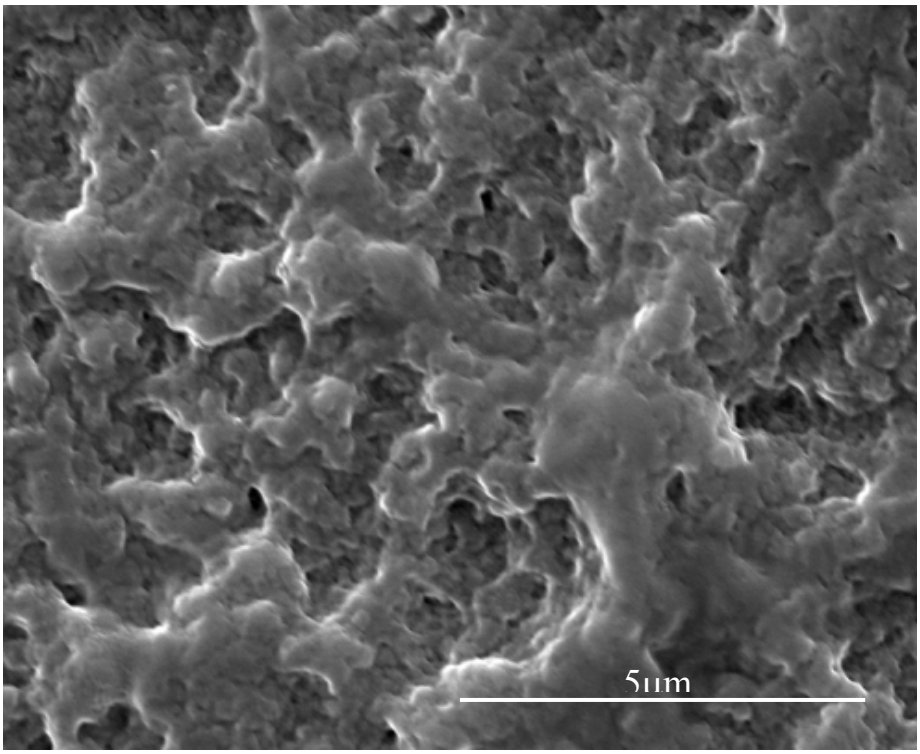

(f)

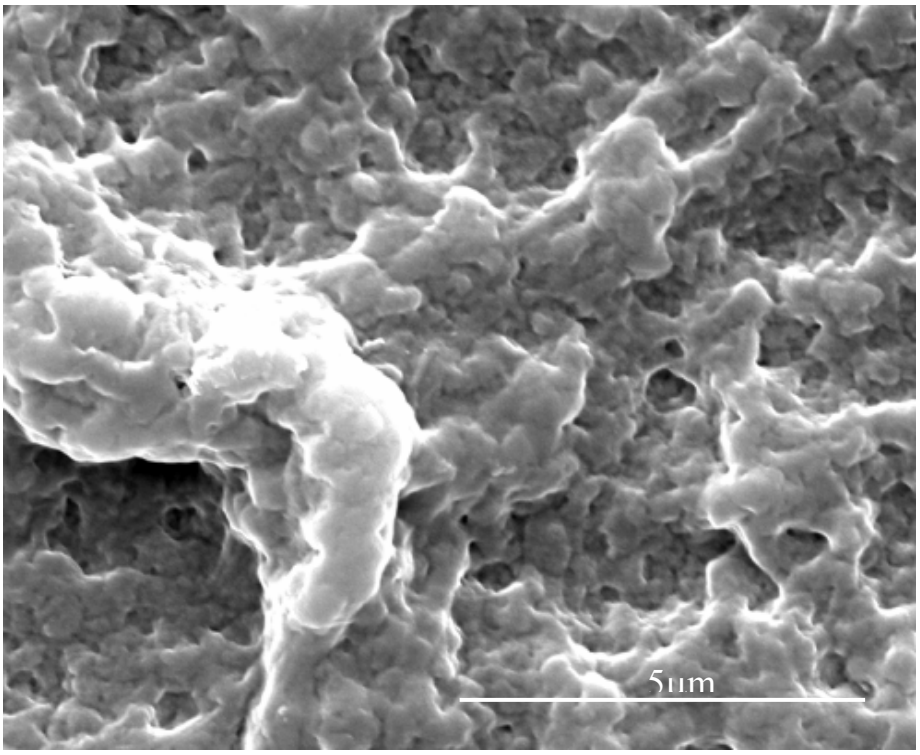

(g)

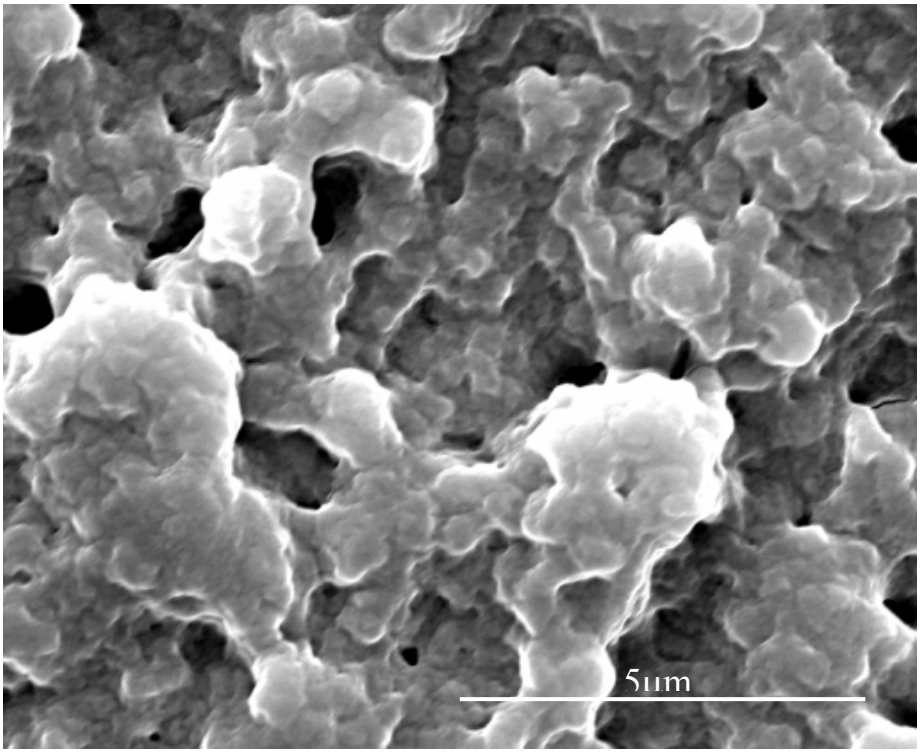

(h)

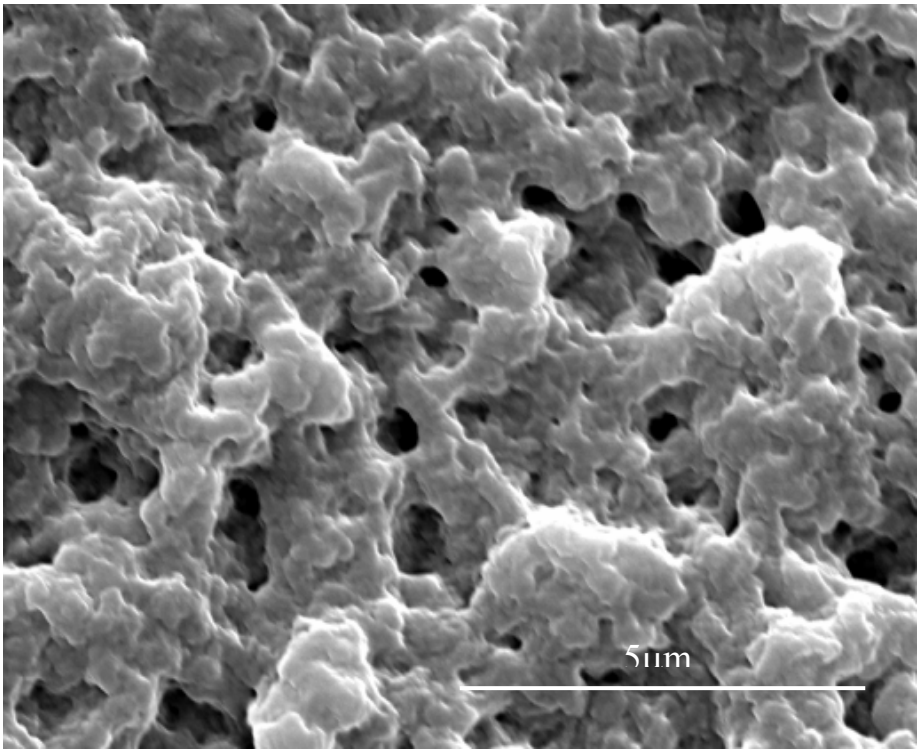

(i)

Figure 4.16 SEM images of microstructures of crosslinked fibrinogen membranes exposed in $CuSO_4$ solution for (a) 30sec, (b) 1min, (c) 5mins, (d) 10mins, (e) 30mins, (f) 1hour, (g) 2hours and (i) 24hours

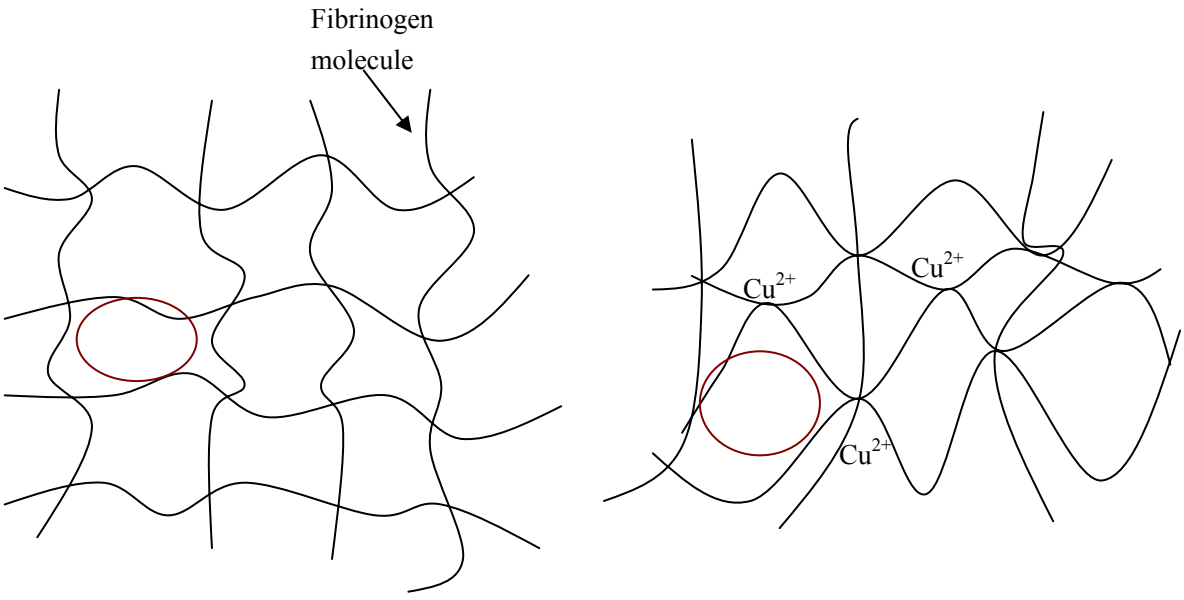

Figure 4.17 Fibrinogen membrane with copper images

4.7.1.2 Surface structure of the crosslinked copper BSA membrane

Figure 4.18 shows the surface morphology of the BSA crosslinked membrane and the BSA membrane exposed to 250mM $CuSO_4$ solution for 30sec, 1min, 5mins, 10mins, 30mins, 1hour, 12hours and 24hours respectively. Figure 4.18a shows the morphology of the crosslinked BSA membrane, a smoother and more homogeneous porous surface was observed with a superficial pore size of around 50nm (marked by red ellipse). After the membrane expose in $CuSO_4$ solution, a gradual morphological transition can be found with increasing expositive time. Figure 4.18b shows after 30seconds the membrane surface becomes rougher. Different from the fibrinogen membranes of Figure 4.18 (b, c d, e, f, g) showing , there was no difference with the pore size in the membrane surface when increasing the exposure time from 30 seconds to 1 hour, just the membrane surface become more roughness. As seen in Figure 4.18 (h, i), after exposure to $CuSO_4$ solution for 12hours, the membrane surface became more porous, and after 24 hours the morphology of the membrane showed noticeable changes, the surface becoming uneven and more porous.

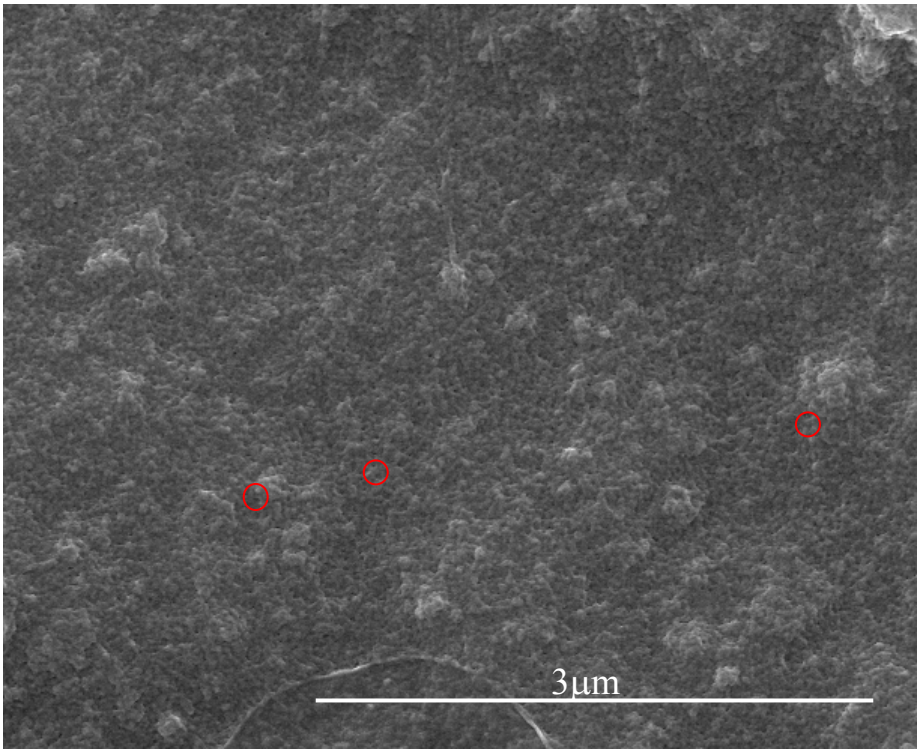

(a)

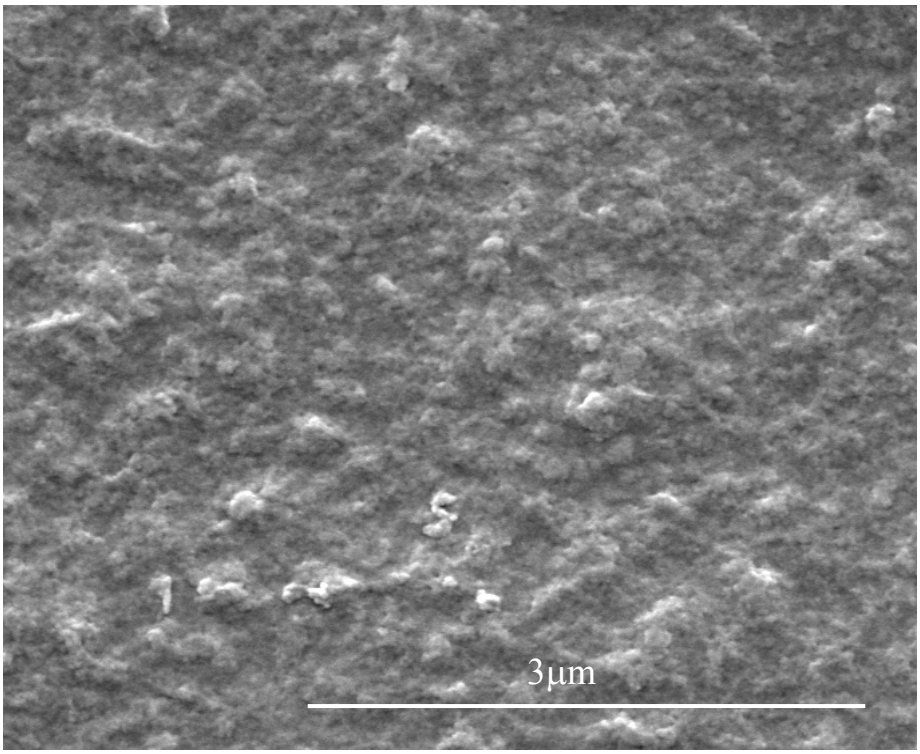

(b)

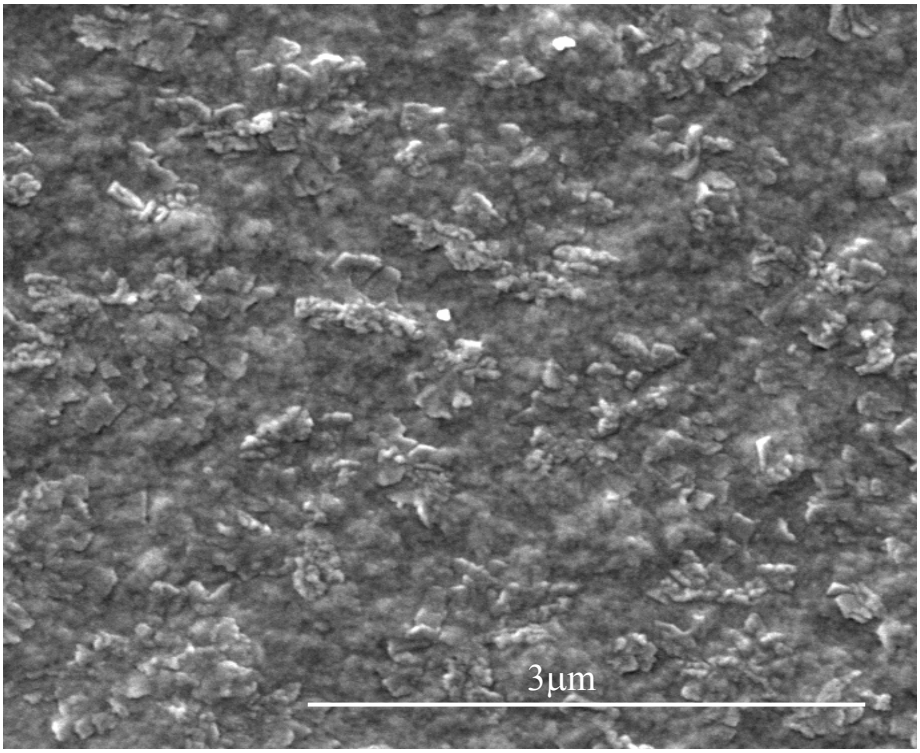

(c)

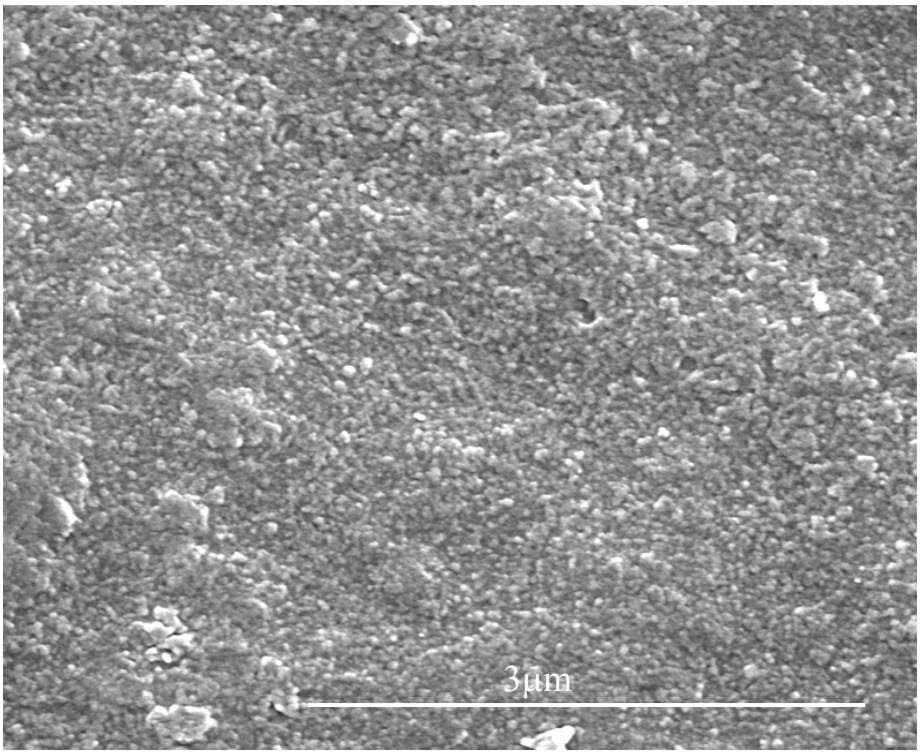

(d)

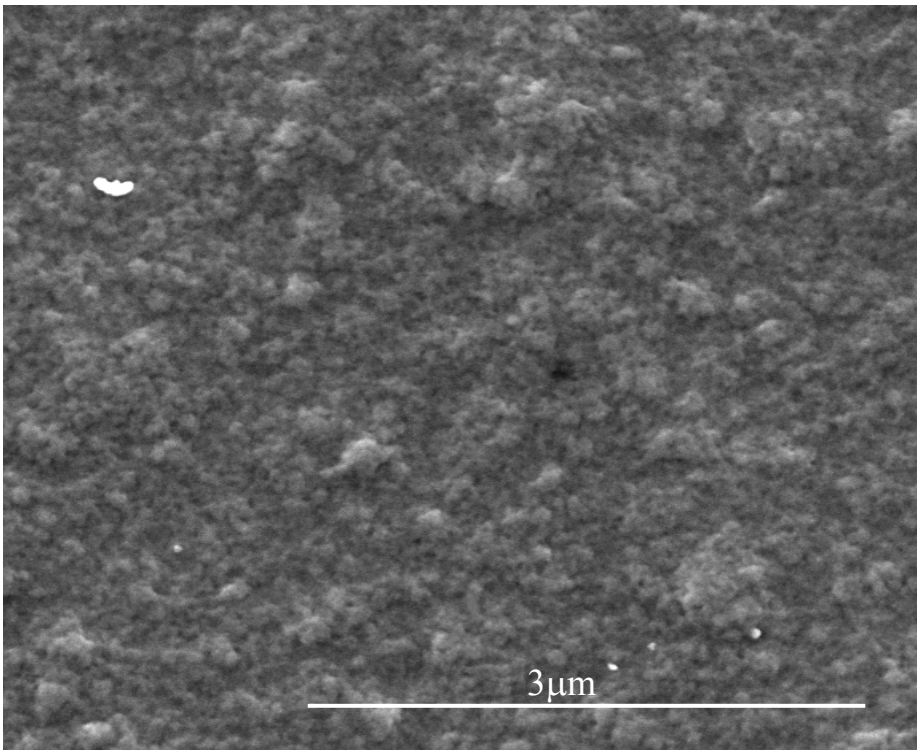

(e)

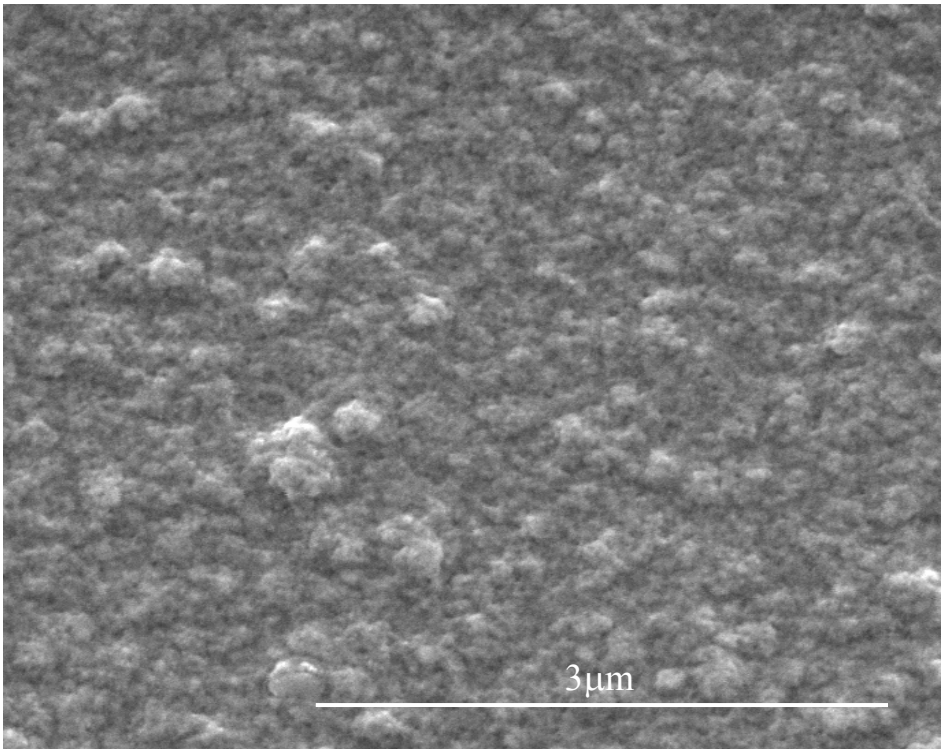

(f)

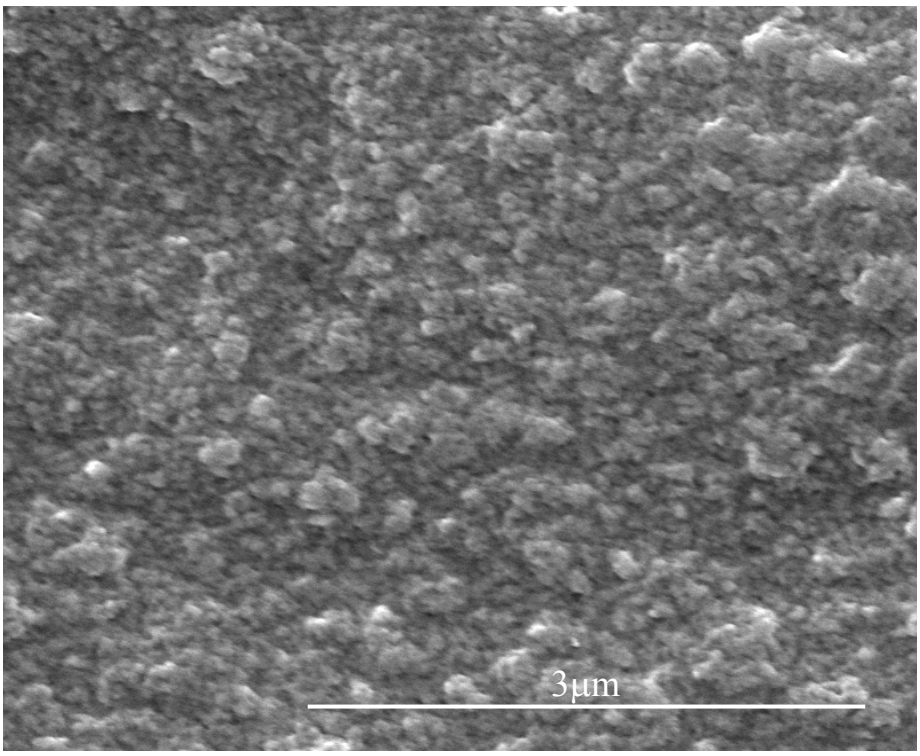

(g)

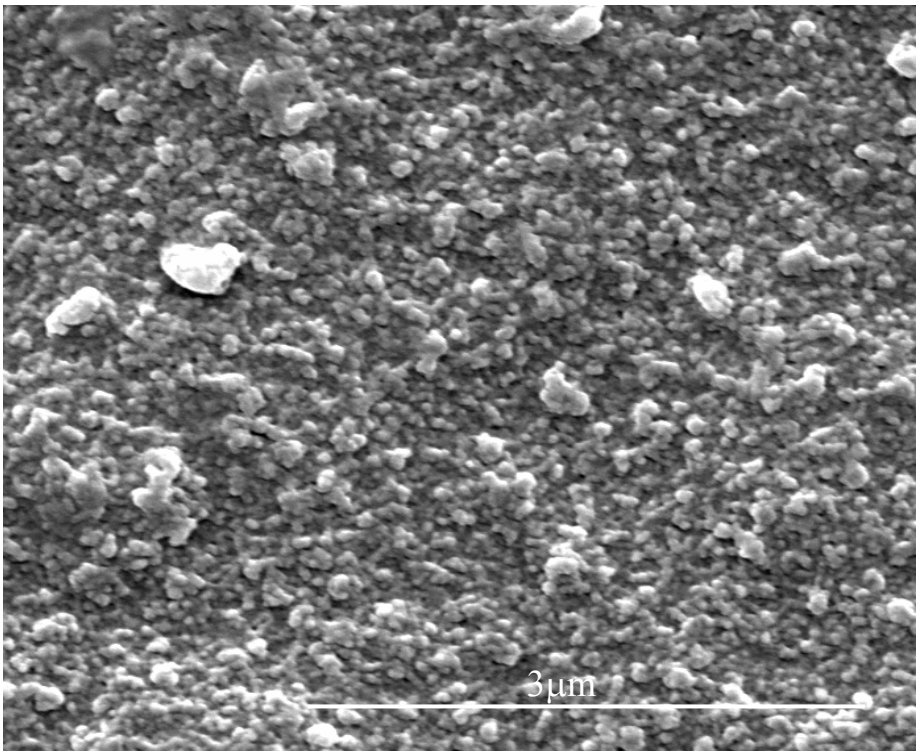

(h)

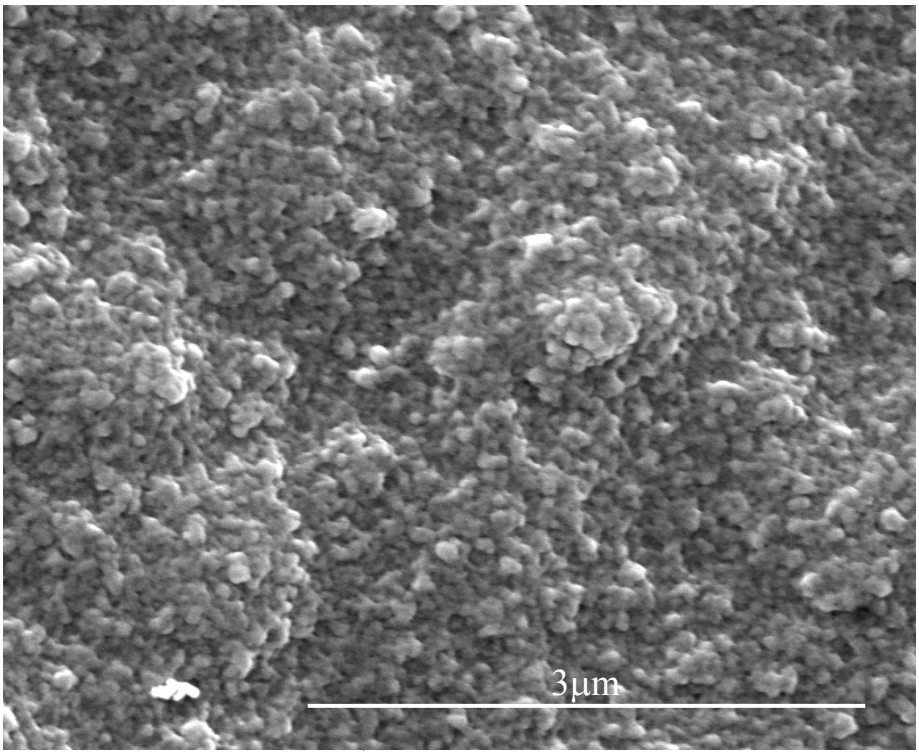

(i)

Figure 4.18 SEM images of microstructures of crosslinked BSA membranes exposed in $CuSO_4$ solution for (a) 30sec, (b) 1min, (c) 5mins, (d) 10mins, (e) 30mins, (f) 1hour, (g) 12hours and (i) 24hours

4.7.2 Energy-dispersive X-ray spectroscopy (EDS) test

There was gold coating on the samples, so spectra also showed Au (not mentioned in below table), the total amount is 100 (all results in weight %).

Table 4.1 The amount of copper compared with carbon in copper fibrinogen membranes with the exposing time increased

Spectrum	C	O	Cu	Cu/C
plain	56.25	22.86		
30sec	56.73	24.68	2.24	3.9%
1min	55.09	25.62	2.73	4.96%
5mins	55.69	23.03	3.17	5.69%
10mins	57.11	21.91	3.19	5.59%
30mins	61.25	35.20	3.55	5.8%
1 hour	62.08	33.92	4.0	6.44%
2 hours	62.88	32.62	4.50	7.16%
24 hours	59.83	35.06	5.11	8.54%

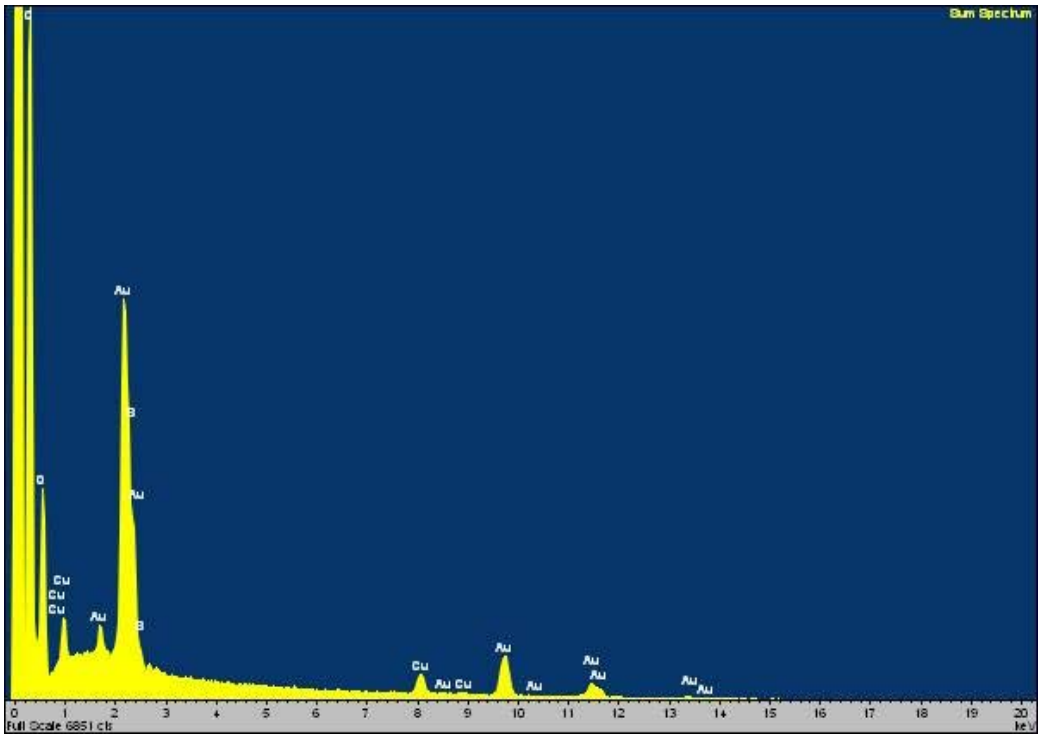

Figure 4.19 EDS profile of copper fibrinogen membrane

Element analysis of samples was undertaken using EDS. EDS (Fig 4.19) of the copper fibrinogen membrane confirms the presence of copper. Excess of gold is due to the coating used during analysis. Table 4.1 shows the weight percent of copper compared with carbon. Around 3.9% (w/w) of copper was present in the 30s sample. That means the reaction between copper (II) and the protein is rapid, happening within 30 seconds. After 1min around 5% of copper was present, the rate of copper (II) absorption slowed compared to the first 30 seconds. After 48 hours there was 8% of copper in the protein membrane. The EDS analysis showed the presence of the copper to be time dependent, which means that control over copper treatment is possible.

4.7.3 FTIR analysis

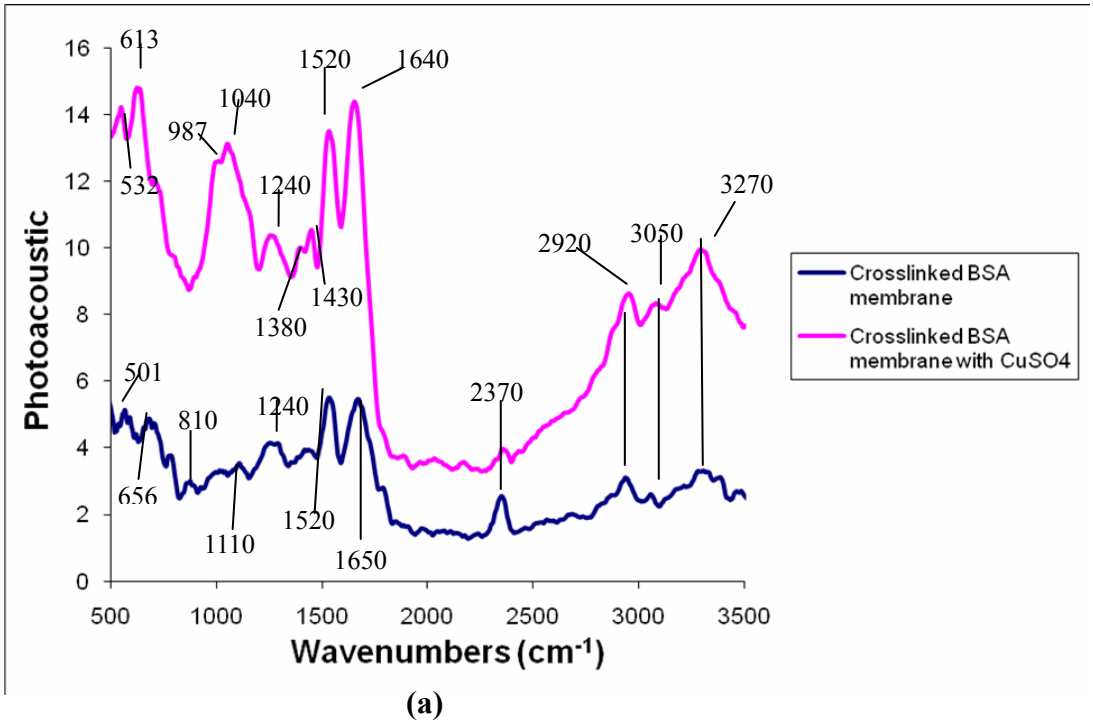

(a)

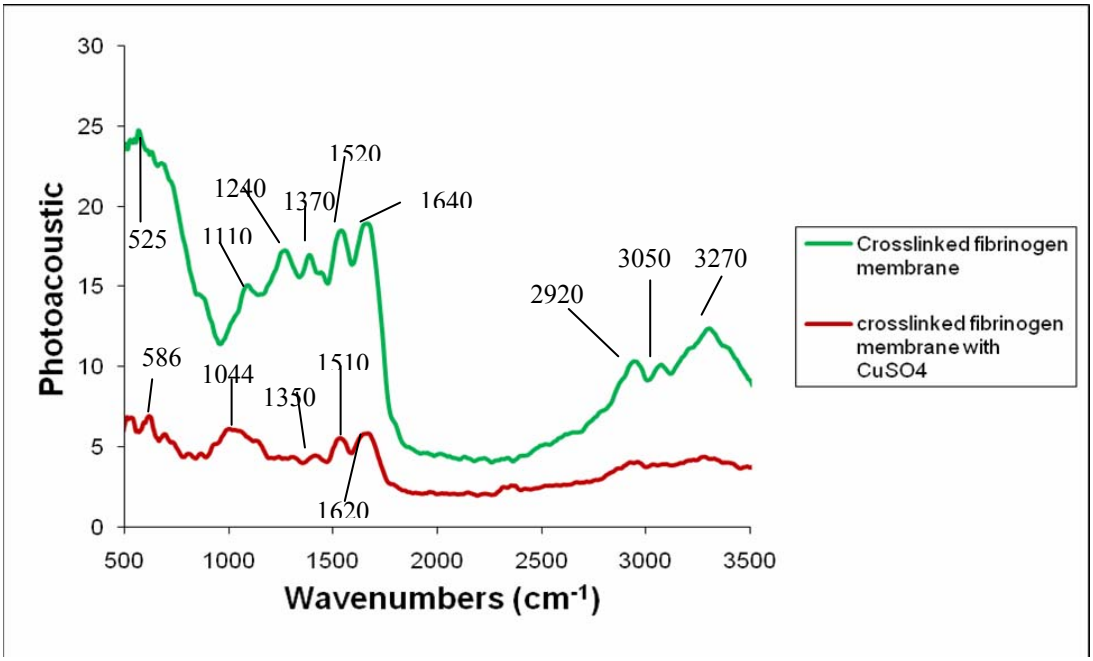

(b)

Figure 4.20 FTIR of (a) BSA membrane compare with BSA copper membrane (b) fibrinogen membrane compare with fibrinogen copper membrane

Table 4.2 Chemical bands for crosslinked membranes

Wavenumber (cm^{-1})	Assignments
3270	N-H binding
3050	C-H stretching
2920	C-H stretching
1640-1650	Amide I, α˜-Helix
1620	Amide I, β-Sheet
1510-1520	Amide II, N-H bending vibration/C-N stretching vibration
1350-1380	$N(CO_2)$ sym. stretching, CH_3 sym. Def.
1240	Amide III, C-N stretching vibration/N-H bending vibration
1110	HPO_4^{2-}
1040-1044	$N(SO_4^{2-})$ asym. stretching

Figure 4.20 shows FTIR for a BSA membrane and a BSA membrane treated with $CuSO_4$. A suggested spectral band spectrum is given in Table 4.2 based on the literature data published by Socrates [143] and in Aldrich Library.

The observed vibrational bands can be attributed to the following modes: 1620 cm^{-1}, amide I of the β-sheet; 1650 and 1640 cm^{-1}, amide I of the α-helix;

1240cm^{-1}, the amide III band of the β-sheet; 1040 and 1044 cm^{-1}, ν(SO_4^{2-}) asymmetric vibrational modes of the sulfates. The bands below 900 cm^{-1} are difficult to interpret since this part is very variable.

With the BSA membrane some spectral changes were seen after treating the sample with $CuSO_4$. Thus, there was a minor difference in the secondary structure amide I region (1650 cm^{-1}), it was enhanced compare with the amide II band (1510-1520cm^{-1}), and in the lower wave number region (1000–1200 cm^{-1}), where the characteristic SO_4^{2-} bands appear. This situation can be explained by the fact that the crosslinked BSA structure is changed by $CuSO_4$. The emerging SO_4^{2-} bands in the double subtracted spectra suggest that SO_4^{2-} is also coordinated to the proteins. An extra amount of HPO_4^{2-} is detected (1110 cm^{-1}), which could have originated from PBS. The very clear and medium-intensity feature at 2370 cm^{-1} points to the CO_2 mode. The other weak bands are interpreted as characteristic spectral features of different amino acids (Phe, Trp and Tyr) of proteins.

With the fibrinogen membrane the FTIR measurements yielded slightly different results (Fig. 4.20b). For these samples, after the membrane had been treated with $CuSO_4$, the same secondary changes in the peptide structure were seen. The relative intensity of the major band characteristic of the amide I α- helix was at 1640 cm^{-1} was changed to β-sheets at 1620 cm^{-1}. The relative intensities of the bands at 1240 cm^{-1} were decreased with the $CuSO_4$ fibrinogen membrane. Also,

some more changes involved the bands at 3270 cm^{-1} (N-H binding), 3050 cm^{-1} (C-H stretching) and 2920 cm^{-1} (C-H stretching); there become weaker. The weak sulphate features were also apparent in the lower wavelength region (1200–1000 cm^{-1}), but these bands were weaker than were those obtained in the BSA membrane spectra (Fig. 4.20a).

4.8 Summary

The morphology of BSA and fibrinogen crosslinked membranes can be examined by using SEM. The aqueous and organic solution supply sides of the membranes exhibited different morphologies, due to the directional difference in reactive solute diffusion. Discrete pores were observed at both fibrinogen and BSA membranes, but the fibrinogen membranes showed a greater ridge structure. pH and ethanol protein treatment had an effect on resultant membrane permeability and this suggests that pre-formation protein status influences final outcome.

Both BSA and fibrinogen can be formed successfully with different crosslinking agents, but the crosslinked protein membranes obtained very different structured morphology. These results could be rationalized on the basis of crosslinker structure. The thickness of the membranes also mainly depends on the permeability of the developing membrane structure. Fibrinogen and albumin membranes need to be compared before and after exposure copper sulphate

solution. Membranes exposed to copper appeared stronger, and changes in the membrane structure appeared after copper treatment. SEM images indicate that there was some clear time dependent increase in surface porosity. EDS analysis showed fixed the presence of the copper in the membrane to be time dependent, from about 4% (30sec) to about 8% (24hours). This means that control over the copper treatment is possible. A large reactive mass of copper could be introduced into membranes and was readily retained.

Chapter5: Mechanical Properties of BSA and Fibrinogen Crosslinked Membranes

5.1 Introduction

This study aimed to treat the membranes as an entire entity and test it as a material. Its mechanical properties gave it a measure of what the strength of the material made was which can give an indication as to where it compares to other materials. To test the mechanical properties of a membrane which is micrometres thick specialised method have to be implemented. Nanoindentation has been a chosen method for membranes of similar dimensions. Through testing both of the protein membranes in different conditions sensible assumptions and conclusions can be made as to what mechanical properties the films possess.

The aim and objective of the is project was to plan an experiment, execute the experiment, process the data, analysis the data and draw conclusions on the mechanical properties of the crosslinked membranes. The mechanical properties of interest were modulus of elasticity (E), instantaneous shear modulus at zero time (G_0), the shear modulus at infinity ($G\infty$) and the creep ratio (C_r). The project reviewed the current knowledge on the new films, how they were made and possible uses. Investigate the nanoindentation method of how to test them and what can be expected from this type of testing. Process the data and create

useful ways of displaying the data. The data was critically analysed and conclusions made form this analysis.

5.2 Nanoindentation test for crosslinked protein membranes

Table 5.1: Averages of all films for modulus of elasticity (E), instantaneous shear modulus at zero time (G_0), the shear modulus at infinity (G_∞) and creep ratio (C_r).

Membrane	E (GPa)	G_0 (GPa)	G_∞ (GPa)	C_r (0-1)
Fibrinogen-IDCL	1.48	0.0624	0.0609	0.02405
Fibrinogen-TCL	1.75	0.20056	0.08992	0.551657
Albumin-IDCL	1.561	0.08167	0.077267	0.053911
Albumin-TCL	2.13248	0.09756	0.08017	0.91783

5.2.1 Modulus of Elasticity

Both protein membranes were tested in the wet condition (keep moisturizing with PBS). With fibrinogen membranes, the elastic modulus increased by 0.27 GPa when comparing the crosslinker IDCL and TCL. While albumin membranes had a greater increase of 0.57 GPa when comparing the crosslinker to TCL. In both crosslinker the TCL crosslinked proteins are significantly stiffer.

Overall the TCL albumin membranes had the greatest modulus of elasticity with an average value of 2.13 GPa (Table 5.1), the smallest modulus of elasticity was 1.48 GPa belonging to the IDCL fibrinogen membranes. From these values the modulus of elasticity varied from a range of 0.65 GPa.

5.2.2 Shear modulus at zero time (G_0) and infinite time ($G\infty$)

The G_0 for both albumin and fibrinogen membranes were greater with TCL crosslinker. The fibrinogen membranes had more significance changes with TCL and IDCL than Albumin. The largest value was TCL fibrinogen membrane with a G_0 of 0.201 GPa and the smallest value was 0.0624 GPa for the IDCL fibrinogen membrane. The range of the averages was 0.138GPa.

At $G\infty$, the TCL fibrinogen membrane would have the greatest value of

0.08992GPa which is significantly more than IDCL fibrinogen membrane which would be 0.0609GPa. The TCL albumin membrane with a G_∞ 0.08017GPa has a slightly greater value $0.02x10^8$GPa than that of the IDCL albumin membrane. There was no significance change between them.

The difference between the G_0 and G_∞ gives a concept of how time plays a role in the creep of the protein crosslinked membranes. So if the material could creep for infinity, it is a value of what would the shear modulus value be. In the same concept if creep could be measured at zero time. The membranes have different values when they begin to creep, and what would be infinity. The difference between the membranes (Table 5.1) seen to have a positive correlation where the greater the G_0 the higher the G_∞. This would imply that the membranes which have a large shear modulus from the start will still maintain the momentum and have a larger shear modulus compared to the others. This seems to be the case in both crosslinked fibrinogen and albumin membranes.

5.2.3 Creep Ratio

The creep ratio is designed to determine how much elastic or viscous the viscoelastic membranes are. All the membranes were closer to 0 meaning they are more elastic than viscous. The IDCL membranes were more elastic than the TCL membranes in both cases of the proteins. The TCL albumin membranes had the most viscous properties compared to the other films with a ratio value of

0.918. The most elastic membrane was the IDCL fibrinogen membrane its value of 0.024 was the closest to 0. There is extreme difference between two different crosslinker of the protein membranes.

5.2.4 Comparisons between the crosslinkers

The shear modulus at infinity and creep ratio between TCL proteins and IDCL proteins had great difference. The TCL protein membrane was predicted to have a higher shear modulus at infinity than the IDCL protein membrane. As the TCL protein membrane was suggested to possess more viscous properties than the TCL protein membranes (Table 5.1), this would imply that the shear modulus at infinite time is higher in more viscous membranes. The ratio of elastic to viscous properties in the film effect the films a manner which the more viscous membrane has greater GPa in the case of E, G_0 and G_∞ . This implies that the less elastic the film is the greater the mechanical properties. The variance in creep ratio was proven to be significant.

5.2.5 Comparisons between the proteins

Albumin produces a more rigid membrane when crosslinked with TCL and IDCL than fibrinogen. This could be due to albumins globular structure allowing crosslinking sites within the entanglement of the protein. Albumin is used to

harbour components within its molecule for transportation purposes. This function as well as the presence of many functional reactive groups along the polymer chain can be an explanation as to why the crosslinked albumin membrane showing more tense polymerisation structure. Fibrinogen in comparison is a much larger molecule which has given a less rigid mechanical property after crosslinking compared to albumin.

The aim of crosslinking is to control and enhance the properties of the monomer alone, in this case the albumin or fibrinogen. These crosslinked protein membranes have done this successfully. The mechanical properties are defined by the different crosslinker which plays an important role in how the crosslinked proteins behave.

5.3 Nanoindentation test for crosslinked copper protein membranes

There are three membranes crosslinked fibrinogen membrane, crosslinked fibrinogen with copper membrane and crosslinked albumin with copper; they are tested in wet and dry conditions. Crosslinker is terephthaloyl chloride (TCL).

Table 5.2 Averages of all membranes in wet condition for modulus of elasticity (E), instantaneous shear modulus at zero time (G_0), the shear modulus at infinity (G_∞) and creep ratio (C_r)

Membrane	E (GPa)	G_0 (GPa)	G_∞ (GPa)	C_r (0-1)
Fibrinogen(TCL) + copper	4.55	1.152	0.7681	0.333228
BSA(TCL) + copper	4.51	1.011	0.5876	0.418814
Fibrinogen(TCL)	1.75	0.20056	0.0899	0.551657
BSA(TCL)	2.13248	0.09756	0.00802	0.91783

Table 5.3 The modulus of elasticity values in comparison to other polymers. *Values from W.Callister (2007)

Material	E (GPa)
Fibrinogen(TCL)+copper (dry)	4.92
BSA(TCL)+copper (dry)	5.82
Epoxy	2.41*
Polyester (thermoset)	2.06-4.41*
PVC	2.14-4.14*

Table 5.4 Averages of copper membranes in wet and dry condition for modulus of elasticity (E), instantaneous shear modulus at zero time (G_0), the shear modulus at infinity (G_∞) and creep ratio (C_r)

Membrane	E (GPa)	G_0 (GPa)	G_∞ (GPa)	C_r (0-1)
Fibrinogen(TCL)+copper (Wet)	4.55	1.152	0.7681	0.333228
Fibrinogen(TCL)+copper (Dry)	4.92	1.301	0.9094	0.30155
BSA(TCL)+copper (Wet)	4.51	1.011	0.5876	0.418814
BSA(TCL)+copper (Dry)	5.28	1.517	1.0163	0.330027

5.3.1 Comparisons between the copper membrane with normal membrane

With the comparisons of Modulus of Elasticity, the membranes were tested in the wet condition. With copper fibrinogen membranes, the elastic modulus had a great increase which is 2.8 GPa more than the membrane without copper, while the copper BSA membranes had a slightly less increase of 2.38 GPa compared

with crosslinked BSA membrane. That means the copper crosslinked protein membrane showing great stiffness. With comparisons between the proteins, BSA membranes' modulus of elasticity was 0.38GPa greater than that of the fibrinogen membranes. However the copper fibrinogen membrane becomes stiffer than copper BSA membrane.

With the comparisons of Shear modulus at zero time (G_0) the copper protein membranes were showed much greater than normal protein membranes. Compare with copper BSA the copper fibrinogen membrane had a slightly increase of 0.14GPa. At infinite time ($G\infty$), the copper fibrinogen membrane would have the greatest value of 0.7681GPa which is more than copper BSA membrane which would be 0.5876GPa. As the difference between the G_0 and $G\infty$ gives a concept of how time plays a role in the creep of the protein crosslinked membranes. So both of the copper protein membranes (Table 5.4) seen to have a positive correlation where the greater the G_0 the higher the $G\infty$. This would imply that the copper protein membranes same like the normal protein membranes which have a large shear modulus from the start will still maintain the momentum and have a larger shear modulus compared to the others.

The membranes which creep ratio were closer to 0 meaning they are more elastic than viscous. As table1 showing in the wet condition copper protein membranes were more elastic than the normal protein membranes in both cases

of the proteins. The crosslinked BSA membranes had the most viscous properties compared to the other membranes with a ratio value of 0.918, however after adding copper the creep ratio had a significantly changes to the value of 0.42. The most elastic membrane was the copper fibrinogen membrane its value of 0.33. There is less changes between fibrinogen membranes.

Overall despite the differences in the mechanical properties of all the membranes they both have been triumphant in the crosslinking. Although the precise mechanical properties of the natural proteins are unknown the crosslinked protein has improved greatly from just blood proteins. After expose them in copper solution some of the mechanical properties even enhance more. The copper protein membranes had the greatest modulus of elasticity and they are more elastic than the membrane without copper. Table 5.3 shows that these crosslinked copper protein membranes can be more rigid than some common polymers such as Eproxy, Polyester (thermoset) and PVC. It is known that the metal ion induced formation of a curly fibrillar network [144]. Therefore after exposing the crosslinked membrane in copper solution the membrane was crosslinked one more time.

5.3.2 Comparisons between wet and dry conditions with copper membranes

The membranes were stiffer when they were tested in the dry condition giving each protein an extremely significant comparison between the two conditions. The elastic modulus of the copper fibrinogen membranes increased by 0.37 GPa, while the copper BSA membranes had a greater increase of 0.77 GPa after the transition from wet to dry. In the dry condition the copper BSA membrane's modulus of elasticity was 0.36 GPa greater than that of the copper fibrinogen membrane. Although the elasticity was slightly greater for the copper fibrinogen membrane when dry, the copper BSA membrane is significantly stiffer when wet.

The G_0 for both copper BSA membranes and copper fibrinogen membranes were greater in the dry condition. The copper BSA membrane had more significance between wet and dry conditions than copper fibrinogen. There was no significance between the two proteins in the wet condition. The largest value was copper BSA membrane in the wet condition with a $G_0$of 1.517 GPa and the smallest value was1.011 GPa for the copper BSA membrane in the dry condition. The range of the averages was 0.506 GPa.

At G_∞ , the copper BSA membrane in the dry condition would have the greatest value of 1.0163GPa which is significantly more than fibrinogen in the

dry condition which would be 0.9094GPa. In the wet condition the copper fibrinogen membrane has a 0.18GPa greater value than that of the copper BSA membrane. The difference in the conditions for both proteins is quite different fibrinogen dry has a G_∞ which is 0.124GPa greater than fibrinogen wet. Copper BSA membrane has an even greater difference between wet and dry having 0.43GPa separating the two values. The smallest difference between G_0 and G_∞ is the copper BSA membrane in the wet condition. The membrane with the largest difference between G_0 and G_∞ is the copper BSA membrane in the dry condition

The dry membranes were more elastic than the wet membranes in both cases of the proteins. Interestingly the viscoelastic ratio was almost the same for the copper fibrinogen wet membrane (0.333228) and the copper BSA dry membrane (0.330027). The copper BSA wet membrane had the most viscous properties compared to the other membranes with a ratio value of 0.418814. The most elastic membrane was the copper fibrinogen in the dry condition its value of 0.30155 was the closest to 0.

5.3.3 Effect of hydration on mechanical properties

The way in which water interacts with the membranes makes a considerable difference to the mechanical properties of these membranes. In both cases of the copper protein membranes the presence of water makes the membranes less

rigid the evidence of this is the smaller modulus of elasticity in the wet conditions compared to the dry conditions.

In the case of the shear modulus at zero time the water provides a greater value but in the case of the shear modulus at infinity the presence of water gives a smaller value. This theory applies to both of the protein membranes. The water in the membrane causes the membranes to be more viscous and less elastic. The creep ratio values for copper fibrinogen and copper BSA membranes both display an increase in viscosity (Table 5.4) in the wet condition. The membranes with the most elastic tenancies is the copper fibrinogen membrane in the wet condition with a ratio of 0.314; followed by the copper BSA membrane in the dry condition with a ratio value of 0.33; followed by copper fibrinogen membrane in the dry condition with a ratio value of 0.301. The copper BSA membrane in the wet condition has the least elastic ration with a value of 0.41.

As the water molecules are in between the crosslinks of the membrane this could put a strain on the bonds and cause them to relax slightly. This would allow the membrane to be less rigid and thus have a lower modulus of elasticity than the membrane without water. The presence of water can make two unlike crosslinked proteins such as albumin and fibrinogen behave similarly in the matter of the modulus of elasticity and shear modulus at zero time. So the matter of that they were different proteins had no effect on these properties as they had similar results.

In both protein membranes when in the wet condition the E, G_0 and G_∞ are significantly smaller than the dry counterpart. Thus water has a negative effect on the modulus of elasticity as well as the shear modulus' at zero and infinity time.

5.3.4 Effect of hydration on different protein membranes

In all cases the wet and dry conditions for each protein were significant, the copper fibrinogen membrane overall had better mechanical properties when in the wet condition but only G_∞ was significant. Without the water (dry conditions) the copper fibrinogen membrane is more elastic than the copper BSA membrane. Fibrinogen has five more polypeptide chains than albumin which could have given it the advantage when in the wet condition as there are more bonds to make the film rigid and withstand the interruption of the water molecules. Although being larger does not help the rigidity when in the dry condition. Fibrinogen in its natural form is soluble in water but less than albumin [145]. This could explain why fibrinogen can remain stiffer than BSA in the wet condition.

The mechanical properties are mainly affected by the water content which plays an important role in how the copper crosslinked proteins behave. There is a clear difference in all mechanical properties when they are influenced by water.

5.4 Summary

The membranes produced by interfacial crosslinking with microfludic flow with albumin or fibrinogen used as the protein, and TCL in copper sulphate solution as the crosslinker have been successfully tested to determine their mechanical properties. Nanoindentation using a spherical indenter proved to be an effective way of testing the protein films. These films can now be catered for a use, now they have been tested; their mechanical properties are now known.

BSA produces a more rigid membrane than fibrinogen. The mechanical properties are also affected by the different crosslinker. The IDCL membranes were more elastic than the TCL membranes in both cases of the proteins.

Fibrinogen and BSA membranes have been compared through exposure with and without copper sulphate solution. Membranes exposed with copper appeared stronger.

Changes in the membranes after copper treatment indicate:

(1) Increased stiffness by at lease three fold

(2) Stiffness of two fold greater than that of some commercial polymers (polyester, PVC), also twice higher as commercial epoxy resin

The elasticity modulus of BSA copper membrane in the dry averaged at 5.28 GPa which was higher than the other membranes. The membranes were known

to be viscoelastic but all showed that the ratio was more toward elastic that viscous and even more so when the membranes were dry. The presence of water affected all membranes; their mechanical properties were significantly lower when the membranes were tested in the wet condition. There was no significant difference between the copper protein membranes in the wet condition yet they were completely comparative in the dry condition. Water can therefore definitely be used to alter the mechanical properties of these membranes.

Chapter6: Application of Crosslinked Protein Membranes with microfluidics

6.1 Introduction

The aim of this study was to prepare crosslinked porous protein membranes in microfluidic channels using parallel streams of solutions carrying desired reagents to establish a reaction at the interface between the streams. For achieving the interfacial crosslinking reaction, terephthaloyl chloride as a selected crosslinker requested to diffuse in the microchannel across the flow direction. Finally, these membranes were planned to be used as barrier layers to ensure stable contact of different phases such as gas/liquid or liquid/ liquid and the permeation of chemical species through the membrane. The surface of crosslinked protein membranes also has the facility functional groups for modification of surface chemistry, or the addition of reactive agents to allow chemical transformation of permeated chemical species. Analysis would be possibly by optics or electrochemistry. These capabilities could lead to the development of complicated and sophisticated chemical systems involving membrane permeation and chemical reactions.

This microfluidics and membrane system could also be used as a biosensor or bioreactor. As different types of membranes can be formed in the microchannel, the system can, further, promote cell growth or prevent bacterial contamination.

The effect of cell adhesion, growth and proliferation on different crosslinked protein membranes has been investigated here. Moreover the toxic effect of copper membrane has been tested.

6.2 In situ membrane

6.2.1 In situ membrane formation

The glass structure was low cost and adhesive bonding was stable in xylene; this allowed numerous iterative design changes as previously reported [8, 9]. To prevent growth of dense, viscous crosslinked protein that formed initially right across the flow channel, the dual laminar streams were chosen to be of immiscible solvents. However, it was also vital that the interfacial polymerisation was rapid, and for this reason the two acyl chlorides were chosen. Reaction rates of acid chlorides with amines have been reported to be rapid, measured as between 10^2 and 10^4 l/mol/s in homogenous solution [146]; rates were likely to be of a similar order for the amino groups of the protein. The basic reaction scheme is shown in chapter 2.1.4 (Scheme 1). The net outcome was a thin, continuous, intact membrane, tightly adherent to the base and the top of the microchannel (Fig. 6.1) which was stable to fluid flows. The thickness of the crosslinked fibrinogen membrane was 60 μm; reaction time was 5 min, after which the flow channel was perfused with pH7.4 PBS.

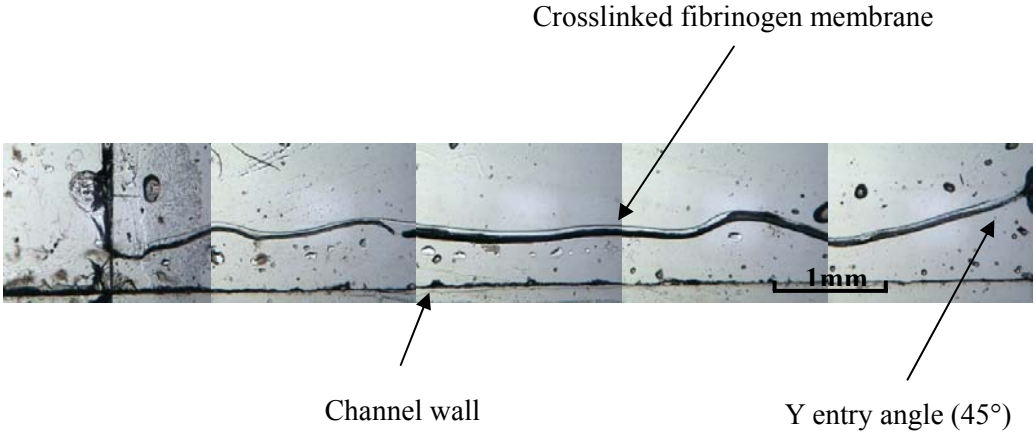

Figure 6.1 Edge view of crosslinked fibrinogen membrane inside a micofluidic channel observed with optical microscopy

6.2.2 Surface structure of in situ fibrinogen membrane

Figure 6.2 showing the crosssection of a fibrinogen membrane formed inside the micro-channel. The crosssection of the protein membrane shows an hourglass type of crosssection with thickness greater near the channel wall boundary, but tapering in the middle. The reason for this was because the flow velocity was higher in the middle and lower at the boundary. Therefore, there was a longer time for interaction of the flows near the boundary. More importantly the seeding effect should be considered. The glass slides act as seeding surfaces for membrane formation. Secondly, once the membrane formed the membrane and the glass slides form corners, where flow velocity decreased further and shear stress reduced to enhance membrane formation.

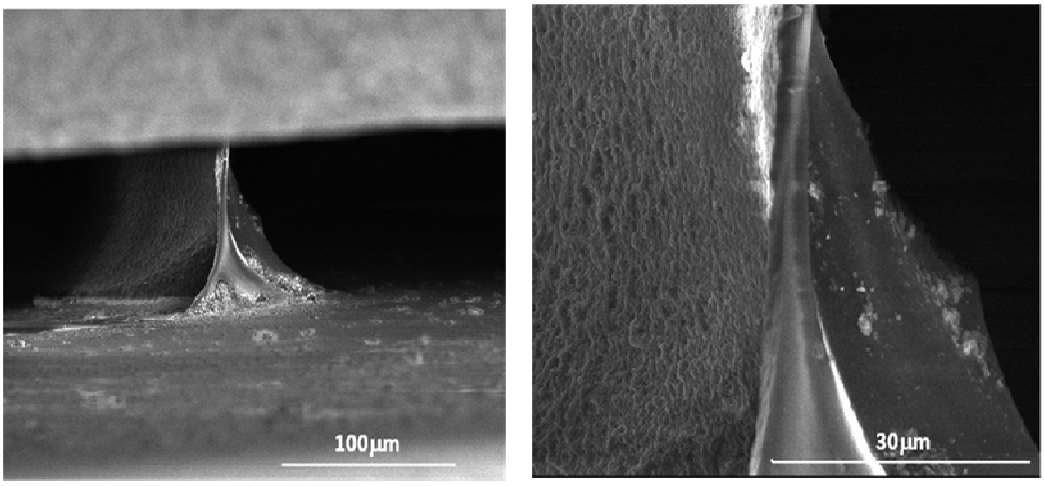

(a) (b)

Figure 6.2 Crosslinked fibrinogen (TCL) membrane in the microfluidics

The surface topography of *in situ* fibrinogen membranes and large surface fibrinogen membranes (15mm in diameter) were examined to assess if there was any microstructural difference due to the membrane formation method. Scanning electron microscopy (SEM) was used to confirm physical appearances. As Figure 6.3 shows, the protein side had a ridge-and-valley structure, whereas the organic side showed a smooth skin surface for both membranes. The formation process is diffusion limited there should be very little difference between the *in situ* membrane here and the large surface membrane, both being generated at static, parallel (stopped-flow) or unstirred dual layers.

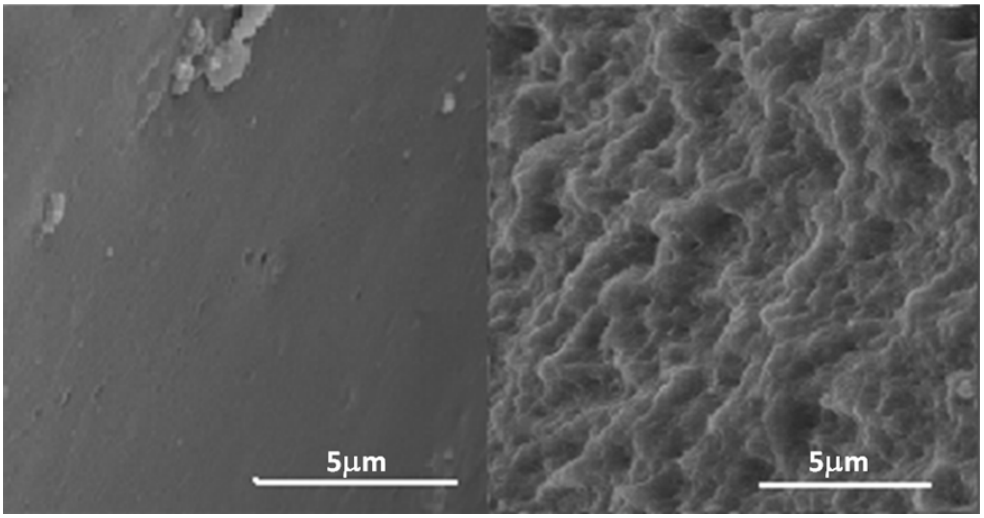

(a) organic side protein side

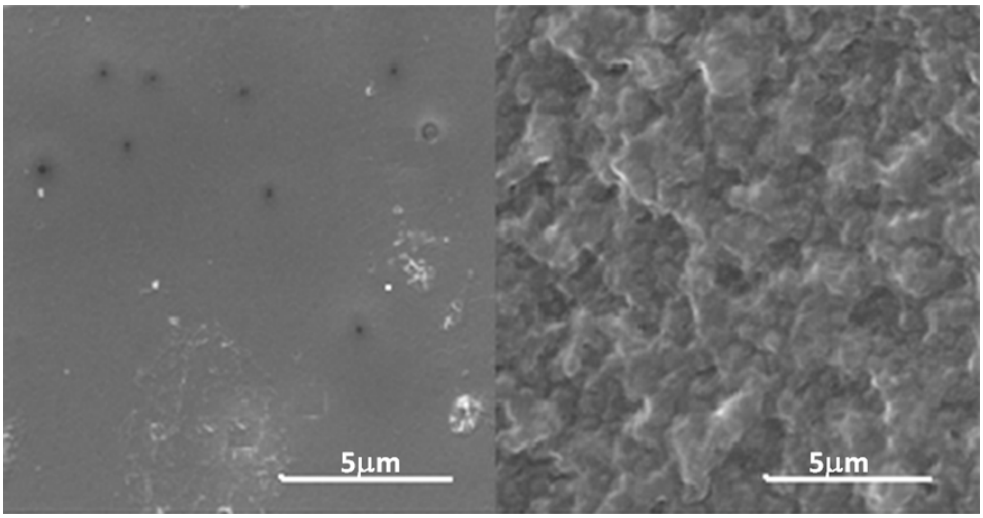

(b) organic side protein side

Figure 6.3 (a) fibrinogen terephthaloyl chloride *in situ* membrane (b) fibrinogen terephthaloyl chloride large surface membrane

6.2.3 Diffusion study of membranes formed within microfluidic channels

To assess the integrity and the continuity of the membrane, as well as to determine permeability properties, dye diffusion studies were conducted. Images (Fig. 6.4) were taken under a stopflow regimen at 0 s and at 30 s. Fig 6.4 (a) and (b) show the dye images and also density profiles for Ponceau S and Meldola Blue, respectively, through a fibrinogen membrane, the latter using Image Tool (http://ddsdx.uthscsa.edu/dig/itdesc.html). There were no structural breaks in the membrane formed. The dye profile in grey scale across the channel for Meldola Blue at 30s *vs* 0s shows that some dye transfer across the membrane does occur; the heights of the grey scale profiles on either side of the membrane approximate more closely after 30s. By contrast, the Ponceau S grey scale profile is unchanged at 30s, strongly indicating impermeability to this dye. By contrast, no dye diffusion occurred across crosslinked albumin [9]. Though Ponceau S is larger (761 Da) than Meldola Blue (379 Da), this is unlikely to be the sole reason for an absolute lack of transport of the former. More likely, it is the highly anionic nature of the former azo dye resulting from its four sulphate pendent groups and the inherent negative charge of the fibrinogen barrier (fibrinogen isoelectric point 5.8) that will alternatively, have attenuated Ponceau S membrane access. The cationic nature of the Meldola Blue will have facilitated transport. This mechanism does not, however, explain why the BSA did not allow either dye to be transported. One possibility for the membrane dominated effect is the

difference in membrane pore structure. As chapter 4.2.2 Fig 4.2 shows, SEMs of albumin and fibrinogen membranes show no obvious pore structure for the albumin membrane, but for the fibrinogen, there are defined pores in the range 0.01 – 0.10 μm and if they are continuous through the material, not only would this account for the membrane permeability differences, but nanopores, if negatively charged would still be able to reject the anionic dye on the basis of charge.

A further factor that requires study is the extent of dye adsorption by the protein membrane which could be not cross-diffusion.

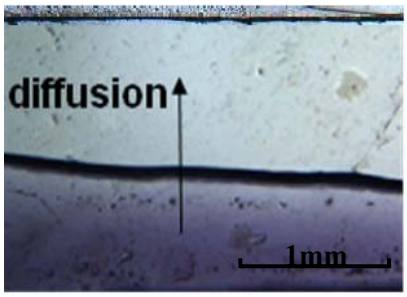

(a) 0 sec image of meldola blue

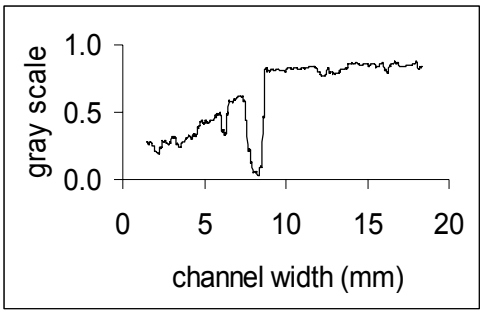

Graph of absorbance grey scale

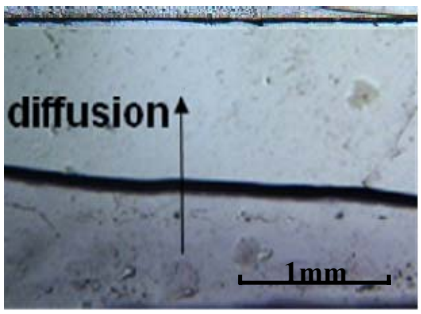

(b) 30 sec image of meldola blue

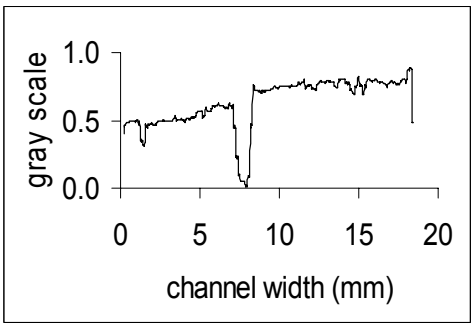

Graph of absorbance grey scale

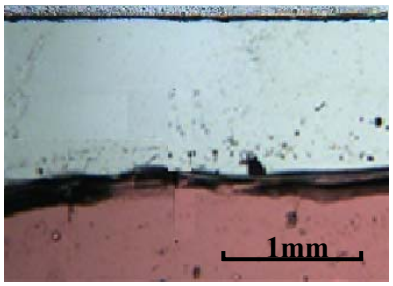

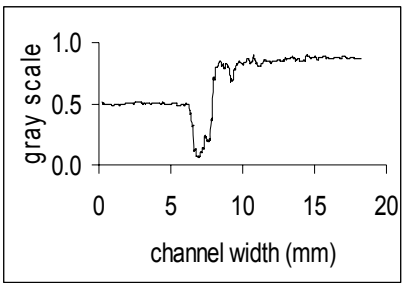

(c) 0 sec image of ponceau S **Graph of absorbance grey scale**

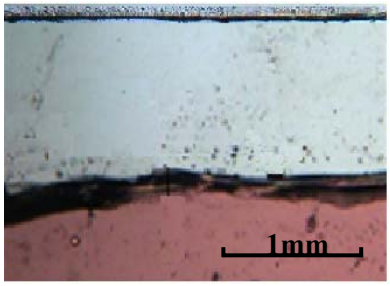

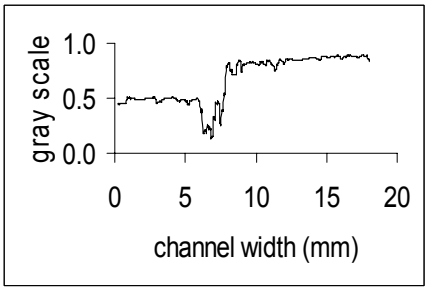

(d) 30 sec image of ponceau S **Graph of absorbance grey scale**

Figure 6.4 Images and grey scale curves for Meldola Blue (a) and Ponceau S (b) diffusion through the crosslinked fibrinogen membranes; TCL crosslinker used.

6.3 Diffusion through in protein membranes

6.3.1 Diffusion of model solutes through fibrinogen and BSA crosslinked membranes

The diffusion coefficients of model solutes through the protein membranes were determined by fitting simulated amperometric sensor current responses at membrane covered electrodes to experimental data following a step change in diffusion concentration. Typical amperometric currents for hydrogen peroxide,

acetaminophen and catechol at membrane covered electrodes are shown in Figure 6.5. It can be seen that the amperometric current for hydrogen peroxide reaches a plateau response earlier than those for acetaminophen and catechol. The hydrogen peroxide, thus, has a higher diffusivity than acetaminophen and catechol at both membranes. This is more clearly seen for calculated diffusion coefficients (Figure 6.6). There also appears to be a relation between transfer of these neutral species and their molecular weights (MW: hydrogen peroxide, 16; catechol, 110; acetaminophen, 151).

The BSA crosslinked membrane displays a less permeable structure due to its denser, tightly cross linked network. The diffusivities of hydrogen peroxide, acetaminophen and catechol through the fibrinogen membranes were 35×10^{-7}, 12.5×10^{-7} and 8×10^{-7} cm^2 s^{-1}, respectively (Figure 6.6). Undoubtedly, the BSA membrane was denser and less porous. The higher overall diffusivity observed with crosslinked fibrinogen membrane supports the possibility of a penetrating pore structure.

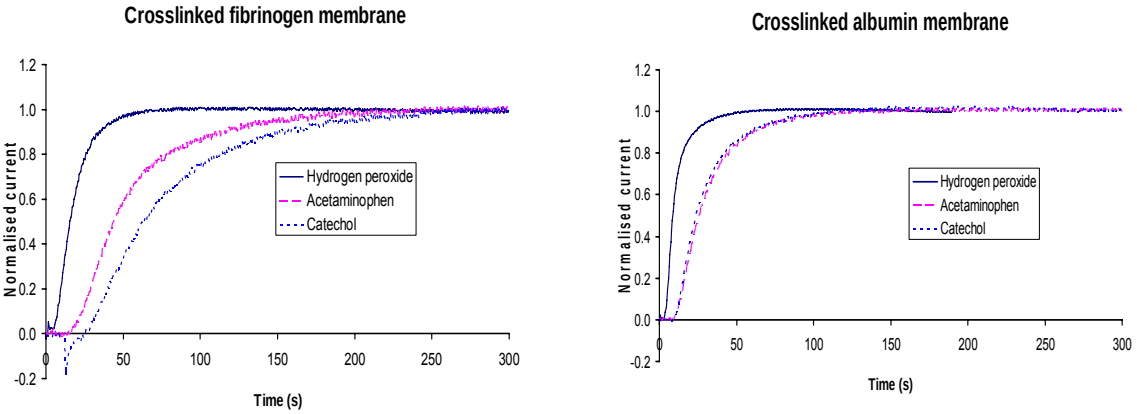

Figure 6.5 Electrode responses to hydrogen peroxide, acetaminophen and catechol through (a) fibrinogen and (b) albumin membrane.

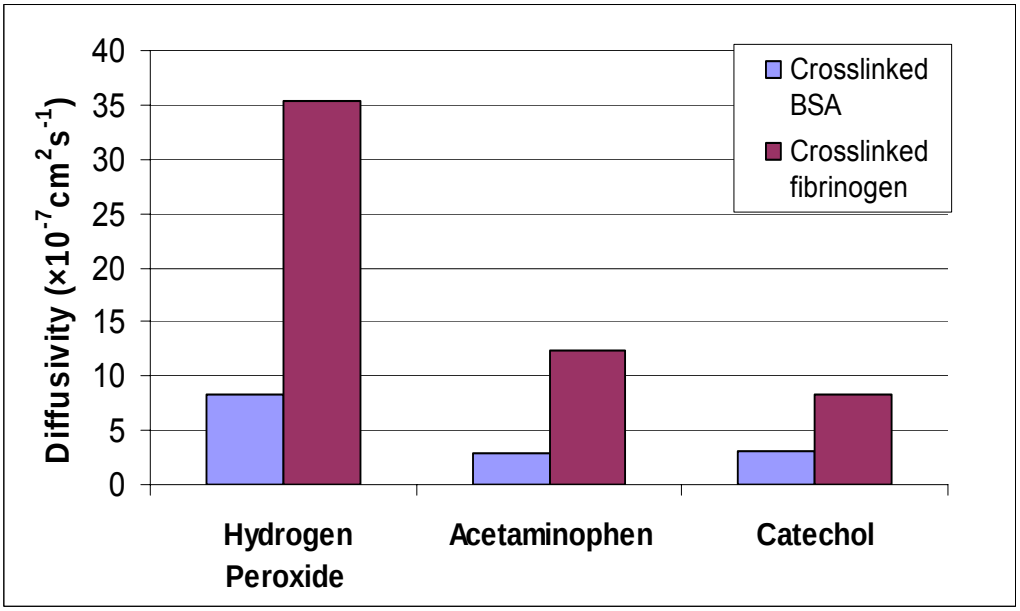

Figure 6.6 Diffusion coefficients of hydrogen peroxide, acetaminophen and catechol through albumin (a) and fibrinogen (b) membranes.

6.3.2 Diffusion cross different pH fibrinogen crosslinked membranes

Table 6.1 Porous structures and diffusion coefficients ($\times 10^{-7}$ cm^2/s) of membranes statically interfacial formed with different pH and proteins

	Fibrinogen		
	pH6.0	pH7.4	pH9.0
[a]average pore diameter (μm)	0.17±0.06	0.46±0.27	0.53±0.31
pore density (μm^{-2})	15.73	3.20	0.76
[b]porosity	0.024	0.024	0.0072
D_a (acetaminophen)	19.6±3.0	6.1±0.4	3.2±0.8
D_c (catechol)	5.2±0.3	5.9±1.1	2.6±0.4
D_d (hydrogen peroxide)	24.0±3.6	16.0±1.9	5.4±0.4
[c]D_a/D_{H2O} (acetaminophen)	0.18	0.06	0.03
[c]D_c/D_{H2O} (catechol)	0.07	0.08	0.03
[c]D_d/D_{H2O} (hydrogen peroxide)	0.18	0.09	0.04

[a]Pore diameter refers to the maximum cross sectional diameter where the pore is elliptical in shape.

[b]Ratio of pore area over geometrical membrane area.

[c]Relative diffusion coefficient in membrane to reported value in water [147,148]. The diffusion coefficient values are given as mean and S. D. for 3 or 4 repeat measurements, where there is no S. D. given the result is a single measurement as the experimental data was not sufficient for calculating the diffusion coefficient.

It can be seen from Table 6.1 that the pore size of the protein membrane increases with pH, but pore density decreases with pH. So pH has an effect on pore organization. Overall, porosity of the fibrinogen membrane goes down with increasing pH and in line with this the diffusion coefficient for all three solutes going down. The ratio of the diffusion coefficients for the solutes against water is generally lower for the pH9 membrane, and this is possibly related to greater solute-membrane interaction due to a low porosity, low permeability membrane e.g. more pore-wall interactions. Catechol shows generally lower permeability than the other two solutes, and again this was the result of greater pore-wall or binding interactions. For the albumin membrane, both lower permeability and porosity is seen compared with all the fibrinogen membranes, and this is manifest in the lower permeability shown for the three solutes.

6.3.3 Diffusion cross Ethanol albumin membranes

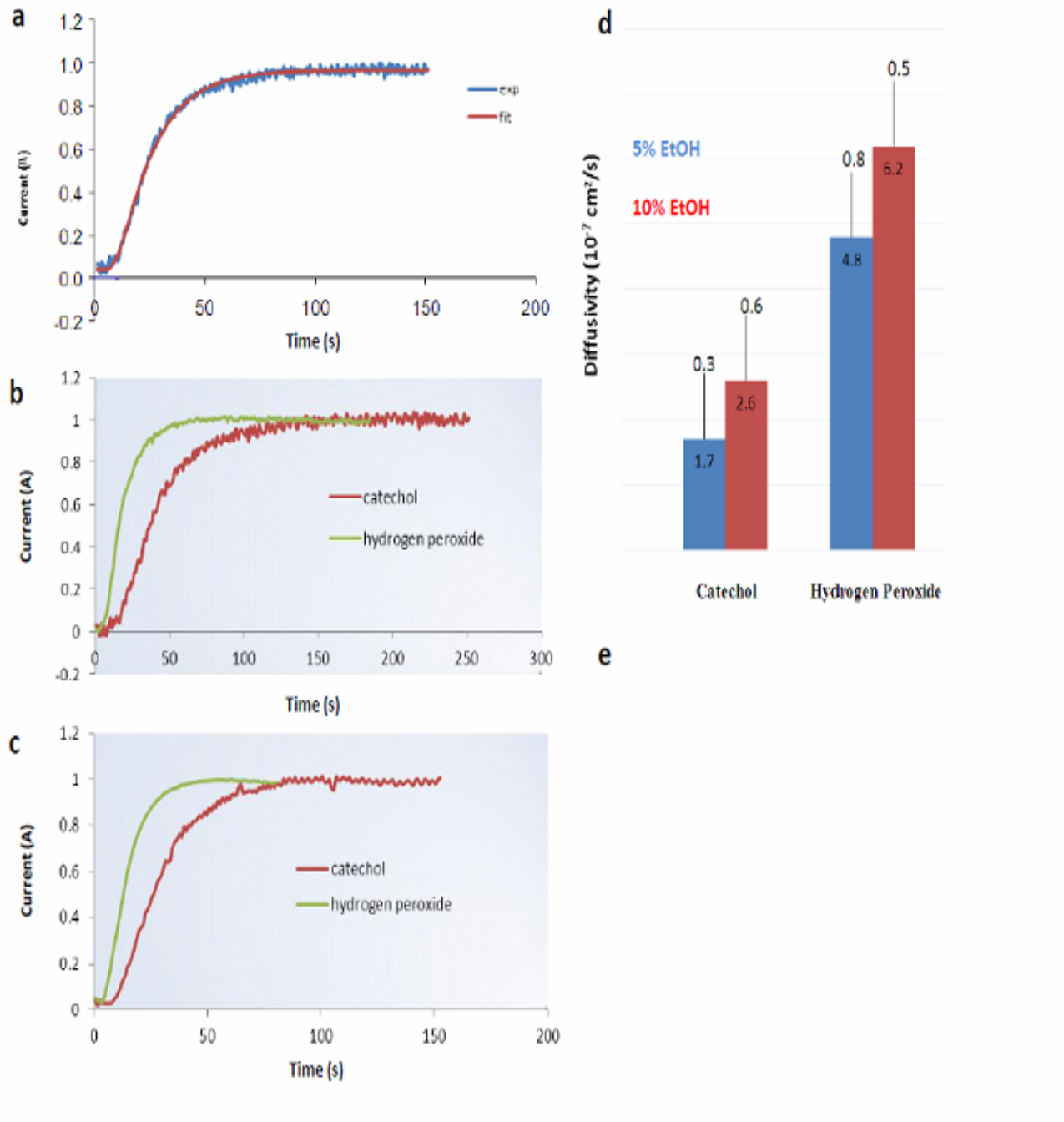

Figure 6.7 Diffusion across membranes. (a) Normalised experimental (solid diamond blue) and simulated (solid square red) transient amperometric currents for catechol diffusion through cross-linked BSA (5 wt. % ethanol) membrane. Amperometric responses of electrode to hydrogen peroxide,

acetaminophen and catechol diffusing through cross-linked BSA membranes with (b) 5% ethanol and (c) 10% ethanol. (d) Diffusion coefficients of the 2 membranes with 5 and 10 wt. %

To identify the behaviour and transport properties of these ethanol BSA membranes, diffusion properties were studied. The diffusion coefficients of model solutes, catechol and hydrogen peroxide through the membranes were measured by fitting simulated amperometric currents to experimental data. A typical fit of catechol diffusion through a crosslinked BSA (with 10% v/v ethanol) membrane is shown in Figure 6.7a. Because the diffusion coefficient was determined through a multiple data set of the time dependent on electrode response, the accuracy could be guaranteed. The standard deviation for the normalised amperometric currents in Figure 6.7a is less 0.01. The method thus gives an exceptionally precise and readily validated measure of diffusion coefficient. Any differences in measured diffusion coefficients are, therefore, an indication of true differences between membranes as shown in Figure 6.7d.

Typical amperometric currents for catechol and hydrogen peroxide are shown in Figures 6.7b and c. It can be seen that the amperometric current for hydrogen peroxide reaches a plateau response earlier than that of catechol. The hydrogen peroxide, thus, has a higher diffusivity than catechol. This is further seen by calculating the diffusion coefficients from the response profiles, Figure 6.7d.

There appears to be a relationship between transfer of these neutral species and their molecular weights (MW: hydrogen peroxide, 16; catechol, 110). The higher overall diffusivity observed with 10% v/v ethanol crosslinked BSA membrane supports a higher permeable structure.

The generated thicknesses of 5 and 10 % (v/v) ethanol BSA membranes were 81 and 78 μm respectively. The 5 % (v/v) ethanol BSA membrane display a less permeable structure due to a denser, tightly cross linked network. The diffusivities of hydrogen peroxide and catechol through the 10% (v/v) ethanol BSA membranes were 6.2×10^{-7} and 2.6×10^{-7} cm^2 s^{-1}, respectively, which were higher than those for the 5% (v/v) ethanol BSA membranes as, 4.8×10^{-7}, and 1.7×10^{-7} cm^2 s^{-1}, diffusivities, respectively (Figure 6.7d). Undoubtedly, the 10% (v/v) ethanol BSA membrane was more permeable.

6.3.4 Diffusion coefficient of crosslinked fibrinogen membrane with different crosslinker

With terepthaloyl chloride (TCL) was used as the crosslinking agent to form fibrinogen membranes. After 24 hours of crosslinking, membrane thickness was 151μm; with isophthaloyl dichloride (IDCL) thickness was 153μm, and with sebacoyl chloride (SCL) the membrane thickness was 145μm. As showing in Figure 6.8, the membrane morphology with IDCL would suggest a less permeable structure. Indeed, diffusivities of hydrogen peroxide, acetaminophen and catechol through the SCL crosslinked fibrinogen membranes of 10.32×10^{-7}, 10.36×10^{-7} and 18.64×10^{-7} cm^2 s^{-1}, respectively, were an order of magnitude higher than for the TCL crosslinked membrane, 8.90×10^{-7}, 8.00×10^{-7} and 14.40×10^{-7} cm^2 s^{-1}, respectively. The IDCL membrane showed the lowest diffusivities which were 1.89×10^{-7}, 1.63×10^{-7}, 9.93×10^{-7} cm^2 s^{-1}. Undoubtedly, the crosslinked IDCL membrane was denser and less porous. The hydrogen peroxide, thus, has a higher diffusivity than catechol and acetaminophen. There appears to be a relationship between the transfer of these neutral species and their molecular weights. This has been previously suggested in Chapter 6.3.2.

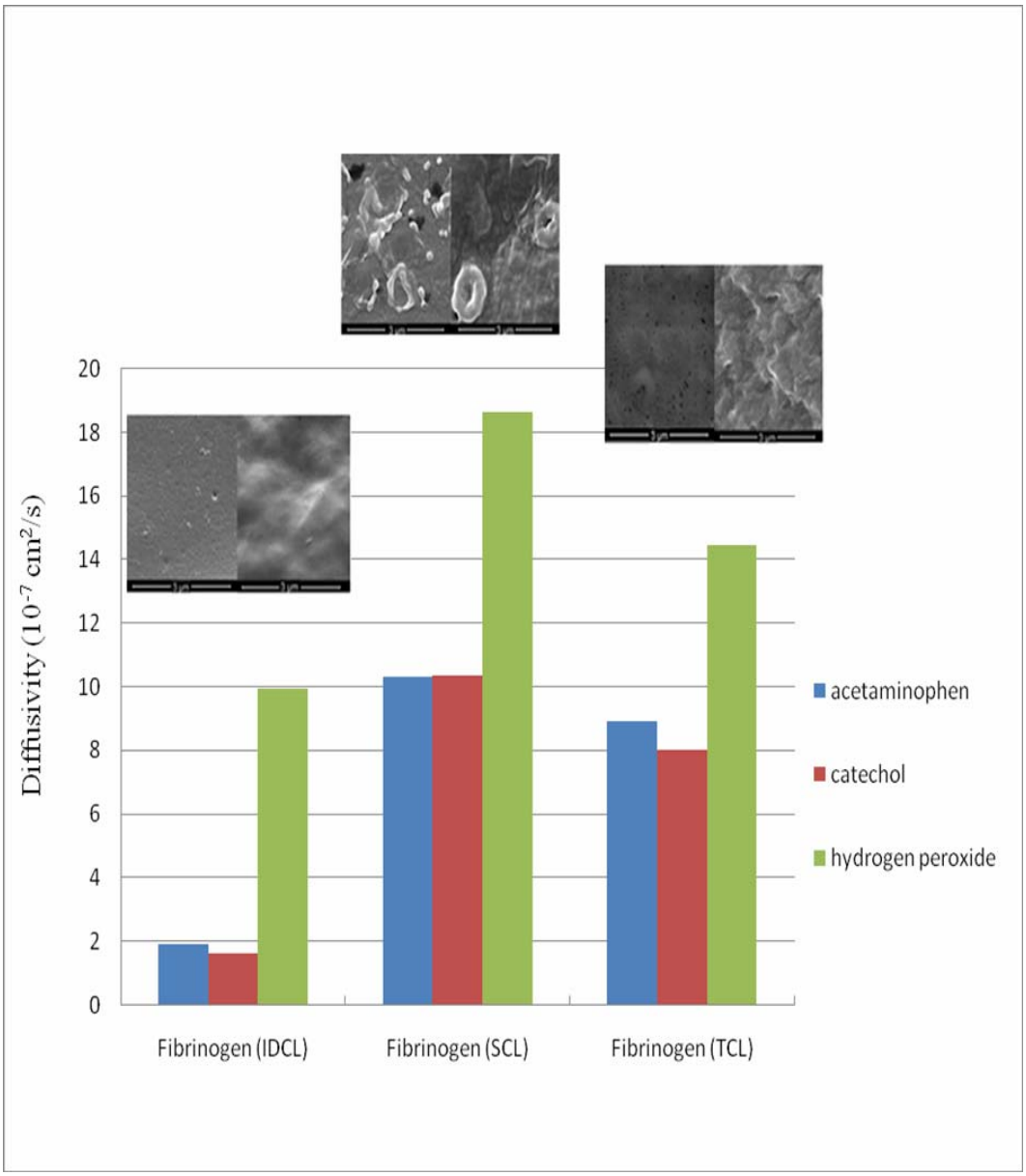

Figure 6.8 diffusion coefficients (×10^{-7} cm^2/s) of membranes statically interfacial formed with different crosslinker

6.4 Antibacterial test for crosslinked copper protein membranes

The antimicrobial efficacy of the crosslinked copper BSA membrane and fibrinogen membrane examined against gram-positive S. epidermidis, which are well-characterized bacteria that have been used as model bacterial systems for various antimicrobial tests. In Figure 6.9, the antimicrobial results of test membranes were observed by SEM.

The crosslinked fibrinogen membrane (Fig. 6.9a) showed that after 24 hours moderate bacterial spread and adherence on the surface of the membrane. The enhanced population cell showed the bacteria also start to grow. By contrast, the copper treated fibrinogen membrane displayed a reduction in the number of adherent bacteria (Fig. 6.9b). The morphology of the bacteria showed reduction in the size of aggregates, which were reduced to small clusters or even single cells.

After 24 hours the bacteria on the crosslinked BSA membrane appeared less spread compared to the crosslinked fibrinogen membrane (Fig. 6.10a). Also, the cell morphology appeared to indicate the promotion of slightly less cell growth. Treated copper BSA membrane (Fig. 6.10b) showed cell growth in a similar fashion to crosslinked BSA membrane. However the bacteria still appeared to exhibit a reduced adhesion and spreading.

After 48 hours, the bacteria replicate, develop as micro colonies and in some cases there was indication of enhanced cell growth (Fig. 6.9c, 6.10c). However, there seemed no difference between cell density and growth on BSA and fibrinogen.

By contrast, the copper treated BSA membrane appeared to show limited bacteria spread on the membrane (Fig. 6.10d), and with the enlarged image the bacteria appear to be of rounded morphology which is a sign of cell death. Surprisingly, the copper treated fibrinogen membrane (Fig. 6.9d) showing a clear surface, where there were no bacteria at all.

Overall, these results show that the fibrinogen copper membrane had a strong antimicrobial obtrude effect after 48 h of bacterial suspension incubation. With copper BSA membranes there is a significant reduction of adherent bacteria. Thus, the copper membrane demonstrated extremely high antibacterial efficacy, the greater efficacy of the fibrinogen membrane may have been because of its greater permeability, allowing better outward release / permeation of copper ion as compared with the loosely crosslinked BSA.

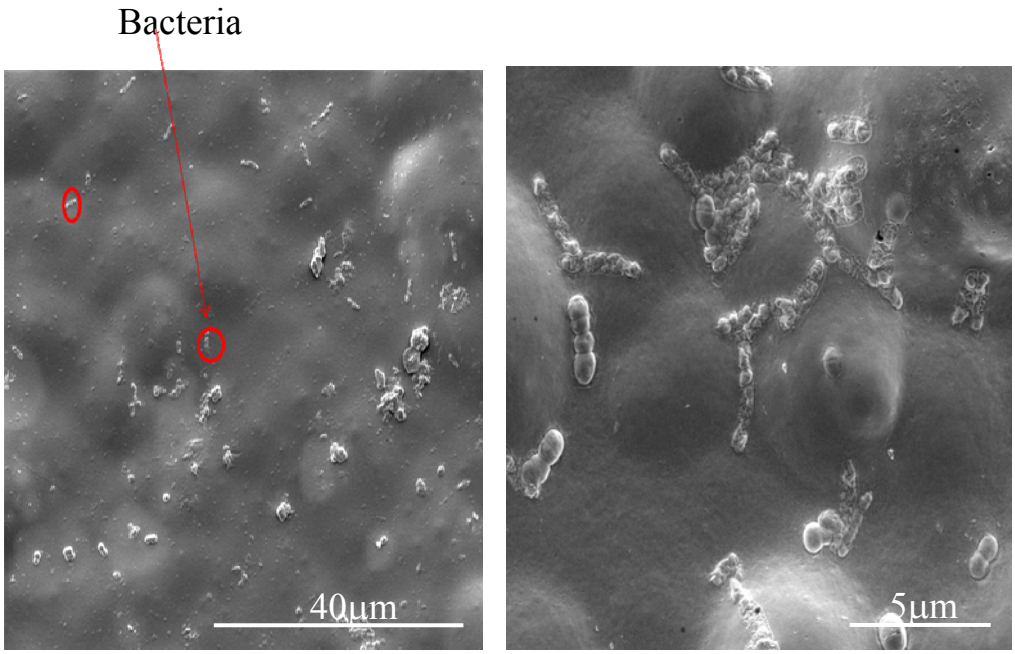

(a)

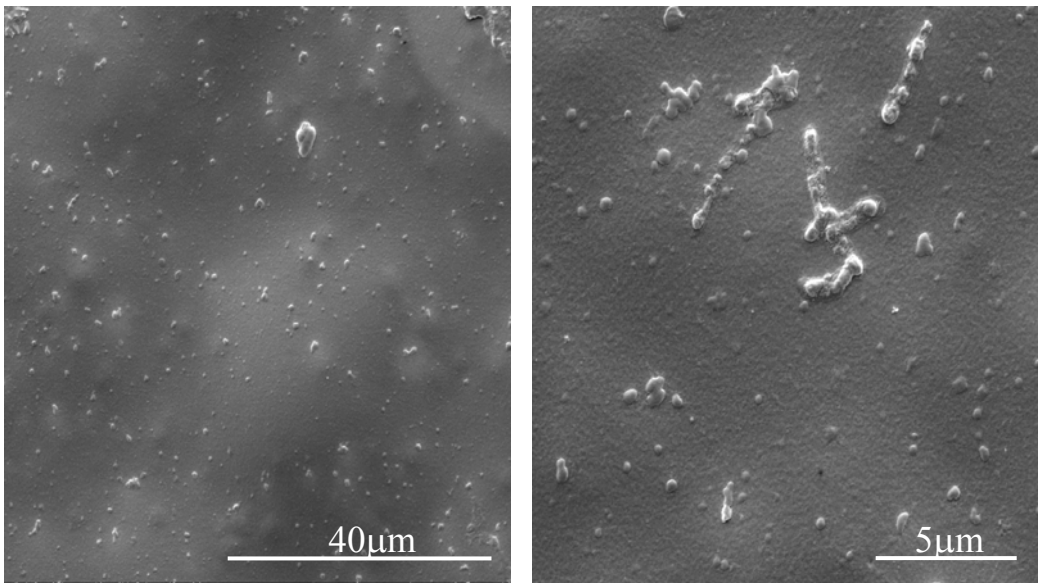

(b)

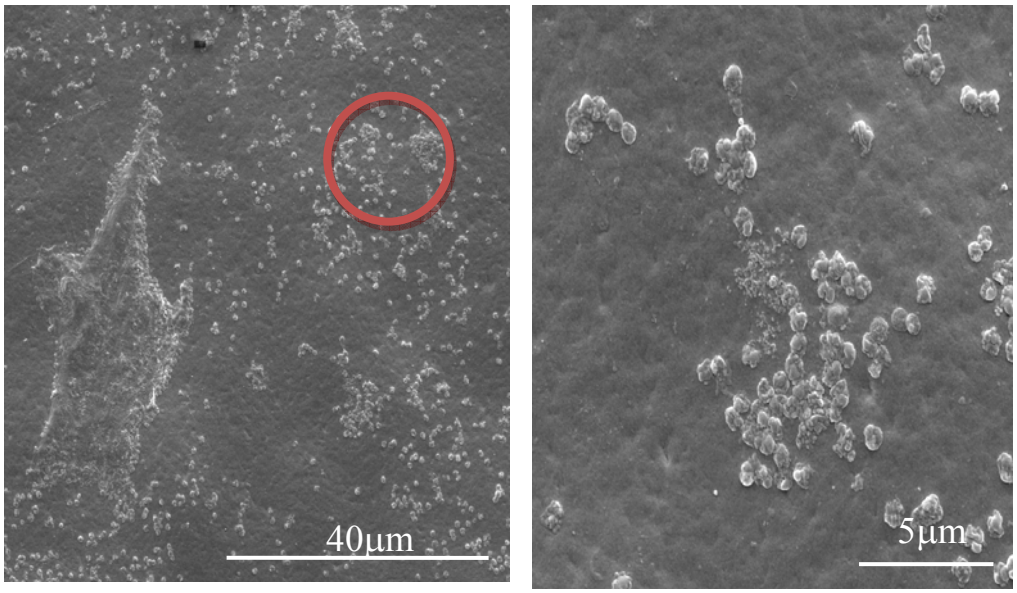

(c)

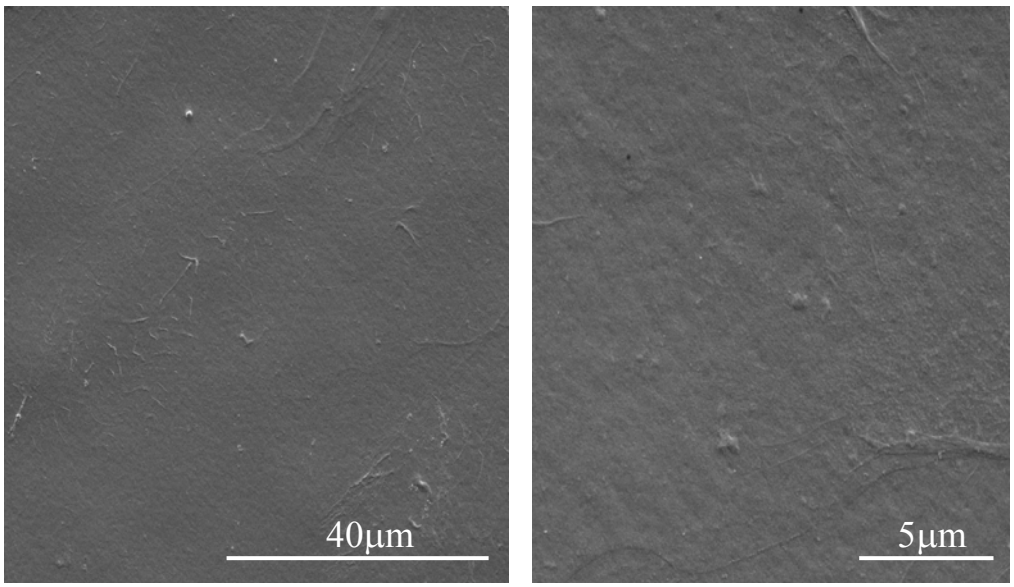

(d)

Figure 6.9 SEM images of gram-positive S. epidermidis with (a) fibrinogen membrane (culture time 24 hours) (b) fibrinogen copper membrane (culture time 24 hours) (c) fibrinogen membrane (culture time 48 hours) (d) fibrinogen copper membrane (culture time 48 hours)

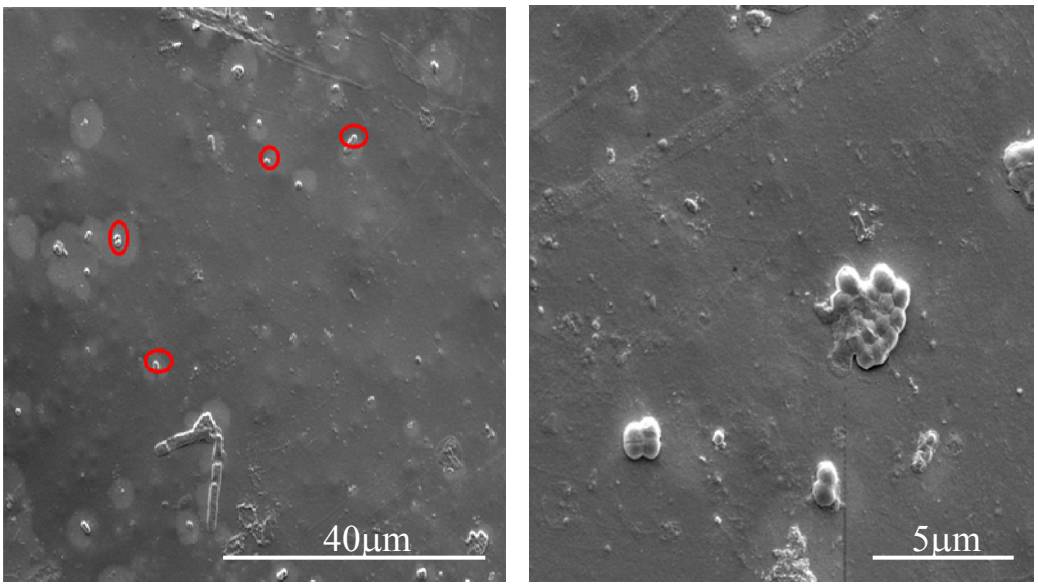

(a)

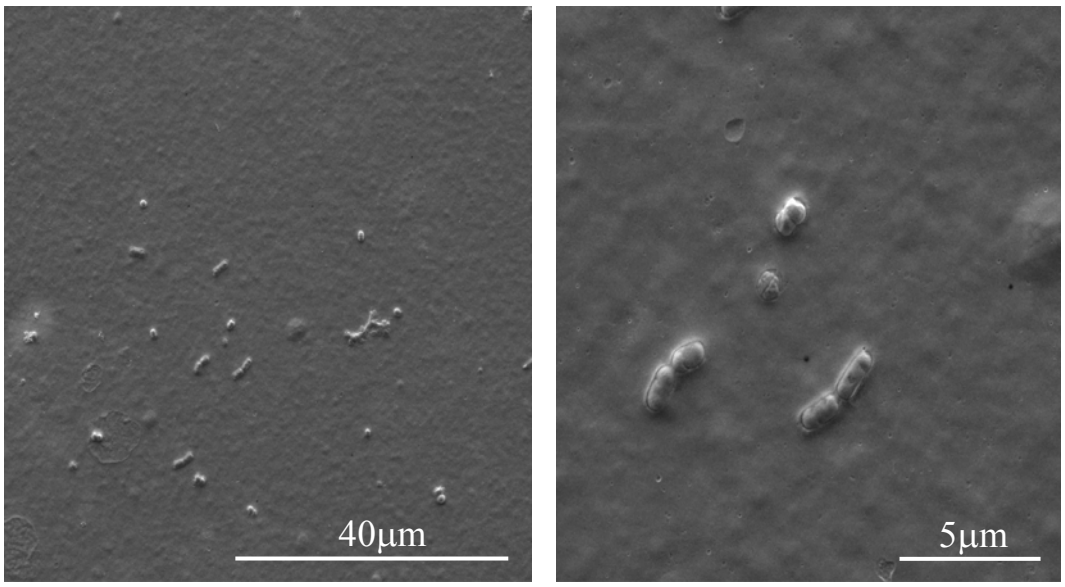

(b)

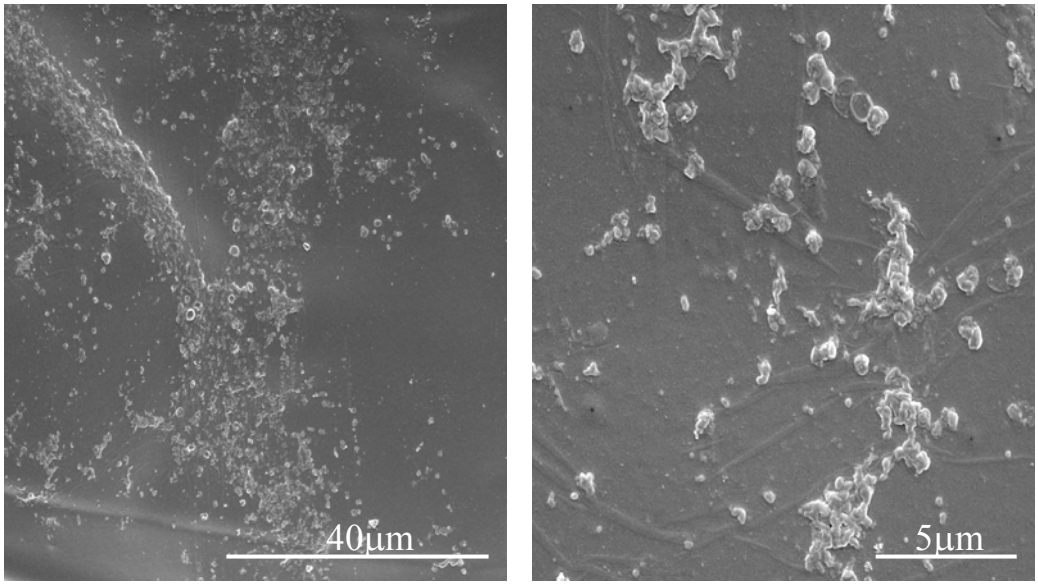

(c)

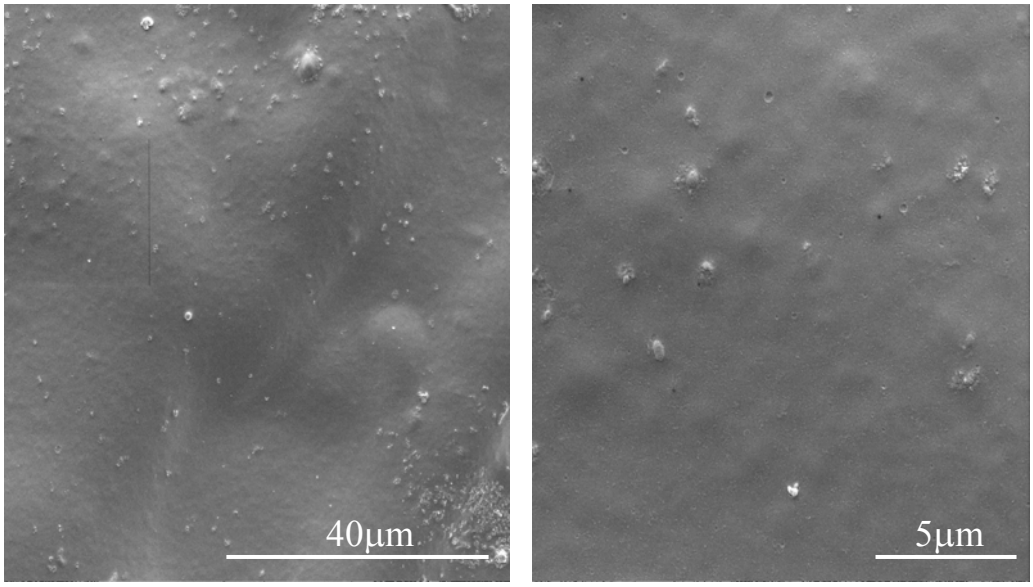

(d)

Figure 6.10 SEM images of gram-positive S. epidermidis with (a) BSA membrane (culture time 24 hours) (b) BSA copper membrane (culture time 24 hours) (c) BSA membrane (culture time 48 hours) (d) BSA copper membrane (culture time 48 hours)

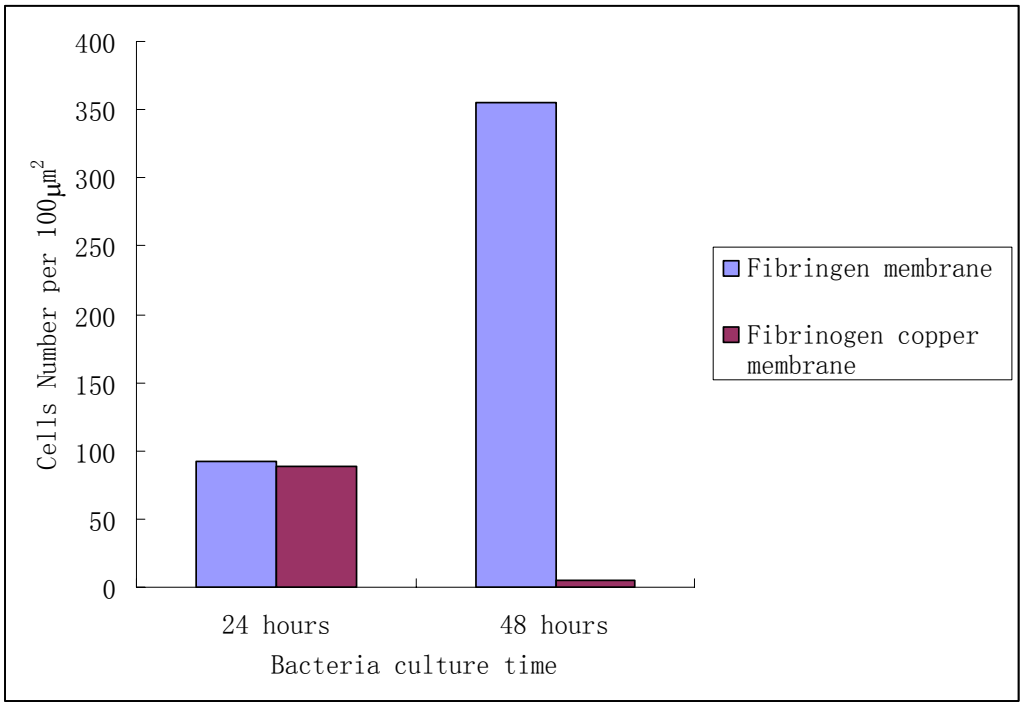

(a)

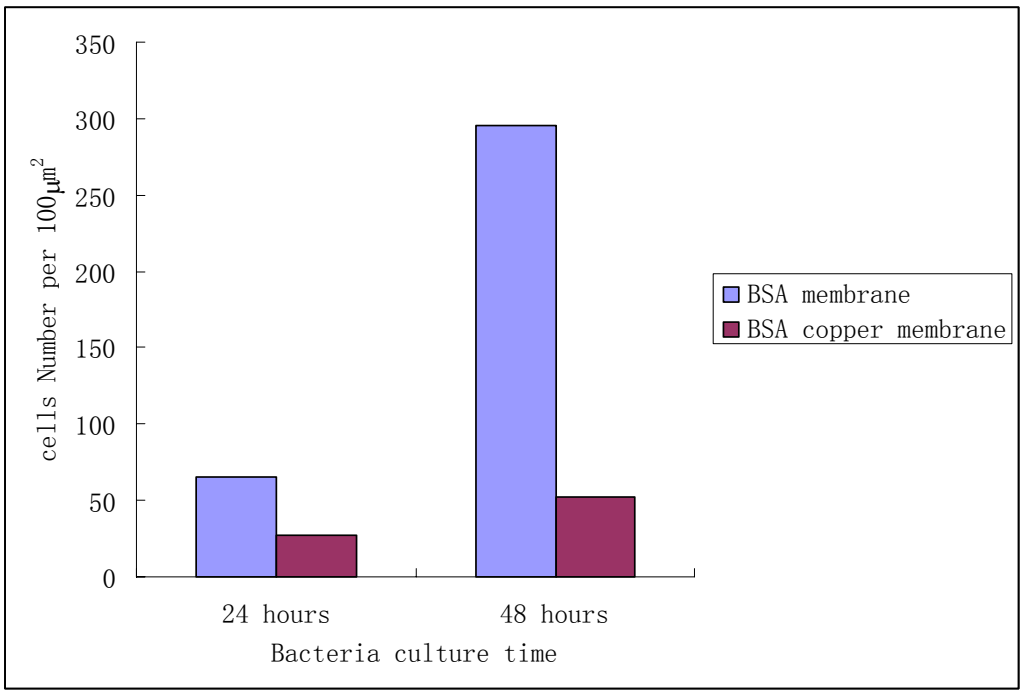

(b)

Figure 6.11 Bacteria density with the bacteria culture time increase (a) fibrinogen and fibrinogen copper membrane (b) BSA and BSA copper membrane

Additionally study: Cells attachment to protein membranes

Studies revealed crosslinked membranes were found to be non-toxic to B50 cells Figure 6.12 compares B50 cells on different planar membranes; cells appeared attached and in some cases indicated enhanced growth, in contrast to glass surfaces Figure 6.13. However there seemed no difference between density and growth on albumin and fibrinogen. Although we can conclude there to be some advantages in using crosslinked fibrinogen for cell growth, further studies will need to be conducted.

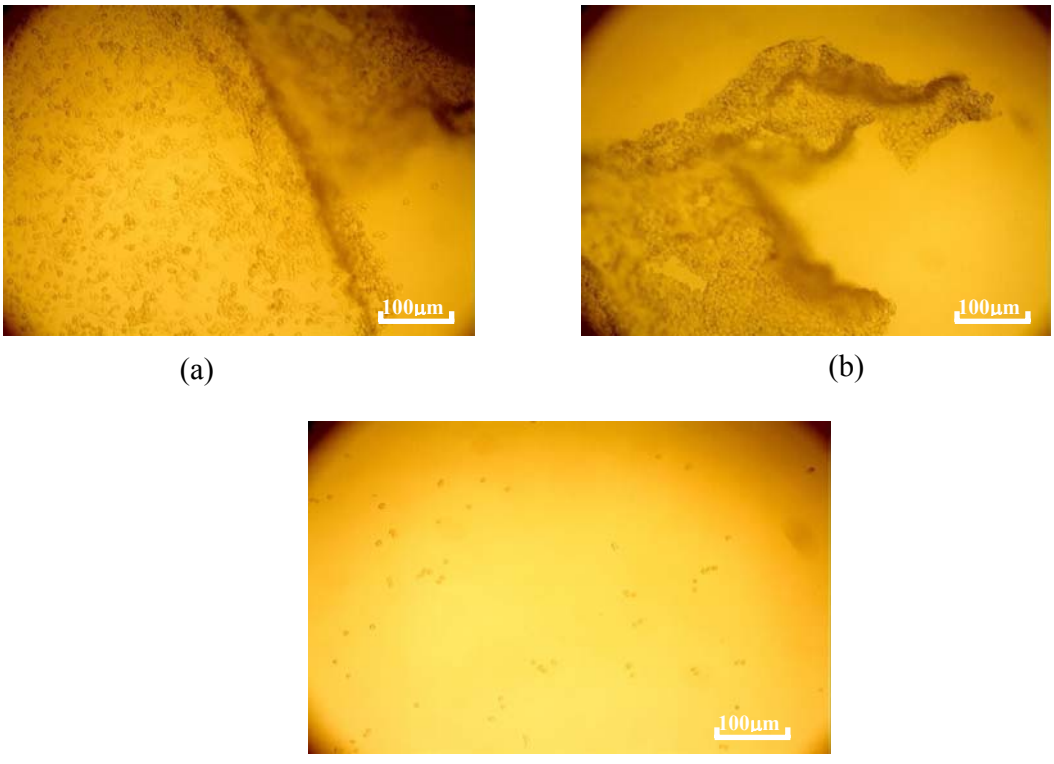

(a) (b)

(c)

Figure 6.12 Light microscopy of B50 rat neuronal cells at 24h growth on crosslinked fibrinogen membranes (a), (b) and glass cover slip (c). Both fibrinogen membranes have partially lifted off the supporting glass surface.

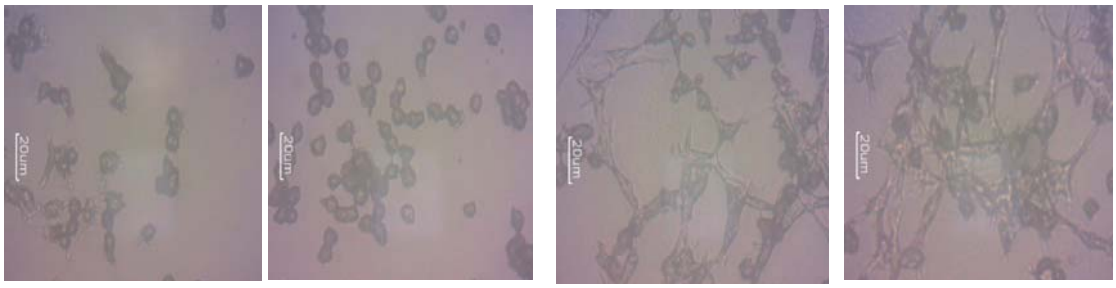

(a) (b) (c) (d)

Figure 6.13 B50 cells on (a) crosslinked BSA (20wt%), (b) crosslinked BSA (20wt%) with fibronectin (0.05wt%) (c) crosslinked fibrinogen (3.8wt%), (d) crosslinked fibrinogen (3.8wt%) with fibronectin (0.05wt%).

6.7 Summary

BSA and fibrinogen crosslinked membranes were successfully formed inside microfluidics channels by interfacial polymerisation. The benefit of using this technology is that one can create a very thin porous membrane already fixed inside a microchannel so it does not require additional bonding processes. The crosssection structure has checked by using SEM. Porosity was likely to be the main basis for diffusional resistances of different membranes, certainly as judged different electroactive by dye and microsolute transport, different crosslinker also influenced diffusivity. The porosity of the membrane was readily changeable by simply changing the crosslinking agents. Generally, this is hard to achieve with conventional fabrication methods because of the very high aspect ratios involved and difficulties in manipulating such a small and thin structure.

The SEM results showed bacterial adhesion to the protein membrane surfaces. With the normal protein membranes, after 48 hours the bacterial develop and form colonies. The novel copper protein membrane can be readily produced and in able to reduce or prevent bacterial contamination.

With some additionally study the crosslinked membranes exposed to B50 rat neuronal cells under microflow conditions, or in static culture medium, confirmed good cellular attachment to all crosslinked protein membranes, but an improved adhesion at fibrinogen.

Chapter7: Conclusion and Future Work

7.1 Conclusion

The fabrication of protein membranes and their contributions to microfluidics system have been extensively studied but are not yet fully understood. It is known that the protein membranes can be crosslinked with different crosslinker by large surface method and the *in situ* interfacial method inside the microchannel.

7.1.1 Morphology of membranes

- Protein can be crosslinked with acly chloride rapid, and the crosslinked membrane was stable and porous.
- With the same membrane its aqueous and organic sides exhibited different morphologies, because the solute was diffused uneven from crosslinker solution to protein solution.
- With the same crosslinker fibrinogen membrane shows more porous structure due to its molecule size.
- Crosslinking agent effect on resultant membrane permeability. The crosslinker sebacoyl chloride led to more permeable membranes than terephthaloyl chloride and isophthaloyl dichloride that could link into differences in pore changes (SEM)

- PH and ethanol effect on resultant membrane permeability suggests that pre-formation protein status influences final outcome. FTIR also conform that the crosslinked protein membranes do influenced by ethanol
- surface structure of crosslinked fibrinogen membrane is no signify difference between two crosslinking temperature (22°C and 4°C)
- The thickness of the membrane depends on the crosslinking time.
- With the same crosslinking time the thickness of BSA membrane is less than fibrinogen membrane. the BSA membrane forming reaction was reagent limited due to the diffusion barrier imposed by the crosslinked membrane structure
- With the same crosslinking time, different crosslinker also influences the thickness of the membranes, due to the different permeability of the membrane.
- Membranes exposed with copper appeared that there was some clear time dependent increase in surface porosity. This means that control the copper treatment is possible.

7.1.2 Mechanical Properties of BSA and Fibrinogen Crosslinked membranes

- The mechanical properties of protein membranes was been tested by nanoindentation method. BSA produces a more rigid membrane than fibrinogen.
- The mechanical properties are also defined by the different crosslinker, IDCL membranes were more elastic than TCL membranes. SCL membrane was too viscous that the indenter was stick on the membrane, which leads to the failure of measurement.
- Protein membranes were compared through exposure with and without copper sulphate solution. Membranes exposed with copper appeared stronger.
- Protein membranes were compared with both dry and wet conditions. The BSA copper membrane in the dry condition showing higher value in all mechanical aspects

7.1.3 Application of Crosslinked Protein Membranes with microfluidics

- Protein membranes can be formed with in the microchannel by interfacial polymerisation method.

- The surface structure of the *in-situ* membrane is same with the membrane which made with lager surface method.
- fibrinogen membranes showing greater solute permeability than albumin based on dye and microsolute diffusion study
- Copper ion was crosslinked as antimicrobial agent into protein membranes.
- The copper ion crosslinked with the protein membrane, this cooper membrane also showing stronger mechanical properties, which might provide long-term antibacterial function.

This thesis has demonstrated that the novel protein membranes can be produced by using fast interfacial polymerization. The porosity of membranes can be controlled by changing the pre-formation protein status or changing the crosslinker. Also a robust antimicrobial copper protein membrane was developed. Those membranes can form in side the microfluidics channel within a few minutes, and the whole system can be used as microbioreactor. The membranes serve as bio-catalyst surfaces or allow cell adhesion.

7.2 Future Work

7.2.1 Bioreactor for cell growth

The application of microfluidics to cell-based research appears to be particularly promising. Microtechnology has been used to fabricate structures for almost every step in the cell research process: cell acquisition; cell culture, trapping, and sorting; cell treatment; and finally analysis [149, 150]. Microflow control permits precise routing of fluids in order to create predictable and reproducible gradients at the microscale, allowing us to better study these biological phenomena. Finally, microscale devices are ideal for studies involving small cell populations, such as primary cancer cells obtained from needle biopsies, or stem cells.

My work has showed the protein membrane can be formed within the microfluidics channel and also has emphasized membranes for selectivity and biocompatibility. Therefore the membrane microfluidics systems will be used for allowing reagents and nutrients which needed for cell growth to be supplied from another side (see Fig. 7.1) in a more controlled and reproducible manner than that often found in traditional cell culture technologies [149,151,152]. Different type of cells will be cultured within microchannel. The cell growth will be determined by confocal microscopy.

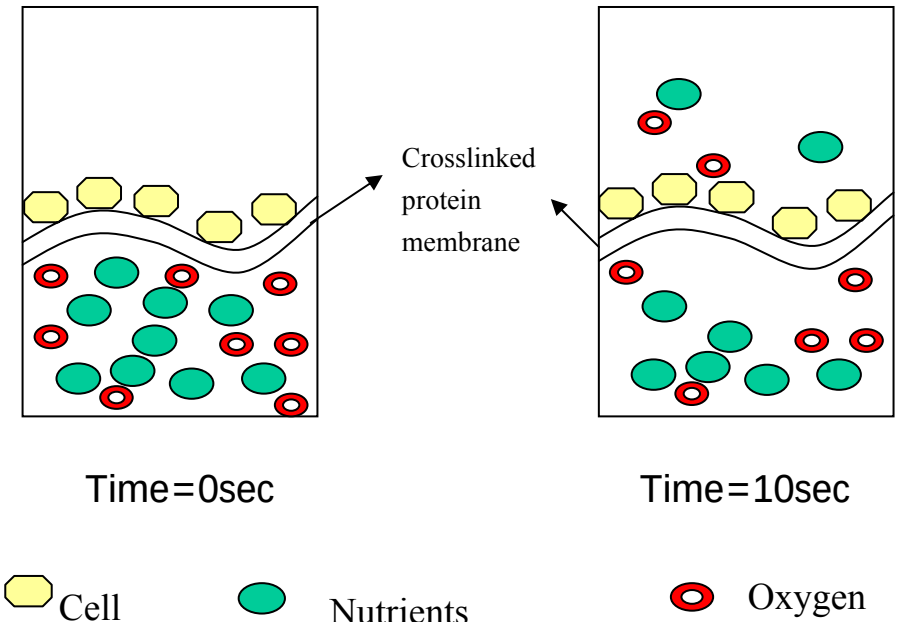

Figure 7.1 Schematids of nutrients and oxygen through protein membrane

7.2.2 Sensor with microfluidic channels

Integrating sensors and detectors within microfluidic channels reduces the need for external infrastructure such as analyte vessels to take measurements from the device [153]. More importantly, incorporating sensors inside the microfluidic channel permits direct *in situ* measurements, as the data is recorded at the time of interest rather than after the fluid has exited the channel. As it is often desirable to accurately monitor various parameters in the cell culture environment, there has been an effort to integrate many types of sensors into microfluidic channels for cell culture, including dissolved oxygen and carbon dioxide [154], pH [155,156], and temperature [157,158].

7.2.3 Fabrication of sensor with microfluidics

Flow channel designs will be based on those currently in use by me (see chapter). Materials used initially will be acrylic and PDMS. PDMS is well established for microfluidics devices [159], with acrylic being currently utilized in this study. Narrow inlets will be located along the side of the main flow channel to allow the introduction of working and counter reference electrodes. The size and exact location of these inlets will vary according to the electrodes used and whether measurements are amperometric or impedimetric. Design will also have the angle between the inlet channels varied (10°, 40°, 80°, 170°) to investigate the effect of initial shear on membrane formation. Finally the crosslinked protein membrane will be formed in the middle of the channel. The system is intended to measure the diffusants (oxygen and glucose) with and without cell seeding on the membrane, and precise control over the culture microenvironment.

References

[1] Beebe D J, Mensing G A, and Walker G M 2002 Physics and applications of microfluidics in biology *Annu. Rev. Biomed. Eng.* 4 261–86

[2] Wu Z, Willing B, Bjerketorp J, Jannson J K and Hjort K 2009 Soft inertial microfluidics for high throughput separation of bacteria from human blood cells *Lab Chip* 9 1193-1199

[3] Erickson D and Li D 2004 Integrated microfluidic devices *Analytica Chimica Acta* 507 11-26

[4] Huang C J, Chen Y H, Wang C H and Lee G B 2006 Integrated micofluidic systems for automatic glucose sensing and insulin injection *Sens Actuator* B 122 461-468.

[5] Cabodi M, Choi N W, Gleghorn J P, Lee C S D, Bonassar L J and Stroock A D 2005 A Microfluidic Biomaterial *J. Am. Chem. Soc*. 127 13788-9

[6] Ziaie B, Baldi A, Lei M, Gu Y and Siegel R A 2004 Hard and soft micromachining for BioMEMS: review of techniques and examples of applications in microfluidics and drug delivery *Adv. Drug Deliver. Rev*. 56 145-72

[7] McDonald J C, Duffy D C, Anderson J R, Chiu D T, Wu H, Schueller O J A and Whitesides G M 2000 Fabrication of microfluidic systems in poly(dimethylsiloxane) *Electrophoresis* 21 27-40

[8] Gargiuli J, Shapiro E, Gulhane H, Nair G, Drikakis D and Vadgama P 2006

Microfluidic systems for *in situ* formation of nylon 6,6 membranes *J. Membrane Sci*. 282 257–265

[9] Nair G, Gargiuli J F, Shiju N R, Rong Z, Shapiro E, Drikakis D and Vadgama P 2006 In situ fabrication of cross-linked protein membranes by using microfluidics *ChemBioChem* 7 1683–9

[10] Peterson D S 2005 Solid supports for micro analytical systems *Lab Chip* 5 132-9

[11] Jong J, Lammertink R G H and Wessling M 2006 Membranes and microfluidics: a review *Lab on a Chip* 6 1125-1139

[12] Moskvin L N and Nikitina T G 2004 Membrane methods of substance separation in analytical chemistry *Journal of Analytical Chemistry* 59 2-16

[13]Wang P C, Devoe D L and Lee C S 2001 Integration of polymeric membranes with microfluidic networks for bioanalytical applications *Electrophoresis* 22 3857-3867

[14] Freger V 2003 Nanoscale heterogeneity of polyamide membranes formed by interfacial polymerization *Langmuir* 19 4791-4797

[15] Moorthy J and Beebe D J 2003 In situ fabricated porous filters for Microsystems *Lab Chip* 3 62-66

[16]Song S, Singh A K, Shepodd T J and Kirby B J 2004 Microchip dialysis of proteins using in situ photopatterned nanoporous polymer membranes *Analytical Chemistry* 76 2367-2373

[17] Hisamoto H, Shimizu Y, Uchiyama K, Tokeshi M, Kikutani Y, Hibara A and

Kitamori T 2003 Chemicofunctional membrane for integrated chemical processes on a microchip *Anal*. *Chem*. 75 350-4

[18] Freger V 2005 Kinetics of film formation by interfacial polycondensation *Langmuir* 21 1884-94

[19] Freger V and Srebnik S 2003 Mathematical model of charge and density distributions in interfacial polymerization of thin films *J*. *Appl*. *Polym. Sci*. 88 1162-9

[20] Dollwet, H.H.A. and Sorenson, J.R.J. Historic uses of copper compounds in medicine, *Trace Elements in Medicine*, Vol. 2, No. 2, 1985, pp. 80–87.

[21] French, F. A., and Freedlander, B. L. Chemotherapy studies on transplanted mouse tumors. Cancer Res. 21: 505-538 (1960).

[22] Gutteridge J, Halliwell B 1990 Reoxygenation injury and antioxidant ant protection- a tale of 2 paradoxes *archives of biochemistry and biophysics* 283 223-226

[23] Bagchi D, Stohs SJ 1995 Oxygen radical scavenging ability of optizinc *Faseb Journal* 9 144-144

[24] Valko M; Morris H; Cronin MTD 2005 Metals, toxicity and oxidative stress *Current Medicinal Chemistry* 12 1161-1208

[25] Bernier G M, Putnam F W 1964 Myeloma proteins and macroglobulins: hallmarks of disease and models of antibodies. *Progress in hematology* 4 160-86

[26] Hughes W L, Sinexf M 1954 Chemistry of the proteins, peptides, and amino acids. *Annual review of biochemistry* 23 177-214

[27] Bloomfield V 1966 The structure of bovine serum albumin at low pH. *Biochemistry* 5 684-9

[28] Wright AK, Thompson MR 1975 Hydrodynamic structure of bovine serum-albumin determined by transient electric birefringence *Biophysical Journal* 15 137-141

[29] Bendedouch D, Chen SH 1983 Structure and interparticle interactions of bovine serum-albumin in solution studied by small-angle neutron-scattering *Journal of Physical Chemistry* 87 1473-1477

[30] Feng L, Hu CZ, Andrade JD 1988 Scanning tunneling microscopic images of adsorbed serum-albumin on highly oriented pyrolytic-graphite *Journal of Colloid and Interface Science*126 650-653

[31] Bos OJM 1989 Albumin, the jack-of-all-trades in the protein world *Pharmaceutisch weekblad-scientific edition* 11 242-243

[32] Peters T (1975). Putman FW. ed. *The Plasma Proteins*. Academic Press. pp. 133–181.

[33] Cater J 1989 Restructuring Britain-the changing social-structure-hamnett C mcdowell L Sarrep *Transactions of the Institute of British Geographers* 14 503-504

[34] Bowman B 1993 A technical comparison between AC and DC furnaces *Revne DE Metallurgie-cahiers D Informations Techniques* 90 809-816

[35] Nair Lakshmi S.; Laurencin Cato T. 2006 Polymers as biomaterials for tissue engineering and controlled drug delivery *Advances in Biochemical*

Engineering-Biotechnology 102 47-90

[36] Jie Hu, Songjun Li and Bailing Liu 2005 Adsorption of BSA onto sulfonated microspheres *Biochemical Engineering Journal* 23 259-263

[37] Brown JR 1975 Structure of bovine serum-albumin *Federation proceedings 34* 591-591

[38] Patterson JE, Geller DM 1977 Bovine microsomal albumin-amino terminal sequence of bovine proalbumin *Biochemical and Biophysical Research Communications* 74 1220-1226

[39] McGillivray R T; Chung D W; Davie E W1979 Biosynthesis of bovine plasma proteins in a cell-free system. Amino-terminal sequence of preproalbumin. *European journal of biochemistry* 98 477-85

[40] Reed RG, Putnam FW, Peters T 1980 Sequence of residues 400-403 of bovine serum-albumin *Biochemical journal* 191 867-868

[41] Hirayama K, Akashi S, Furuya M, et al. 1990 Rapid confirmation and revision of the primary structure of bovine serum-albumin by seims and frit-fab LC MS *Biochemical and Biophysical Research Communications* 173 639-646

[42] Hall C E, Slayter H S 1959 The fibrinogen molecule: its size, shape, and mode of polymerization. *The Journal of biophysical and biochemical cytology* 5 11-6

[43] Mosesson M W; Sherry S 1966 The preparation and properties of human fibrinogen of relatively high solubility. *Biochemistry* 5 2829-35

[44] J. de Jong, R. G. H. Lammertink and M. Wessling 2006 Membranes and

microfluidics: a review *Lab on a Chip* 6, 1125–1139

[45] Merrill E W, Shon Cheng C, Pelletier G A 1969 Yield stress of narmal human blood as a function of endogenous fibrinogen. *Journal of Applied Physiology* 26 1-3

[46] Doolittle RF 1984 Fibrinogen and fibrin *Annual review of biochemistry* 53 195-229

[47] Yang Z; Kollman JM; Pandi L; et al.2001 Crystal structure of native chicken fibrinogen at 2.7 angstrom resolution *Biochemistry* 40 12515-12523

[48] P. Bermabeu and A. Caprrani 2003 Influence of surface charge on adsorption of fibrinogen and/or albumin on a rotating disc electrode of platinum and carbon *Biomaterials* 4 258-264

[49] McKenzie SB: Clinical Laboratory Hematology. Upper Saddle River, N.J.:Prentice Hall, 2004:688.

[50] Jerry H. Brown, Niels Volkmann, Gyo Jun, Agnes H. Henschen-Edman, and Carolyn Cohen 1999 The crystal structure of modified bovine fibrinogen *Biochemistry* 97 85-90

[51] Hantgan, R.R., et.al., in Haemostasis and Thrombosis, 2nd edition, pp 269-289, Bloom, A.L., Forbes, C.D., Thomas, D.P. and Tuddenham, E.G.D., eds, Churchill Livingstone, 1991.

[52] Roach P; Farrar D; Perry CC 2006 Surface tailoring for controlled protein adsorption: Effect of topography at the nanometer scale and chemistry Journal of the *American Chemical Society* 128 3939-3945

[53] Kent P W 1953 Chemical synthesis of hexose polymers. *The Biochemical journal* 55 361-5

[54] Alger MM, Stanley TJ 1989 Measurement of transport parameters in polymer-films-flux overshoot produced by a step change in temperature *Journal of membrane science* 40 87-99

[55] Arshady R 1999 In the name of particle formation *Colloids and surface a-physicochemical and engineering aspects* 153 325-333

[56] William R. Berti, Barry W. Wolstenholme, John J. Kozlowski, Raymond L. Sobocinski, and Robert W. Freerksen 2006 Hydrolytic Stability of Terephthaloyl Chloride and Isophthaloyl Chloride *Environ. Sci. Technol* 40 6330-6335

[57] Dollwet, H. H. A., and J. R. J. Sorenson. 1985. Historic uses of copper compounds in medicine. *Trace Elem. Med.* 2:80–87.

[58] Gregor Grass, Christopher Rensing, and Marc Solioz 2011 Metallic Copper as an Antimicrobial Surface *American Society for Microbiology.* 77 1541–1547

[59] Kuhn, P. J. 1983. Doorknobs: a source of nosocomial infection? Copper Development Association, New York, NY. http://www.copperinfo.co.uk /antimicrobial/downloads/kuhn-doorknob.pdf.

[60] Sudha, V. B. P., K. O. Singh, S. R. Prasad, and P. Venkatasubramanian. 2009. Killing of enteric bacteria in drinking water by a copper device for use in the home: laboratory evidence. *Transact. R. Soc. Trop. Med. Hyg.* 103: 819–822.

[61] Karlin, K. D. 1993. Metalloenzymes, structural motifs, and inorganic

models. *Science* 261:701–708.

[62] Yoshida, Y., S. Furuta, and E. Niki. 1993. Effects of metal chelating agents on the oxidation of lipids induced by copper and iron. Biochim. Biophys. *Acta* 1210:81–88.

[63] Macomber, L., and J. A. Imlay. 2009. The iron-sulfur clusters of dehydratases are primary intracellular targets of copper toxicity. *Proc. Natl. Acad. Sci. U. S. A.* 106:8344–8349.

[64] Cha, J. S., and D. A. Cooksey. 1991. Copper resistance in *Pseudomonas syringae* mediated by periplasmic and outer membrane proteins. *Proc. Natl. Acad. Sci. U. S. A.* 88:8915–8919.

[65] Cooksey, D. A. 1994. Molecular mechanisms of copper resistance and accumulation in bacteria. *FEMS Microbiol. Rev.* 14:381–386.

[66] Rensing, C., and G. Grass. 2003. *Escherichia coli* mechanisms of copper homeostasis in a changing environment. *FEMS Microbiol. Rev.* 27:197–213.

[67] Rouch, D., J. Camakaris, B. T. Lee, and R. K. Luke. 1985. Inducible plasmidmediated copper resistance in *Escherichia coli*. *J. Gen. Microbiol.* 131:939–943.

[68] Solioz, M., H. K. Abicht, M. Mermod, and S. Mancini. 2010. Response of Gram-positive bacteria to copper stress. *J. Biol. Inorg. Chem.* 15:3–14.

[69] Solioz, M., and J. V. Stoyanov. 2003. Copper homeostasis in *Enterococcus hirae*. *FEMS Microbiol. Rev.* 27:183–195.

[70] Tottey, S., P. R. Rich, S. A. Rondet, and N. J. Robinson. 2001. Two

Menkestype ATPases supply copper for photosynthesis in Synechocystis PCC 6803. *J. Biol. Chem.* 276:19999–20004.

[71] Balasubramanian, R., and A. C. Rosenzweig. 2008. Copper methanobactin: a molecule whose time has come. *Curr. Opin. Chem. Biol.* 12:245–249.

[72] Kusumaningrum, H. D., G. Riboldi, W. C. Hazeleger, and R. R. Beumer. 2003. Survival of foodborne pathogens on stainless steel surfaces and crosscontamination to foods. *Int. J. Food Microbiol.* 85:227–236.

[73] Magnani, D., and M. Solioz. 2007. How bacteria handle copper, p. 259–285. *In* D. H. Nies and S. Silver (ed.), Molecular microbiology of heavy metals. *Springer, Heidelberg, Germany.*

[74] Solioz, M., S. Mancini, H. K. Abicht, and M. Mermod. The lactic acid bacteria response to metal stress. *In* K. Papadimitriou and E. Tsakalidou (ed.), Stress response of lactic acid bacteria, in press. *Springer, Heidelberg, Germany.*

[75] Magnani, D., O. Barre´, S. D. Gerber, and M. Solioz. 2008. Characterization of the CopR regulon of *Lactococcus lactis* IL1403. *J. Bacteriol.* 190:536–545.

[76] LaMarche Matthew J.; Leeds Jennifer A.; Dzink-Fox JoAnne; et al.2011 4-Aminothiazolyl analogs of GE2270 A: Design, synthesis and evaluation of imidazole analogs *Bioorganic & Medicinal chemistry letters* 21 3210-3215

[77] Sun Li-ming; Zhang Chen-lu; Li Ping 2011 Characterization, Antimicrobial Activity, and Mechanism of a High-Performance (-)-Epigallocatechin-3-gallate (EGCG)-Cu(II)/Polyvinyl Alcohol (PVA) Nanofibrous Membrane. *Journal of*

agricultural and food chemistry 59 5087-5092

[78] Sivakumar P. M.; Prabhawathi V.; Doble Mukesh 2011 2-Methoxy-2 ',4 '-dichloro chalcone as an antimicrofoulant against marine bacterial biofilm *Colloids and surfaces B-biointerfaces* 81 439-446

[79] Qiu Jian-Hua; Zhang Yan-Wu; Zhang Ya-Tao; et al.2011 Synthesis and antibacterial activity of copper-immobilized membrane comprising grafted poly(4-vinylpyridine) chains *Journal of colloid and interface science* 354 152-159

[80] Bhushan B 1998 Micro/nanotribology using atomic force microscopy/friction force microscopy: state of the art. *Proceedings of the institution of mechanical engineers part J-journal of engineering tribology* 212 1-18

[81] Rablbauer R; Fischer R; Frommeyer G 2004 Mechanical properties of NiAl-Cr alloys in relation to microstructure and atomic defects. *Zeitschrift fur metallkunde* 95 525-534

[82] Chung YW, Li D, Lin XW, et al. 1993 Synthesis and characterization of ultrahigh strength carbon nitride thin-films prepared by magnetron sputtering *Vide-science technique et applications* 49 181-188

[83] Doerner MF, Nix WD 1988 Stresses and deformation processes in thin-films on substrates. *CRC critical reviews in solid state and materials sciences* 14 225-268

[84] Cook RF; Morris DJ; Thum J 2004 Toughness and contact behavior of

conventional and low-k dielectric thin films. *Symposium on Thin Films - Stresses and Mechanical Properties X held at the 2003 MRS Fall Meeting* 795 119-130

[85] Zheng XJ; Zhou YC; Li JY 2003 Nano-indentation fracture test of Pb(Zr(0.52)Ti(0.48))O(3) ferroelectric thin films *Acta materialla* 51 3985-3997

[86] Vella JB; Adhihetty IS; Junker K; et al.2003 Mechanical properties and fracture toughness of organo-silicate glass (OSG) low-k dielectric thin films for microelectronic applications *International journal of fracture* 119 487-499

[87] Park YJ; Pharr GM 2004 Nanoindentation with spherical indenters: finite element studies of deformation in the elastic-plastic transition regime *Thin solid films* 447 246-250

[88] Herbert EG; Pharr GM; Oliver WC; et al.2001 On the measurement of stress-strain curves by spherical indentation *Thin solid films* 398 331-335

[89] Swain MV 1998 Mechanical property characterisation of small volumes of brittle materials with spherical tipped indenters *Materials science and engineering a-structural materials properties microstructure and processing* 253 160-166

[90] Cheng L; Xia X; Scriven LE; et al.2005 Spherical-tip indentation of viscoelastic material *Mechanics of materials* 37 213-226

[91] Spary I. J.; Bushby A. J.; Jennett N. M.2006 On the indentation size effect in spherical indentation *Philosophical magazine* 86 5581-5593

[92] Cepheid 2003 http://www.Cepheid.com

[93] ChipRX. 2003 http://www.ChipRX.com

[94] Shawgo G M, Richards Grayson A C, Li Y and Cima M J 2002 Bio-MEMS for drug delivery, Curr. Opin. Solid State Mater. *Sci*. 6 329-334

[95] Efimenko K, Wallace W E and Genzer J 2002 Surface Modification of Sylgard-184 Poly (dimethyl siloxane) Networks by Ultraviolet and Ultraviolet/Ozone *Treatment Journal of Colloid and Interface Science* 254 306–315

[96] Konrad R, Ehrfeld W, Freimuth H, Pommersheim R, Schenk R and Weber L 1998 Microreaction Technology: Proceedings of the first internation conference on microreaction technology *pp*. 348-356

[97] Brody J P, Yager P, Goldstein R E and Austin R H 1996 Biotechnology at low Reynolds numbers *Biophys. J*. 71 3430-3441

[98] Li P C H and Harrison D J 1997 Transport, manipulation and reaction of biological cells on-chip using electrokinetic effects *Anal. Chem.* 69 1564-1568

[99] Woolley A T and Mathies R A 1995 Ultra-high-speed DNA-sequencing using capillary electrophoresis chips *Anal. Chem.* 67 3676-3680

[100] Liu S, Shi Y and Ja W W 1999 Optimization of high-speed DNA sequencing on microfabricated capillary electrophoresis channels *Anal. Chem.* 71 566-573

[101] Chiem N and Harrison D J 1997 Microchip-based capillary electrophoresis for immunoassays: Analysis of monoclonal antibodies and theophylline *Anal. Chem.* 69 373-378

[102] Colyer C L, Tang T, Chiem N and Harrison D J 1997 Clinical potential of microchip capillary electrophoresis systems *Electrophoresis* 18 1733-1741

[103] Hadd A G, Raymond D E, Halliwell J W and Ramsey J M 1997 Microchip device for performing enzyme assays *Anal. Chem.* 69 3407-3412

[104] Van den Bery A, Grisel A, Verney-Norberg and De RooijN F 1993 On-wafer fabricated free-chlorine sensor with ppb detection limit for drinking-water monitoring *Sensors and Actuators B: Chemical* 13 396-399

[105] Kugelmass SM; Lin C; DeWitt SH 1999 Fabrication and characterization of three-dimensional microfluidic arrays *Microfluidic devices and systems II* 3877 88-94

[106] Hwang TJ; Popa D; Sin J; et al.2004 BCB wafer bonding for microfluidics *Micromachining and microfabrication process technology IX* 5342 182-191

[107] Larsen Ryan J.; Dickey Michael D.; Whitesides George M.; et al. 2009 Viscoelastic properties of oxide-coated liquid metals *Journal of rheology* 53 1305-1326

[108] Chen ZF; Gao YH; Su RG; et al.2003 Fabrication and characterization of poly(methyl methacrylate) microchannels by in situ polymerization with a novel metal template *Electrophoresis* 24 3246-3252

[109] Madou MJ; Lu YM; Lai SY; et al.2000 A centrifugal microfluidic platform - A comparison *Micro total analysis systems* 2000, 565-570

[110] Situma Catherine; Hashimoto Masahiko; Soper Steven A.2006 Merging microfluidics with microarray-based bioassays *Biomolecular engineering* 23

213-231

[111] White R 2007 SU-8 Photoresist Processing

[112] Abgrall P.; Gue A-M 2007 Lab-on-chip technologies: making a microfluidic network and coupling it into a complete microsystem - a review *Journal of micromechanics and microengineering* 17 R15-R49

[113] Kumar Ashok; Srivastava Akshay; Galaev Igor Yu; et al.2007 Smart polymers: Physical forms and bioengineering applications *Progress in polymer science* 32 1205-1237

[114] Inamdar Niraj K.; Borenstein Jeffrey T.2011 Microfluidic cell culture models for tissue engineering *Current opinion in biotechnology* 22 681-689

[115] Liu Changchun; Thompson Jason A.; Bau Haim H.2011 A membrane-based, high-efficiency, microfluidic debubbler *Lab on a chip* 11 1688-1693

[116] Srigunapalan Suthan; Lam Cameron; Wheeler Aaron R.; et al 2011 A microfluidic membrane device to mimic critical components of the vascular microenvironment *Biomicrofluidics* 5

[117] Luo Xiaolong; Berlin Dean Larios; Betz Jordan; et al. 2010 In situ generation of pH gradients in microfluidic devices for biofabrication of freestanding, semi-permeable chitosan membranes *Lab on a chip* 10 59-65

[118] Lu Yao; Shi Weiwei; Qin Jianhua; et al. 2010 Fabrication and Characterization of Paper-Based Microfluidics Prepared in Nitrocellulose Membrane By Wax Printing *Analytical chemistry* 82 329-335

[119] Letourneau Suzanne; Hernandez Luiza; Faris Andrea N.; et al.2010 Evaluating the effects of estradiol on endothelial nitric oxide stimulated by erythrocyte-derived ATP using a microfluidic approach *Analytical and bioanalytical chemistry* 397 3369-3375

[120] Moorthy J and Beebe D J 2003 In situ fabricated porous filters for Microsystems *Lab Chip* 3 62-66

[121] Baldi A; Lei M; Gu YD; et al.2006 A microstructured silicon membrane with entrapped hydrogels for environmentally sensitive fluid gating *Sensors and actuators B-chemical* 114 9-18

[122] Liu Changchun; Cui Dafu; Cai Haoyuan; et al. 2006 A rigid poly(dimethylsiloxane) sandwich electrophoresis microchip based on thin-casting method *Electrophoresis* 27 2917-2923

[123] Al-Aribe Khaled; Knopf George K.; Bassi Amarjeet S.2006 Reconfigurable microfluidic chip based on a light-sensitive hydrogel *Optomechatronic actuators, manipulation, and systems control* 6374

[124] Adiga Shashishekar P.; Curtiss Larry A.; Elam Jeffrey W.; et al.2008 Nanoporous materials for biomedical devices *JOM* 60 26-32

[125] Rong Zimei; Vadgama Pankaj 2009 An electrochemical method for measurement of mass transport in polymer membranes using acetaminophen as a model system *Electrochimica acta* 54 4949-4953

[126] Ding L and Wang E K 1996 Electrochemical studies of Meldola blue-modified bilayer lipid membranes Chinese *Academy of Sciences* 130022

[127] G.F. Hall, D.J. Best, P.F. Turner 1988 The determination of p-cresol in chloroform with an enzyme electrode used in the organic phase *Anal. Chim. Acta,* 213, 113–119

[128] C. J. Nikles, M. Yelland, C. D. Marc, D. Wilkinson, Am. J. Therap. 2005 The role of paracetamol in chronic pain: an evidence-based approach *American journal of therapeutics* 12, 80–91

[129] R. N. Goyal, S. P. Singh 2006 Voltammetric determination of paracetamol at C-60-modified glassy carbon electrode *Electrochim. Acta* 51, 3008–3012

[130] M. Li, L. Jing 2007 Electrochemical behavior of acetaminophen and its detection on the PANI-MWCNTs composite modified electrode *Electrochim. Acta* 52 3250–3257

[131] Kuei-Sheng Tseng, Lin-Chi Chen, Kuo-Chuan Ho 2005 Amperometric detection of hydrogen peroxide at a prussian Blue-modified FTO electrode *Sensors and Actuators* 108 738–745

[132] Crank J 1979 The Mathematics of Diffusion (2nd ed. Clarendon Press, Oxford)

[133] Gill SR et al., 2005 “Insights on evolution of virulence and resistance from the complete genome analysis of an early methicillin-resistant Staphylococcus aureus strain and a biofilm-producing methicillin-resistant Staphylococcus epidermidis strain.", *J Bacteriol,* 187 (7) :2426-38

[134] Sapelkin A, Bayliss S, Unal B and Charalambou A, 2006, Interaction of B50 rat hippocampal cells with stain-etched porous silicon, *Biomater* 27

842-846

[135] Schubert MA; Wiggins MJ; Anderson JM; et al.1997 The effect of strain state on the biostability of a poly(etherurethane urea) elastomer *Journal of biomedical materials research* 35 319-328

[136] Matthew L. Clarke, Jie Wang, and Zhan Chen 2005 Conformational Changes of Fibrinogen after Adsorption *J. Phys. Chem.* 109 22027-22035

[137] Fay M and Hendrix B M 1931 The effect of acid denaturation upon combining power of fibrinogen *J. Biol. Chem*. 93 667-75

[138] Wasilewska M, Adamczyk Z and Jachimska B 2009 Structure of fibrinogen in electrolyte solutions derived from dynamic light scattering and viscosity measurements. *Langmuir* 25 3698-704

[139] Militello V; Casarino C; Emanuele A; et al. 2004 Aggregation kinetics of bovine serum albumin studied by FTIR spectroscopy and light scattering Biophysical chemistry 107 175-187

[140] Pinnau I, Koros WJ 1993 A qualitative skin layer formation mechanism for membranes made by dry wet phase inversion *Journal of polymer science part B-Polymer Physics* 31 419-427

[141] Qiu Yongzhi; Zhang Ning; Kang Qian; et al.2009 Fabrication of Permeable Tubular Constructs From Chemically Modified Chitosan With Enhanced Antithrombogenic Property *Journal of biomedical materials research part B-applied biomaterials* 90 668-678

[142] Abhay Kumar Thakur, Atul Kumar Srivastava, Volety Srinivas, Kandala

Venkata Ramana Chary and Chintalagiri Mohan Rao 2011 Copper Alters Aggregation Behavior of Prion Protein and Induces Novel Interactions between Its N- and C-terminal Regions *The journal of biological chemistry* 286 38533–38545

[143]Canete Socrates Jose P.; Zhang Zhengzheng; Kong Lingmei; et al. 2011 Application of synchrotron FTIR microspectroscopy for determination of spatial distribution of methylene blue conjugated onto a SAM via "click" chemistry *Chemical communications* 47 11918-11920

[144] Nitin K. Pandey, Sudeshna Ghosh and Swagata Dasgupta 2010 Fibrillation in Human Serum Albumin Is Enhanced in the Presence of Copper(II) *J. Phys. Chem.* 31 10228–10233

[145] Mosesson M W; Sherry S 1966 The preparation and properties of human fibrinogen of relatively high solubility. *Biochemistry* 5 2829-35

[146] Morgan P W and Kwolek S L 1959 Interfacial polycondensation II fundamentals of polymer formation at liquid interfaces *J. Polym. Sci*. XL 299-327

[147] Luz RCS, Damos FS, Oliveira AB, Beck J, Kubota LT, 2006, Development of a voltammetric sensor for catechol in nanomolar levels using a modified electrode with Cu(phen)2(TCNQ)2 and PLL, *Sens. Actuators B* 117 274-281

[148] Henzler T and Steudle E, 2000, Transport and metabolic degradation of hydrogen peroxide in *Chara corallina*: model calculations and measurements

with the pressure probe suggest transport of H_2O_2 across water channels, *J Exp Botany*, 51 2053-2066

[149] Andersson, H.; van den Berg, A. Microfluidic devices for cellomics: A review. *Sens. Actuat B-Chem.* 2003, *92*, 315-325.

[150] Yi, C.Q.; Li, C.W.; Ji, S.L.; Yang, M.S. Microfluidics technology for manipulation and analysis of biological cells. *Anal.Chim. Acta* 2006, *560*, 1-23.

[151] Dittrich, P.S.; Manz, A. Lab-on-a-chip: Microfluidics in drug discovery. *Nat. Rev. Drug Discov.*2006, *5*, 210-218.

[152] El-Ali, J.; Sorger, P.K.; Jensen, K.F. Cells on chips. *Nature* 2006, *442*, 403-411.

[153] Erickson, D.; Li, D.Q. Integrated microfluidic devices. *Anal.Chim. Acta* 2004, *507*, 11-26.

[154] Liebsch, G.; Klimant, I.; Frank, B.; Holst, G.; Wolfbeis, O.S. Luminescence lifetime imaging of oxygen, pH, and carbon dioxide distribution using optical sensors. *Appl. Spectrosc.* 2000, *54*, 548-559.

[155] Kocincova, A.S.; Nagl, S.; Arain, S.; Krause, C.; Borisov, S.M.; Arnold, M.; Wolfbeis, O.S. Multiplex bacterial growth monitoring in 24-well microplates using a dual optical sensor for dissolved oxygen and pH. *Biotechnol. Bioeng* 2008, *100*, 430-438.

[156] Liebsch, G.; Klimant, I.; Krause, C.; Wolfbeis, O.S. Fluorescent imaging of pH with optical sensors using time domain dual lifetime referencing. *Anal. Chem.* 2001, *73*, 4354-4363.

[157] Huang, C.W.; Lee, G.B. A microfluidic system for automatic cell culture. *J. Microme. Microen.* 2007, *17*, 1266-1274.

[158] Lao, A.I.K.; Lee, T.M.H.; Hsing, I.M.; Ip, N.Y. Precise temperature control of microfluidics chamber for gas and liquid phase reactions. *Sens. Actuat. A-Phys.* 2000, *84*, 11-17.

[159] Sanders GHW; Manz A 2000 Chip-based microsystems for genomic and proteomic analysis *Trac-trends in analytical chemistry* 19 364-378

LIST OF PUBLICATIONS

PAPERS

Hong Chang, Rachel Khan, Zimei Rong, Andrei Sapelkin and Pankaj Vadgama 2010 Study of albumin and fibrinogen membranes formed by interfacial crosslinking using microfluidic flow *Biofabrication*

Zeynep Ekemen, **Hong Chang**, Zeeshan Ahmad, Cem Bayram, Zimei Rong, Emir Baki Denkbas, Eleanor Stride, Pankaj Vadgama, and Mohan Edirisinghe 2011 Fabrication of Biomaterials via Controlled Protein Bubble Generation and Manipulation *Maromolecules*

H.Chang, S.Dunn, W.Wang, P.Vadagma Nanomechanical Characterization of the protein membranes (processing)

BOOK

A. Spehar-Délèze, S. Anastasova, Z. Rong, D. Bickham, **H. Chang**, P. Vadgama: General Platform for In vivo Sensors for Oxygen, Glucose and Lactate Monitoring. Portable Chemical Sensors - Weapons Against Bioterrorism, D. Nikolelis (Ed), NATO Science for Peace and Security Series A: Chemistry and Biology (2012) 287-303

ABSTRACT

H.Chang, Z. Rong, S.Dunn, P.Vadagma 2011 Study of an in situ protein membrane in a microfluidics system *2011 MRS Spring Meeting*